UNIVERSITE D'ABOMEY - CALAVI (UAC)

INSTITUT NATIONAL DE L'EAU

Registered under N°: 2030-20/UAC/VR-AA/SA

A DISSERTATION

Submitted

In partial fulfillment of the requirements for the degree of

DOCTOR of Philosophy (PhD) of the University of Abomey-Calavi (Benin Republic)

In the framework of the

Graduate Research Program on Climate Change and Water Resources (GRP-CCWR)

By

Rita HOUNGUE

Public defense on: 02/26/2020

======

CLIMATE CHANGE IMPACTS ON HYDRODYNAMIC FUNCTIONING OF OUEME DELTA (BENIN)

======

Supervisors:

Agnidé Emmanuel LAWIN, Full Prof, University of Abomey-Calavi, Bénin
Abel AFOUDA, Associate Prof, University of Abomey-Calavi, Bénin

======

Reviewers:

Prof Eric A. ALAMOU, Associate Prof, University of Abomey, Bénin
Prof Albert Tié Bi GOULA, Full Prof, University of Nangui Abrogoua, Côte d'Ivoire
Prof Benjamin NGOUNOU NGATCHA, Full Prof, University of Ngaoundéré , Cameroon

======

JURY

Basile KOUNOUHEWA	Full Prof, University of Abomey-Calavi, Bénin	President
Eric A. ALAMOU	Associate Prof, UNSTIM of Abomey, Bénin	Reviewer
Albert Tié Bi GOULA	Full Prof, University of Nangui Abrogoua, Côte d'Ivoire	Reviewer
Benjamin NGOUNOU NGATCHA	Full Prof, University of Ngaoundéré, Cameroon	Reviewer
Sounmaïla MOUMOUNI	Associate Prof, UNSTIM of Abomey, Bénin	Examiner
Agnidé Emmanuel LAWIN	Full Prof, University of Abomey-Calavi, Bénin	Supervisor
Abel AFOUDA	Associate Prof, University of Abomey-Calavi, Bénin	Co-supervisor

Dedication

To the Almigthy God who allows and guides me throughout;

To my beloved Sourou and my son Oladé;

To my life fellows Mendel, Cessac, Rhoyale and Rholan;

To my life givers Lucie ANAGO KPOGLA and Raymond Y. HOUNGUE;

To my second family members the OGNIs;

for your everyday sacrifice, understanding, encouragement and help. Be honored and blessed.

Acknowledgment

This PhD work is realized in the framework of the West African Science Service Center on Climate Change and Adapted Land use (WASCAL) and funded by the **German Ministry of Education and Research (BMBF) in collaboration with the Benin Ministry of High Education and Scientific Research** (MESRS). I am also grateful to the International Fundation for Science (IFS), the African Network of Earth Science Institutions (ANESI) and the Committee on Space Research (COSPAR) for their grant support.

My gratitude to Prof Abel AFOUDA for mentoring me all along my scientific journey till today. Thanks for your patience, your guidance and supervision within this great journey.

My special thanks for my main supervisor Prof Agnidé Emmanuel LAWIN for his untiredfull guidance for today greatful end.

I thank Prof Julien ADOUNKPE, Director of the WASCAL Graduate Research Program Climate Change and water resource (Benin) for his efforts and encouragement througout.

I am gratefull to Prof Daouda MAMA, Director of the National Institute of Water for his effort and committements since I stepped into hydrology.

I would also like to thank Prof Jean Paul Rudant, Prof Pierre Louis Frison from Université Paris Est Marne la vallée for they support during my training at the Laboratoire en Sciences et technologies de l'information géographique (*LaSTIG*) at the University Paris-Est Marne la Vallée.

I am grateful to Prof Arhur MYNETT and Prof Johannes Hans Van Der KAST for they commintment during my training at UNESCO-IHE at Delft.

I would like to thank IRD staff in Benin for their support especially Dr Christophe PEUGEOT, Dr Sylvie GALLE, Dr Maxim WUBDA, Mr Théodore OUANNOU and Mr Simon AFOUDA.

My thanks go to DHI France ingenieers especially Dr Caroline TESSIER who helped me enhancing the use of Mike 21 for hydrodynamic modelling. I won't forget the Late Hans Jacob VESTED who firstly introduced me to this tool.

My gratitude to Salem ELEGBEDE and Imelda DJAGOUN for they support, care and conviviality. Be blessed.

Special thanks to my WASCAL colleagues from the first to the third batch especially Samiratou OUERMI.

I am gratefull to the National Water Institute members especially those from the Laboratory of Applied Hydrology where I got my footprints in hydrology.

Abstract

This work focused on quantification of the effects of climate change on the hydrodynamic functioning of the Ouémé Delta through the following steps. First of all, an analysis of the current state of extreme climate risks was conducted. Then, a future projection of the Ouémé River discharge at Bonou outlet was made in order to quantify the impact of anthropogenic activities and climate change by 2050. In addition, a mean ensemble model approach based on HEC-HMS, HBV and HyMoLAP was applied to better simulate Ouémé River peak flows at Bonou. Indeed, the hydrological simulation is done to generate the current missing flow data from 2011 to 2019. Finally, these flows were used to simulate water level and flows in the Ouémé Delta on the basis of the hydrodynamic model set up. Results showed increasing trend in extreme events. Similarly, the temperature is increasing as result of the current global warming. In addition, flows tend to decrease significantly with representative concentrations RCP4.5 while non-significant growth is observed with representative concentrations RCP8.5. HEC-HMS was the best among the three hydrological models to simulate both the Ouémé River daily and peak flow at Bonou. Thus, the outputs of this model over the period 2011- 2019 are then used for the hydrodynamic modeling. The hydrodynamic model set up allowed the correct simulation of the water level and flows in the Ouémé Delta. Thus, an inter-correlation between the water levels at Bonou, Adjohoun, Hêtin-Sota and So-Ava was established in order to reconstruct the water level and flows at Bonou in 2016. A good match between reconstructed flows and those simulated in HEC-HMS is observed. Thus, from the rain and temperature data over Ouémé catchment at Bonou Outlet, we can simulate water level and flow at any point in the Ouémé delta. Moreover, the combined effects of the governmental project of dams constructing and climate change will probably enhance existing ecosystem services issues in Ouémé Delta as Ouémé River flows in Bonou are expected to decrease by 2050. Therefore, ecological impacts studies have to be done for Ouémé Delta ecosystem sustainable preservation for the stakeholders' wellbeing.

Key words: *Trend analysis, hydrological modeling, land use and cover dynamic, hydrodynamic modeling, Ouémé Catchment, Ouémé Delta early warning system in Bénin.*

Synthesis

Résumé

Le présent travail contribue à la quantification des effets des changements climatiques sur le fonctionnement hydrodynamique du delta de l'Ouémé. Dans un premier temps, une analyse de l'état actuel des risques climatiques extrêmes a été faite. Ensuite, une projection future des débits du fleuve Ouémé à l'exutoire de Bonou a été faite en vue de quantifier l'impact des activités anthropiques et des changements climatiques sur ceux-ci à l'horizon 2050. De plus, une approche de moyenne d'ensemble de modèle utilisant HEC-HMS, HBV et ModHyPMA a été appliquée en vue de choisir le meilleur capable de simuler les débits maximum de l'Ouémé à Bonou. En effet, la simulation hydrologique est faite dans le but de combler les données de débit de 2011 à 2019 actuellement manquantes. Enfin, ces débits ont servi à simuler les côtes et débits dans le delta de l'Ouémé sur la base d'un modèle hydrodynamique.

Il en ressort que l'état acutel montre une tendance à l'augmentaton des événements extrêmes tels que les inondations. De même, la température est croissante du faite du réchauffement climatique actuel. De plus, les débits tendent à décroitre significativement selon les références de concentrations représentatives RCP4.5 tandis qu'une croissance non significative est observée avec les concentrations representatives RCP8.5. HEC-HMS s'est révélé le meilleur parmi les trois modèles hydrologiques utilisés tant lors de la simulation des débits journaliers que des débits de pointe de l'Ouémé à Bonou. Ainsi, ce modèle a permis de simuler les données de débits sur la période 2011 – 2019 pour la modélisation hydrodynamique. Le modèle hydrodynamique mise en place a permis la bonne simulation des côtes et débits dans le delta de l'Ouémé. Ainsi, une intercorrelation entre les côtes de Bonou, Adjohoun, Hêtin-Sota et So-Ava a été établi afin de reconstituer les côtes et débits à Bonou en 2016. Une bonne adéquation entre des débits reconstitués et ceux simulés dans HEC-HMS est observée. Ainsi, à partir de la pluie et de la température sur le bassin de l'Ouémé à Bonou, il est possible donc simuler les côtes et débits à n'importe quel point du delta de l'Ouémé. Les impacts combinés de la contruction de l'ensemble des barrages structurants du bassin de l'Ouémé (Bétérou, Vossa et Dogo-Bis) prévu dans le programme d'action du gourvernement actuel, et des changements climatiques vont probablement aggraver les problèmes liées aux services écosystémiques existants dans le delta de l'Ouémé vue la tendance à la décroissance des débits à l'horizon 2050. Alors, des études devront être faites pour déterminer les débits

environnementaux dans le but de la préservation de l'écosystème du delta de l'Ouémé pour le bien être des communautés environnantes.

Mots clés: *Analyse tendancielle, modélisation hydrologique, dynamique d'utilisation des terre, modelisation hydrodynamique, Bassin de l'Ouémé à Bonou, système d'alerte précoce du delta de Ouémé au Bénin.*

Introduction

Connue comme la zone nourricière du sud du Bénin, le delta de l'Ouémé présente un intérêt socio-économique important, vue les diverses opportunités d'activités qu'il offre telles que : la pêche, la chasse, l'agriculture, l'élevage mais aussi le commerce [1]. *De plus, il est un écosystème abritant diverses espèces animales et végétales qui y dépendent. Par ailleurs, de part sa situation géographique, le delta de l'Ouémé se trouve être la zone tampon des eaux provenant du bassin de l'Ouémé à l'exutoire de Bonou avant leur acheminement vers l'Océan Atlantique. Avec sa superficie d'environ 50 000 km^2 , le bassin de l'Ouémé représente près de la moitié de la superficie du Bénin. Ainsi, le delta de l'ouémé subit de façon saisonnière des inondations qui emportent avec elles des infrastrutures, des récoltes agricoles, du bétail mais aussi des vies humaines. En 2010, les pertes et dommages dues au inondations étaient évaluées à environ 128,3 millliards de francs CFA* [2] *soit 3,72% du produit intérieur brute (PIB) de cette même année. Bien que les inondations apportent des sédiments qui fertilisent les terres cultivées, les pertes et dommages restent non négligeables. De plus, dans le souci de l'amélioration de la fourniture de l'énergie électrique, le gouvernement actuel du Bénin prospecte la construction de barrages hydroelectriques sur certaines de nos rivières. Une de ces priorités porte sur le barrage de Dogo-Bis situé sur le fleuve Ouémé* [3]. *Aussi, la croissance démographique et par conséquent l'augmentation du taux de dégradation des terres qui ne sont pas à occulter avec pour corollaire les variabilités climatiques impactent la disponibilité des ressources en eau dans le delta de l'Ouémé. Il urge donc d'approfondir la compréhension du fonctionnement hydrodynamique du delta de l'Ouémé pour une meilleure gestion des inondations de même qu'une bonne planification des ressources en eau du delta sous l'effet des changements climatiques. C'est dans ce cadre que s'inscrit le présent travail structuré en quatre objectifs à savoir : 1) caractériser l'état climatique actuel du delta de l'Ouémé à travers une analyse tendancielle ; 2) évaluer l'impact des changements climatiques sur les débits du fleuve Ouémé à l'exutoire de Bonou à l'horizon 2050 ; 3) proposer une approche simple de cartographie des inondations dans le delta de l'Ouémé ; 4)*

concevoir un modèle hydrodynamique du delta de l'Ouémé pour sa meilleure gestion sous l'effet des changements climatiques.

Zone d'étude

La zone d'étude est le delta de l'Ouémé qui est alimenté en eau par le bassin versant de l'Ouémé dont il représente la zone tampon avant l'Océan Atlantique. La figure 1. montre le complexe du bassin versant de l'Ouémé et du delta dans lequel la portion du delta de l'Ouémé ici considérée est de couleur violette.

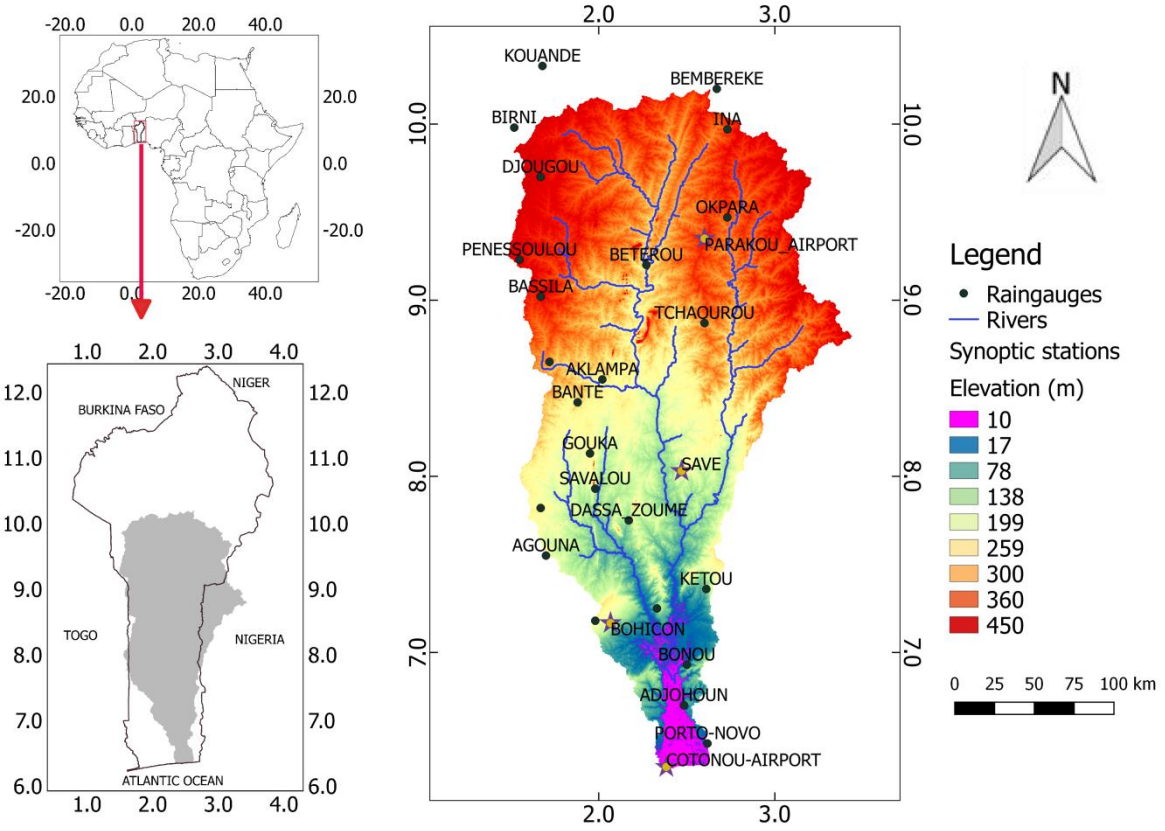

***Figure 1**. Situation géographique du complexe bassin-delta de l'Ouémé.*

Le complexe du bassin et du delta de l'Ouémé est situé entre les latitudes 6,3° et 10,3° Nord et les longitudes 1,5° et 3,5° Est au Bénin en Afrique de l'Ouest. Le Bénin est limité à l'ouest par le Togo, à l'est par le Nigeria, au nord par le Niger, au nord-ouest par le Burkina Faso et au sud par l'océan Atlantique.

Le bassin de l'Ouémé à l'exutoire de Bonou est d'environ 50 000 km^2, dont 0,1 % au Togo et 8 % au Nigeria [4]. *Il est situé entre les latitudes 6,9° et 10,3° Nord, et les longitudes 1,5° et 3,5° Est. Le bassin de l'Ouémé est sous un climat tropical avec trois zones climatiques*

allant du climat subéquatorial au climat soudanien vers le nord. Le bassin versant de l'Ouémé reçoit chaque année entre 724 et 1396 mm de précipitations [5].

Le delta de Ouémé en entier s'étend de la côte Atlantique jusqu'à la latitude de Zagnanado et envelopé par la courbe de niveau d'altitude 15 m. Il est situé entre 6,30° et 7.20° Nord et entre 2,20° et 2,70° Est. Il couvre une superficie d'environ 5000 km^2 [6]. *Compte tenue de la disponibilité des données et du bassin du fleuve Ouémé considéré ici à l'exutoire de Bonou, la portion du delta prise en compte, représente la zone tampon entre le bassin de l'Ouémé à l'exutoire de Bonou et l'Océan Atlantique. Elle représente l'aire de l'envelope de la courbe de niveau d'altitude 10 m à partir de la latitude de la station de Bonou. Elle se situe entre 6,30° et 6,9° Nord et entre 2,20° et 2,70° Est. Il est long de 55 km dans la direction Est-Ouest, de la rivière Djonou jusqu'à la extrémité de la lagune de Porto-Novo au Bénin. Elle est large de 67 km du Nord au Sud de l'Océan Atlantique jusqu'à la station de Bonou. Le delta de l'Ouémé pris en compte dans le présent travail, couvre les communes de Bonou, Adjohoun, Dangbo, Akpro-Missérété, Abomey-Calavi, Aguégué, Porto Novo, Sêmé Kpodji et Cotonou. Il s'agit une zone très riche, qui offre la vie à un grand nombre d'espèces écologiques. Il s'agit d'une région bien adaptée non seulement à l'agriculture en raison du dépôt de nutriments, mais aussi pour la pêche et les transactions fluviales. Il abrite également un nombre considérable d'habitants qui dépendent de ces ressources, en particulier ceux qui vivent sur le lac Nokoué ainsi que le long des rivières Ouémé et Sô dans le delta. Le lac Nokoué est le plus grand du Bénin ; il représente le réceptacle des eaux du delta de l'Ouémé avant leur acheminement vers l'Océan Atlantique. Le lac Nokoué est situé entre 6,30° et 6,50° Nord et entre 2,35° et 2,50° Est. Il est long de 11 km du Nord au Sud et large de 20 km dans sa direction Est - Ouest* [6,7]. *Il couvre 150 km*^{2} *à marée basse et pourrait grossir jusqu'à 450 km*^{2} *en hautes eaux* [6,7]. *Il est limitée à l'Ouest par le plateau d'Abomey-Calavi, à l'Est par la lagune de Porto Novo, au Nord par les rivières Ouémé et Sô de même que la plaine inondable du delta de l'Ouémé, et au Sud par la ville de Cotonou. Les chenaux de Cotonou et Totchè connectent respectivement le lac Nokoué à l'océan Atlantique et la lagune de Porto-Novo qui s'ouvre sur Lagos* [6]. *Le delta de l'Ouémé est caractérisé par une température moyenne variant entre 25 to 29°C et des précipitations variant entre 719 mm and 2470 mm* [8]. *La végétation est composée essentiellement de plantations de palmiers, acacia et teck, de même que des forêts galeries. En plus, il est distingué une végétation aquatique de Paspalum vaginatym le long des marécages* [6]. *Le delta de l'Ouémé est caractérisé par un sol argilo-sableux. Il est observé*

une dégradation croissante des terres, en particulier la conversion des savannes et forets arbustives en terres cultivables [5].

Données, matériels et méthodes

Données

Les données utilisées dans le présent travail sont essentiellement de trois sortes. Il s'agit des données d'observation climatique de 1971 à 2016, des données de projection des modèles climatiques de 2020 à 2050, des données hydrométriques de 1971 à 2010 et des données d'imagerie satellitaire couvrant le delta pendant les années 2010, 2018.

Les données d'observation climatique ont été collectées tant sur les stations environnantes du delta que sur celles du bassin de l'Ouémé à Bonou. Les données collectées sur le delta sont: la pluie, la température, l'humidité relative, la durée d'insolation et l'évaporation bac pour l'analyse de la situation climatique actuelle. Seule la pluie et la température sont collectées pour les simulations pluie-débit et les projections climatiques sur le bassin de l'Ouémé à Bonou. Les données de débit sont collectées à la station de Bonou. Les données de cote sont collectées aux stations de Bonou, Adjohoun, Hêtin-Sota et So-Ava. Les données d'imagerie satellitaire optique Landsat du 10 Décembre 2018 de même que radar Envisat du 10 Octobre 2010 et sentinel 1A du 09 Août à 10 Décembre 2018 ont été collectées.

Matériels et méthodes

Les données climatiques du delta ont servi à calculer huit indices climatiques extrêmes de température et quinze de précipitation parmi les indices établis par l'Organisation Mondiale de la Météorologie. Ces indices ont été calculés à l'aide de l'outil ClimPACT qui est développé sous le language R [9]. *Les indices obtenus ont été analysés par la méthode de Mann Kendall modifiée permettant d'enlever la corrélation sérielle interne qui biaise l'analyse des tendances. Ensuite, une corrélation partielle a été appliquée dans le but de déterminer l'interrelation entre l'évaporation et le reste des variables climatiques sus-citées. Enfin, une regression échelonnée a permis de quantifier la proportion d'influence desdites variables sur l'évaporation qui représente en effet l'une des principales sources de perte dans les ressources en eaux de surface.*

Les données de pluie et de température du bassin de l'Ouémé ont été utilisées pour le calage et la validation des modèles hydrologiques HEC-HMS, HBV et ModHyPMA. Ce calage a été fait sur la période 1971 - 1990 et la validation sur la période 1991 – 2010 tandis que les projections ont été faites sur la période 2020 - 2050. Dans le but de quantifier

l'impact des changements climatiques sur les débits du fleuve, la méthode du taux de ruisselement '' curve number (CN)'' a été utilisée sous le modèle HEC-HMS en vue de la prise en compte des changements d'état de surface. De plus, la méthode de prise en compte de l'humidité du sol '' soil moisture accounting (SMA)'' a été appliquée avec les modèles HEC-HMS et HBV dans le but de prendre en compte les écoulements rétardés liées à l'humidité du sol lors de la simulation des débits de pointe de l'Ouémé à Bonou. Par ailleurs, une approche de moyenne d'ensemble de modèle a été appliquée en vue de déterminer le modèle qui représente au mieux les débits maximum de l'Ouémé à Bonou. Pour ce faire, les modèles ont été évalués individuellement avant d'être couplés comme suit : HBV/HEC-HMS, ModHyPMA/HBV, ModHyPMA/HEC-HMS et enfin ensemble (HMS, HBV et ModHyPMA). Les coefficients d'efficacités retenus sont principalement l'efficience de Kling–Gupta (KGE), le pourcentage de biais (PBias) et l'erreur moyenne absolue (MAE).

Du fait de l'indisponibilité des images satellites optiques dans le delta de l'Ouémé à cause du taux de couverture nuageuse élevée, il s'est avéré nécessaire d'utiliser les images satellitaires radars telles que Sentinel qui sont libres. Par contre, ces données présentent des difficultés de téléchargements, du fait de leur poids surtout dans nos réalités de pays en développement. Une alternative a été d'utiliser la platforme Visioterra qui a permis l'analyse en composition colorée sans téléchargement pour la cartographie de l'utilisation des terres et des inondations dans le delta de l'Ouémé. La modélisation hydrodynamique a été faite avec le modèle HEC-RAS. Le calage a été fait avec l'année 2010 et l'année 2008 a servi à la validation. Le modèle établi a ensuite permis de reconstituer les débits en 2016 et 2018 à Bonou. De plus, l'impact des projets de construction des barrages structurants du bassin de l'Ouémé a été évalué. En effet, lesdits barrages sont prévus pour retenir environ 3,5 millards de m^3 d'eau. De même, l'impact des changements climatiques sur le fonctionnement hydrodynamique du delta a été étudié sur la base du modèle hydrodynamique.

Résultats et discussion

Les résultats montrent que les événements extrêmes ont tendance à augmenter avec la variabilité climatique. En effet, les fortes et les très fortes pluies ont une tendance significativement croissance sur la période 1971-2016. De même, les maxima mensuel des 1, 2 3, 5 et 10 jours de pluie montrent une tendance significative croissante pendant la période de hautes eaux allant de Septembre à Octobre. Aussi, la tendance croissante observée dans les chroniques de température est en cohérence avec le réchauffement climatique global. De même, l'indice indicateur des poches de sécheresse de deux jours consécutifs, il présente une

tendance significative croissante. Quant aux maxima, minima et moyenne d'humidité relative, vitesse de vent et durée d'insolation, ils restent presque inchanger sauf les maxima annuel des humidités relatives maximales qui eux tendent à décroitre significativement compte tenu du réchauffement climatique. De plus, les paramètres influençant beaucoup plus l'evaporation dans le delta de l'Ouémé sont essentiellement la durée d'insolation, la température et la vitesse du vent.

Le modèle hydrologique HEC-HMS a montré une bonne capacité à simuler les débits tout en tenant compte de l'utilisation des terres et de la modification de la couverture des sols avec un KGE de 0,94 et 0,91 respectivement en calage et en validation. Le PBias est de 7 % de surestimation et 1,3 % de sous-estimation des observations respectivement en calage et en validation. De plus, la projection des débits du fleuve Ouémé à l'exutoire de Bonou montre, à l'horizon 2050, une tendance significative à la diminution d'environ 6,58 m^3/s sur la base du scénario RCP 4.5, tandis qu'une tendance à la hausse non significative est observée sur la base du RCP 8.5. Ceci pourrait s'expliquer par la très hausse temperature projetée selon le scénario du RCP 8.5 puisqu'il n'y aura pas une variation significative considérable des précipitations en considérant les deux scénari RCP 4.5 et 8.5 [10]. *Selon la méthode de perte SMA, les performances de HBV et de HEC-HMS sont respectivement de 0,9 et 0,94 en calage avec 0,9 et 0,92 en validation. En calage, la valeur KGE de ModHyPMA est de 0,86 en calage et 0,78 en validation. Les valeurs de PBias sont respectivement en calage et en validation 5,8 et 4,9 pour HBV; 2,1 et 1,9 pour HEC-HMS mais 3,8 et -10,6 pour ModHyPMA. Les valeurs de MAE est respectivement en calage et en validation 41,88 m^3/s et 59,74 m^3/s pour HBV; 41.39 m^3/s et 58.03 m^3/s pour HEC-HMS mais 54.86 m^3/s et 77.28 m^3/s pour ModHyPMA. En comparant les performances de ces trois modèles, HEC-HMS s'est révélé être le meilleur suivi de HBV. En outre, le processus de couplage par l'approche de la moyenne d'ensemble montre la haute performance du couple HBV/HEC-HMS. La même performance est observée sur les débits de pointe du fleuve Ouémé à l'exutoire de Bonou. La faible performance de ModHyPMA est probablement due au manque de composantes de stockage auxquelles HEC-HMS et HBV sont en effet sensibles. Par contre, la prise en compte de la dynamique stockastique des évenements hydrologiques telle que prévue par le modèle ModHyPMA basé sur le principe de moindre action offrirait l'avantage d'être plus propice à la modélisation des phénomenes aléatoires comme les crues, si les pics étaient mieux simuler.l'utilisation de la forme distribuée de ModHyPMA pourrait améliorer les résultats. Par ailleurs, en tenant compte du principe de l'équi-finalité développé par Beven* [11], *ModHyPMA se révèlerait le meilleur puisqu'il ne dispose que de deux paramètres.*

Le modèle hydrodynamique mis en place a été calé et validé aux stations de Bonou et de So-Ava. En effet, les valeurs de KGE en calage et en validation, sont respectivement 0.96 et 0.95 à la station de Bonou tandis qu'elles sont de 0.92 et 0.94 à la station de So-Ava. Sur le base de l'efficience dudit modèle, la reconstruction des données manquantes de 2016 à la station de Bonou a été faite en tenant compte des données des stations de Hêtin-Sota, Adjohoun et So-Ava. Ainsi, les interralations entre ces diverses stations sont établies afin que juste à partir de la connaissance des données à l'une de ces stations, celles des autres puissent être reconstituées. Le scénario de construction des barrages structurants montre une réduction du débit de pointe à Bonou d'environ 454 m^3/s. De plus, la réduction des débits sera accentuée compte tenu des effets des changements climatiques. Les incertitudes obtenues lors des diverses modélisations sont essentiellement dues à la qualité des données d'entrées. En efftet, le delta de l'Ouémé reste une région encore mal connue vue l'importance du manque de données malgré les recents efforts entrepris.

Conclusion

Le présent travail décrit l'état climatique actuel du delta de l'Ouémé qui montre une tendance à l'accroissement des évènements climatiques extrêmes. De même, une augmentation des températures est remarquée. De plus, sous l'effet des changements climatiques, les débits de l'Ouémé à Bonou sont prévus pour dimunuer à l'horizon 2050. Par ailleurs, une étude comparative des modèles hydrologiques nous a permis de comfirmer le modèle HEC-HMS comme le plus éfficace à modéliser non seulement les débits journaliers en général mais également les débits de pointe de l'Ouémé à l'exutoire de Bonou en particulier. Enfin, le modèle hydrodynamique établi a prouvé son éfficacité à simuler la propagation des crues du delta de l'Ouémé. Il a donc été utilisé pour reconstituter les débits de l'Ouémé en 2016 de même qu'en 2018 et comparé avec les sorties du modèle hydrologique. Il en ressort que les modèles hydrologiques et hydrodynamique developpés dans cette étude sont efficaces. En outre, une diminution des débits pourrait survenir sous l'effet combiné des changements climatiques et des aménagements prévus. Bien qu'il subsiste des incertitudes liées à ces diverses modélisations entreprises, le présent travail à le mérite d'automatiser la propagation des crues dans le delta et ainsi d'informer sur la distribution des niveaux d'eau et débits au point de grille du delta de l'Ouémé. Ceci représente en effet une grande contribution à la compréhension du fonctionnement du delta et pourrait servir au système d'alerte précoce dans la delta de l'Ouémé.

Table of contents

Dedication i
Acknowledgment ii
Abstract iv
Synthesis v
Table of contents 1
List of Acronyms and Abbreviations 5
List of figures 6
List of tables 9
List of photos 11
Chapter 1: General introduction 12
1.1. Contexte and problem statement 12
1.2. Literature review 15
1.2.1. Climate change impacts on extremes 15
1.2.2. Regional climate model bias correction in Ouémé catchment in Bénin 17
1.2.3. Hydrological modeling 18
1.2.4. Hydrodynamic modeling and flood mapping in Ouémé Delta 21
1.3. Research questions 22
1.4. Thesis objectives 23
1.4.1. Main objective 23
1.4.2. Specific objectives 23
1.5. Hypothesis 23
1.6. Novelty 23
1.7. Scope of the thesis 24
1.8. Expected results and benefits 24
1.9. Outline of the thesis 25
Chapter 2: Study area 26
2.1. Localization 26
2.2. Relief 28
2.3. Vegetation 28
2.4. Climate 28
2.4.1. Rainfall 28

2.4.2. Temperature 29
2.4.3. Relative Humidity 30
2.4.4. Pan evaporation 30
2.4.5. Wind speed 31
2.5. Hydrography 31
2.6. Soil, land use and cover 33
2.6.1. Soil 33
2.6.2. Land use and cover 34
2.7. Demography 35
2.8. Partial conclusion 37
Chapter 3: Data, materials and methods 38
3.1. Data 38
3.1.1. Data for analysis of current climatic and hydro-meteorological state of Ouémé Delta 38
3.1.2. Data for assessment of climate change impact on Ouémé River discharge as well as peak flow simulation at Bonou outlet at 2050 horizon, under anthropogenic degradation 40
3.1.3. Data for assessment of climate change impacts on hydrodynamic and flood event in Ouémé Delta 41
3.1.4. Ouémé Delta land use and flood event mapping 44
3.2. Materials 44
3.2.1. ClimPACT 44
3.2.2. CMhyd 45
3.2.3. Hydrological models 46
3.2.4. HEC-RAS 48
3.3. Methods 49
3.3.1. Analysis of current climatic and hydro-meteorological state of Ouémé Delta 49
3.3.2. Assessing climate change impact on Ouémé River discharge at Bonou outlet at 2050 horizon, under anthropogenic degradation 52
3.3.3. Model comparison and ensemble model approach 60
3.3.4. Land cover and flood mapping 61
3.3.5. Climate change impacts on Ouémé Delta hydrodynamic 63
3.4. Partial conclusion 67

Chapter 4: Change in Climate Extremes and Pan Evaporation Influencing Factors over Ouémé Delta in Bénin 69
4.1. Rainfall trend analysis 69
4.1.1 Trend analysis in annual precipitation 69
4.1.2. Trend Analysis in Monthly Maximum Precipitation 74
4.1. Trend Analysis in Temperature, Relative Humidity, Pan Evaporation, Sunshine Duration and Wind Speed at 10m Altitude 78
4.2. Ouémé Delta Climate Drivers 82
4.3. Discussions 83
4.4. Partial conclusion 85
Chapter 5: Impact of climate change on Ouémé river discharge 87
5.1 Regional climate model bias correction 87
5.1.1 Rainfall 87
5.1.2. Temperature 90
5.2. Runoff modeling with HEC-HMS using the curve number 91
5.2.1. Model calibration 91
5.2.2. Hydrological model performance 93
5.2.3. Comparison of observation and simulation flow duration curve 95
5.3. Climate change impacts 95
5.4. Discussions 98
5.5. Partial conclusion 98
Chapter 6: Ensemble model approach on peak flow simulation in Ouémé catchment at Bonou outlet in Benin 100
6.1. One by one model performance 100
6.2. Model sensitivity analysis 101
6.3. Ensemble model performance 103
6.4. Quantile curve method 105
6.5. Peak flow comparison 106
6.6. Discussion 106
6.7. Partial conclusion 107
Chapter 7: Flood mapping in Ouémé Delta 109
7.1. Natural color composition of Sentinel1A 109
7.2. Classes differentiation 110
7.3. Built up mapping on Nokoué Lake and Porto-Novo lagoon 112

7.4. Flood mapping in 2018 112
7.5. Discussions 115
7.6. Partial conclusion 116
Chapter 8: Hydrodynamic functioning of Ouémé Delta under climate change and dam construction scenario impacts 117
8.1. Extreme events characterization 117
8.2. Hydrodynamic model calibration and validation 119
8.3. Reconstruction of Ouémé River discharge at Bonou outlet in 2016 and Assessment of the hydrodynamic and hydrological models robustness in 2016 and 2018 124
8.3.1. Reconstruction of Ouémé River discharge at Bonou outlet in 2016 124
8.3.2. Propagation results of the reconstructed discharge at Bonou in 2016 124
8.4. Assessment of the hydrodynamic and hydrological models robustness in 2016 and 2018 126
8.4.1. Assessment of the hydrodynamic and hydrological models robustness in 2016 126
8.4.2. Assessment of the hydrodynamic and hydrological model combination robustness in 2018 126
8.5. Ouémé Delta hydrodynamic functionning 129
8.6. Dam construction scenario and climate change impacts on Ouémé Delta hydrodynamic 133
8.7. Early warning system improvement in Ouémé Delta 135
8.8. Discussions 136
8.9. Partial conclusion 137
Chapter 9: General conclusion and perspectives 138
9.1. Conclusion 138
9.2. Perspectives 141
References 142
Annexes 155
List of published papers 155
List of co-authors published papers 155

List of Acronyms and Abbreviations

DGEau: Direction General de l'Eau

IRHOB: Institut de Recherche Halieutique et océanographique du Bénin

HEC-HMS: Hydrologic Engineering Center's Hydrological Modeling System

HEC-RAS: Hydrologic Engineering Center's River Analysis System

HBV: Hydrologiska Byråns Vattenbalansavdelning

HyMoLAP: Hydrological Model based on the Least Action Principle

ModHyPMA: Modèle Hydrologique base sur le Principe de Moindre Action

SWAT: Soil and Water Assessment Tool

CORDEX: Coordinated Regional Climate Downscaling Experiment

IPCC: Intergovernmental Panel on Climate Change

RGPH: Recensement Général de la Population et de l'Habitat

NASA: National Aeronautics and Space Administration

SMA: Soil Moisture Accounting Method

CN: Curve Number

KGE: Kling-Gupta Efficiency

MAE: Mean absolute Error

PBias: Percentage of Bias

List of figures

Figure 1. Situation géographique du complexe bassin-delta de l'Ouémé. vii
Figure 2. Ouémé catchment and Delta complex geographical position. 26
Figure 3. Ouémé Delta geographical position. 27
Figure 4. Monthly mean rainfall in Ouémé Delta from 1971 to 2016. 29
Figure 5. Daily (a) and monthly mean (b) temperature variation in Ouémé Delta. 29
Figure 6. Daily (a) and monthly mean (b) relative humidity variation. 30
Figure 7. Daily (a) and monthly mean (b) pan evaporation variation. 30
Figure 8. Daily (a) and monthly mean (b) wind speed variation. 31
Figure 9. Ouémé Delta hydrography 32
Figure 10. Ouémé delta complex soil types (a) and textures (b) 33
Figure 11. Land use and cover change from the years 1975, 2000 and 2013. 34
Figure 12. Ouémé Delta population effectif variation. 35
Figure 13. Ouémé Delta municipalities' population density variation from 1979 to 2013. 36
Figure 14. Ouémé Delta municipalities' population growth variation from 1979 to 2013. 36
Figure 15. Bed and lowest bank elevation in Ouémé River (a) and (b), as well as Bed and lowest bank elevation in Sô River (c) and (d). 43
Figure 16. Bias correction framework. 46
Figure 17. HBV model components structure. 47
Figure 18. Schema of rainfall runoff modeling in HEC-HMS. 47
Figure 19. HyMoLAP model components structure. 48
Figure 20. HEC-RAS model components. 48
Figure 21: Trend analysis process sketch. 49
Figure 22. Structure of HEC-HMS (a) and HBV (b). 57
Figure 23. HyMoLAP structure. 59
Figure 24. Image processing diagram. 62
Figure 25. Hydrodynamic model calibration. 66
Figure 26. Plot of Annual total precipitation (PRCPTOT), R10mm, R20mm trend, and consecutive wet day (CWD) over Ouémé Delta. 71
Figure 27. Plot of Simple daily intensity index (SDII), very wet day (R95pTOT), and extremely wet days (R99pTOT) trend over Ouémé Delta. 72

Figure 28. Plot of the percentage of pan evaporation variance hold in each of its explanatory variables. 83
Figure 29. Comparison of raw and bias corrected rainfall with observation at seasonal scale over the historical period 1971 – 2005 87
Figure 30. Comparison of raw and bias corrected rainfall with observation at daily scale over the historical period 1971 – 2005 89
Figure 31. Comparison of raw and bias corrected temperature with observation at seasonal scale over the historical period 1971 – 2005 90
Figure 32. Model parameter sensitivity. 92
Figure 33. Model parameter elasticity ratio. 92
Figure 34. Hydrological model calibration from 1971 - 1990 (a) and validation over 1991 - 2010 (b) graph. 94
Figure 35. Flow duration curve of daily observed and simulated discharge in calibration over 1971 – 1990 (a) and validation over 1991 - 2010 (b). 95
Figure 36. Change in annual rainfall (a), temperature (b), potential evapotranspiration (c) and peak flow (d) from observation to projection based on the RCP 4.5 and RCP 8.5 over the period 1971 – 2050. 96
Figure 37. Flow duration curve comparison between observation, RCP 4.5 and RCP 8.5 discharge. 97
Figure 38. One by one model calibration and validation. 101
Figure 39. Sensitivity analysis of HEC-HMS and HBV 102
Figure 40. Ensemble models simulation. 104
Figure 41. one by one model calibration (a) and validation (b) as well as ensemble model calibration (c) and validation (d) 105
Figure 42. Visual comparison of Sentinel 2A (a) and Sentinel 1A (b) images. 109
Figure 43. Comparison between natural color composition and ESA land use and cover map 111
Figure 44. Acadja and built up map over Nokoué Lake and Porto-Novo lagoon on December 2018. 112
Figure 45. Ouémé Delta flood mapping results from September to November 2018. 113
Figure 46. Water extent during 2018 Ouémé Delta flood event. 114
Figure 47. GPM rainfall over Ouémé Delta 115
Figure 48. Flow duration curve over the period 1971 – 2010. 118
Figure 49. Water level duration curve over the period 1971 – 2010. 118

Figure 50. Plot of discharge in relation with water level from 1971 – 2010. 119
Figure 51. Calibration and validation of Ouémé River discharge at Bonou station and water level at So-Ava station. 121
Figure 52. Comparison between October 18, 2010 satellite image (a) and simulated flood map (b). 122
Figure 53. Calibrated Mannings number regions relatively to land cover types over Ouémé Delta 123
Figure 54. Relationship between Bonou and Adjohoun water level. 124
Figure 55. Bonou water level reconstructed (a), So-Ava validation (b), Hêtin-Sota validation (c) and Adjohoun validation (d) in the year 2016. 125
Figure 56. Comparison between simulated discharge from the hydrodynamic and hydrological model in 2016. 126
Figure 57. Water level reconstruction at Bonou, Adjohoun, Hêtin-Sota and Nokoué Lake station in 2018. 128
Figure 58. Tidal effect extent in Ouémé Delta. 130
Figure 59. Tide influence on water level So and Hêtin (a) and Bonou and Adjohoun (b). ... 130
Figure 60. Water level station positions (a) and water level at each station (b). 131
Figure 61. water level relationship between various stations 132
Figure 62. Daily discharge scenario in the case of dam construction. 133
Figure 63. Ouémé Delta flood map before (a) and after (b) dam construction scenario with the scale in meters. 134
Figure 64. Early warning system improvement in Ouémé Delta. 136

List of tables

Table 1.Characteristics comparison between SWAT and HEC-HMS. 20
Table 2. Percentage of change in land use and land cover within 1975 – 2000 and 2000 – 2013. 34
Table 3. Summary of available stations over Ouémé Delta with latitude and longitude. 38
Table 4 : Indices of Expert Team on Climate Risk and Sector-specific Indices (ET CRSCI) core indices where TN = minimum temperature and TX = maximum temperature, p = daily precipitation, and prcp = annual total precipitation [98]. 39
Table 5. Rain gauges and synoptic stations geographical position details. 40
Table 6. Details of the regional climate models used. 41
Table 7. List of data used for the hydrodynamic model. 42
Table 8. Sentinel 1A and 2 A data collected. 44
Table 9. Model performance criteria. 53
Table 10. Hydrological modeling processing. 54
Table 11. Hydrodynamic model simulation periods. 65
Table 12. Annual rainfall intensity indices trends. 70
Table 13. Significant trend results of annual rainfall frequency indices. 71
Table 14. Annual rainfall intensity indices with no trend. 73
Table 15. Annual consecutive dry day (CDD), very wet day (R95p), and extremely wet day (R99p) indices trend with no trend 73
Table 16. Monthly trend analysis of one-day precipitation amount (RX1day) and two-day precipitation amount (RX2day) during high water. 75
Table 17. Monthly trend analysis of three-day precipitation amount (RX3day) and five-day precipitation amount (RX5day) during high water. 76
Table 18. Monthly trend analysis of ten-day precipitation amount (RX10day) during high water. 77
Table 19. Temperature based indices trend. 79
Table 20. Maxima relative humidity based on annual minimum, maximum, and mean. 79
Table 21. Wind speed at 10 m altitude based on annual minimum, maximum, and mean 79
Table 22. Monthly and annual significant trend for sunshine and pan evaporation. 81
Table 23. Correlation coefficient of pan evaporation with mean relative humidity (RH), maximal relative humidity (Hmax), minimal relative humidity (Hmin), minimal temperature

(Tmin), maximal temperature (Tmax), mean temperature (Tmean), wind speed at 10 m altitude (WIND), precipitation (PRCP), and sunshine duration (SUND). 82
Table 24. Stepwise regression coefficient of pan evaporation and relative humidity (RH), mean temperature (Tmean), wind speed at 10 m altitude (WIND), precipitation (PRCP), and sunshine duration (SUND). 83
Table 25. Bias correction efficiency at seasonal scale 88
Table 26. Bias correction efficiency at daily scale 89
Table 27. Efficiency of temperature bias correction 91
Table 28. Optimized model parameters 91
Table 29. Results of Monte Carlo Analysis with 500 Trials. 93
Table 30. Trend in annual rainfall, discharge, temperature and potential evapotranspiration. 97
Table 31. One by one model calibration and validation performance. 100
Table 32. Ensemble models calibration and validation performance 103
Table 33. Peak flow trend statistics. 106
Table 34. Model performance over peak flow. 106
Table 35 . Extreme event corresponding to the return period 5, 20, 50 and 100. 117
Table 36. Efficiency coefficient of model calibration and validation results. 120
Table 37. Calibrated Manning's numbers with actual region and chow description 123
Table 38. Data reconstruction efficiency in 2016. 125
Table 39. Data reconstruction efficiency in 2018. 127
Table 40. Annual volume of water corresponding to each discharge scenario 133

List of photos

Photo 1. Tomato field (at left), school (in a middle) and houses (in the right) flooded during 2018 flood event in Ouémé Delta (source: Rita HOUNGUE). 13
Photo 2. Agriculture field (at left) and fishing devices (in the right) (Source: Rita HOUNGUE) 14
Photo 3. Fuel transport (at left) and sand extraction (in the right) (Source: Rita HOUNGUE) 14

Chapter 1: General introduction

This chapter presents the context and problem statement in section 1.1 In addition, literature review is detailed in Section 1.2 relatively to climate change impacts on extremes, regional climate model bias correction in Ouémé catchment, hydrological modeling approach and hydrodynamic modeling in Ouémé Delta. Moreover, Section 1.3 provides research questions whereas Section 1.4 presented the thesis main and specific objectives. Furthermore, the hypothesis, novelty, scope, expected results and benefits as well as the outline of the thesis are provided respectively in Section 1.4, 1.5, 1.6, 1.7, 1.8 and 1.9.

1.1. Contexte and problem statement

The global climate system is suffering from considerable modification which are amplified by natural and anthropogenic factors not only at regional scale but also local [12]. Thus, West Africa and Benin are experiencing climate variability. Analysis of the impacts of these erratic climate evolutions shows clearly harmful sequences for sustainable development. Most impacted sectors by climate change are water resources, energy, coastal zone, health, agriculture and forestry [13]. Indeed, it is noticed in Southern parts of Benin, exacerbation of extremes phenomena as predicted by the Intergovernmental panel on Climate Change (IPCC) in their 5^{th} report. As consequences, deficit and shortness of the second rainy season (in the case of bimodal rainy regime) on one hand and erratic increase of rain leading to flood on other hand are observed [14].

Urban flood is a prominent issue, not only at local scale but also at global level. In 2008, over half of the world's population was living in urban conglomerations, many of which are situated at locations where large river systems meet the ocean, called Deltas. Hence these megacities in delta areas are quite naturally exposed to flood events coming from either direction: inland or ocean [1]. Flooding in urban areas often causes huge economic damage as most of the structural developments and activities take place in cities. It is common knowledge that the poor tend to suffer most from floods. In addition to loss of life and structural damages, flooding often creates non-point source pollution when toxic substances, sediment, nutrients, pathogens and garbage are washed away into the water bodies, deteriorating the water quality [15].

In fact, in 2010, flood disaster in Benin affected more than 680,000 people and caused the death of 46 people. 55 out of 77 municipalities were affected. More than 50,000 houses

were destroyed and 150,000 people were left without shelter. In addition, 278 schools were flooded, 128,000 hectares of crops and farmland were ruined, and an estimated 12,000 metric tons of food stocks were lost due to destroyed storage facilities. The overall damages and losses were estimated to more than 46,847,399 US dollars [16]. Flooded tomato field, school and houses photos snapped during 2018 flood event are illustrated on Photo 1.

Photo 1. Tomato field (at left), school (in a middle) and houses (in the right) flooded during 2018 flood event in Ouémé Delta (source: Rita HOUNGUE).

Unfortunately, the disaster will increase because of climate change effects [17]. Hence, these delta cities around the world become even more vulnerable to disasters, especially in developing countries. Due to limited adaptation measures in developing countries like Benin, surface water needs to be well managed especially in wetlands like Ouémé Delta to avoid sudden shrunk as in Chad Lake. Climate change scenarios predicted by the IPCC identify tropical regions as the most vulnerable areas due to increased probabilities of the occurrence of disasters [18]. So the occurrence of floods cannot be ignored or denied especially fluvial flood in tropical coastal regions. The primary focus should be on identifying probable measures to develop Integrated River Management in order to preserve the resources from sudden disappearance for their sustainability. It is necessary to analyze and apply the latest scientific tools in data acquisition and management, combination of hydrological and hydrodynamic modeling, data assimilation and improved forecasting capabilities as well as geographical information system to deal with this issue. So handling this problem means good knowledge of the river system in order to apply these tools efficiently especially in complex areas like Deltas.

The Ouémé Delta which is situated in the southern Benin with Nokoué Lake as buffer zone, used to aggravate flood event in Cotonou city every year. In fact, Cotonou is the most populous town in Benin which population is still increasing. This causes a heavy pressure on land use, water resource management and supply. Moreover, many anthropogenic activities

are going on Delta such as agriculture, fishing, sand extraction and trade exchanges (Photo 2 and 3).

Photo 2. Agriculture field (at left) and fishing devices (in the right) (Source: Rita HOUNGUE)

Photo 3. Fuel transport (at left) and sand extraction (in the right) (Source: Rita HOUNGUE)

Moreover, some gutters' outlets in Cotonou are directed to Nokoué Lake the biggest of the country; which causes pollution and contamination in addition to everyday waste discharge from the regional Dantopka market. Apart from that, Ouémé Delta is under marine water pressure because of its contact with the Atlantic Ocean.

These entire reasons make complex the understanding of Ouémé Delta hydrodynamic functioning, which is the most important characteristic in conceiving an efficient management plan for resources sustainability. Therefore, this work focuses on the: **Hydrodynamic functioning of Ouémé Delta under climate change impacts.**

Benin is a West African country which receives in average 1200 mm annual rainfall. In addition, it holds a lot of rivers and water ponds among which is the Ouémé River which length is about 510 km with a trans-boundary catchment of about 50 000 km^2. Moreover, in the downstream of the Ouémé River catchment, lies the Ouémé Delta of about 5000 km^2 which is rich of nutrient for agriculture. Furthermore, Ouémé Delta hosts Nokoué Lake which is the biggest in Benin as well as Sô and Ouémé Rivers. However, the country still suffers

from agriculture products shortage especially in dry period. Thus, garden products are mostly imported in that period from Burkina Faso and Niger that are Sahelian countries as well as Nigeria. These last years, there was a great interest in developing dam construction project along some rivers in Benin. One of the prioritized one is Dogo Bis dam that is planned to be built not far from the entrance of Ouémé Delta [19].

Moreover, the issue of data availability remains an obstacle in modeling the hydrodynamic of a complex area like Ouémé Delta for its sustainable management. Therefore, there is a need to find simple process for generating accurate information based on limited data. In order to model hydrodynamic functioning of Ouémé Delta under climate change impacts the following steps are proposed. First of all, current climate state of Ouémé Delta should be known. In addition, climate change impacts on Ouémé River discharge under emission scenarios as well as land use and cover change conditions should be addressed. Moreover, effects of projected hydraulic infrastructures on Ouémé Delta hydrodynamic should be assessed.

1.2. Literature review

1.2.1. Climate change impacts on extremes

Quantifying impacts of changes in climate variables over natural resources in a given region is important at area level where micro climate variability and impacts on daily life are significant. For instance, in the process of developing adequate water resources management plan, this is important in order to cater for everyday demand and supply of users, especially in developing countries where the economy is mainly based on rainfed agriculture [20].

In West Africa, there was a drier period during 1970s and 1980s whereas a gradual return to wetter condition was observed since the 1990s especially in Sahelian and Soudanian areas [21]. However, there are contrasting trends throughout seasonal variations of rainfall. Such situation is reported since early 2000s across Algeria and Tunisia and from 2008 in Morocco by Nouaceur et al. [22]. Nevertheless, extreme rainfall is declining in Cote d'Ivoire [23] and annual precipitation tends to reduce in Nigeria [24]. No significant trends were detected in Ghana [25]. In Bénin, annual total precipitation, annual number of wet days and maximum 30 days rainfall present a significant decreasing trend [26]. Interpolated change in heavy rainfall of different return periods revealed an east-west gradient from negative to positive along the lower Ouémé basin, whereas from the middle to the upper Ouémé, a

decreasing tendency of heavy rainfall is dominant [27]. In the upper Ouémé basin, Attogouinon et al. [28] noticed the absence of clear cumulative annual rainfall trend over the period 1951–2014. However, when considering the entire Ouémé Basin, N'Tcha M'Po et al. [29] reported significant decline in the number of heavy and very heavy rainfall days, heavy, and extremely heavy rainfall, consecutive wet days and annual wet-day rainfall total from 1950 to 2014, confirming that trend in rainfall depends on spatial scale as reported by Lawin et al. [30].

Thus, extreme events like flood threaten humid zone like Deltas [1]. Then, knowledge about hydro-climatologic trends of relatively small area like Ouémé Delta is of great interest, since Deltas are food basket of countries [31]. They are of extremely fertile soils for agriculture and provide easy access to fishery [1]. Even though Deltas were usually subjected to flood as humid area, extreme climatic risks are expected to increase because of climate variability and changes [32]. Over West Africa, the Coupled Model Intercomparaison Project Phase 5 (CMIP5) showed an increase in heavy rainfall by the end of 21st century [33]. Furthermore, regional climate models projected increasing number of extreme rainfall in the period of May and July [34]. Observed minimum air temperature increased more rapidly than maximum temperatures [35]. This results in narrow difference between maxima and minima air temperature known as diurnal temperature over most parts of Africa [36]. Near surface temperature has increased by 0.5 °C or more during the last 50 to 100 years [37]. In West Africa, significant increase in temperature is also shown over the period 1961 to 2000 using indices that were developed by the Expert Team on Climate Change Detection and Indices (ETCCDI) [38].

Trends in other climatic variables, like sunshine, wind speed, and relative humidity are less explored. However, a lot of works on trend in pan evaporation have been done in diverse climate regions. Results showed that both decreasing and increasing trends that are observed, coexist [39]. Decrease in pan evaporation under a warming climate is known as the pan evaporation paradox because of the contradiction to common expectation. This phenomenon can either be explained by an increase in cloudiness and aerosol concentrations, which results in a decrease in solar radiation received on Earth's surface; or, an increase in terrestrial evaporation that cools down the air over the pan and reduces the evaporation from that pan [40]. However, an increase in pan evaporation is mostly due to an increase in temperature. In Africa, such phenomenon has been less mentioned probably because of limited data according to Oguntunde et al. [40]. These authors showed that pan evaporation, sunshine, and wind

speed decrease significantly highly (P <0.001), whereas rainfall, minima temperature, and relative humidity showed insignificant increasing trends in Nigeria over the period 1973–2008. Recently, Djaman et al. [41] detected an increasing trend in pan evaporation at Lomé, Tabligbo, and Sokodé, but a decreasing trend at Atakpamé in Togo over the period 1976–2011.

Pan evaporation is basically used to measure evaporation from free water surface [42]. In Australia, it is shown that surface water losses of around 40% of their storage are due to evaporation [43]. In West Africa, river discharge is projected to decrease about 50% by the end of 21st century [44,45]. There is a consensus that climate change impacts are projected to hit more developing countries due to their fragility in terms of adaptation and mitigation capacity [46]. Consequently, primary sectors that are basis of these countries' economy are threatened. Water resources are key element for every development sector, but they are under pressure in Wetlands like Deltas [15]. Moreover, Deltas are likely to face extreme events due to population growth, anthropogenic activities, urbanization, and climate variability [1,18]. However, trend in climate variables over Ouémé Delta is not yet well known.

1.2.2. Regional climate model bias correction in Ouémé catchment in Bénin

Water resources are impacted by climate change with consequences on anthropogenic activities and ecosystems [12,47]. In semi-arid regions, an erratic extremes precipitation is projected due to global warming. As consequences, occurrence of extreme events like flood cannot be ignored because of extreme flows propagation [8,28]. As climate change is projected to heat more developing countries that are limited in adaptation, looking for comprehension of change in hydro-climatic variables for risk and catastrophe prevention remains a goal [48]. To that end, climate models are key elements in future weather projection. They have been largely used these last decades [12,49,50]. However, climate model data hold some biases that need to be corrected before any usage. The concept is based on identifying possible biases between observed and simulated climate variables as a starting point of correcting both control and scenario of regional climate model runs. A lot of bias correction methods exist and are applied around the world [51–59]. In Benin, the correction methods such as delta change, linear scaling and quantile mapping (Empirical, Gamma) are already tested over Ouémé catchment [60–62]. Among these methods M'Po et al. [62] showed that the empirical quantile mapping was the best bias correction method over Ouémé catchment. Similarly, efficiency of this method in climate model bias correction has been

shown worldwide [55,59,63–65]. In the linear scaling method, it is just considered a linear translation coefficient for matching observed and raw data [65]. Delta change method has the disadvantage of holding a constant variance from historical to future what is not consistent since meteorological conditions are random [62,66]. However, the quantile mapping method gives the advantages of preserving the distribution of climate variables and then informs on extreme values [67]

1.2.3. Hydrological modeling

Hydrological models play a key role in predicting extreme events like drought and flood. In order to reduce uncertainties during model calibration, the approach of ensemble modelling is being developed nowadays with satisfactory results. It improves the model representation of river flow. Such method is an input to give broad perspective regarding water resources management and flood control in the context of climate change, especially in developing countries like Benin.

Ouémé River catchment at Bonou outlet with its Delta hold about half of the country's area [60]. The Delta is the buffer zone of the overall water drained before it reaches the Atlantic Ocean [68]. Consequently, Ouémé Delta is flooded every year with considerable damage and losses on agricultural productions, infrastructure and human life. Thus, peak flow modelling in Ouémé catchment remains of great interest in flood management processes. A lot of hydrological models have been applied either on the whole Ouémé catchment or on its sub-catchments [4,69–72]. It comes out that distributed models are more suitable to simulate extreme events because of their capability to integrate gridded data over catchment [73]. In addition, lumped models seem to well handle low water discharge [74]. Moreover, it is noticed that the use of an ensemble modelling approach based on both lumped and distributed models instead of the common one by one modelling method for their mutual compensation. In fact, gathering models which perform well in high water period and others good in low water, showed best fitting than taken solely [74,75]. Such approach is preferable in modelling extremes in the Ouémé catchment. Gaba et al. (2015) found that when using ensemble approach, the mean ensemble is more efficient than the median one in the surrounding of sahelian region. Therefore, the mean ensemble is the one adopted.

Among the models already experienced with good results in Ouémé sub-catchment, HBV (Hydrologiska Byråns Vattenbalansavdelning) and HEC-HMS (Hydrologic Engineering Center's Hydrological Modeling System) are two semi-distributed models that are free,

flexible and offer the advantage of simulating single and continuous events [5,74]. In addition, HyMoLAP (Hydrological Model based on the Least Action Principle) is a lumped model that can also be used as semi-distributed made of only two parameters has given good results over the catchment [4].

It has been showed that semi-distributed models are good at modeling peak flows whereas the lumped simulates best the low flows [74,75]. Consequently, to counterbalance each of these advantages offered by lumped and semi-distributed models, an ensemble approach is thus adopted. Moreover, Gaba et al. [74] found that when using GR4J, HBV and HyMoLAP, the mean ensemble is more efficient than the median one over the Mékrou basin. Thus, ensemble mean approach taking into account two semi-distributed models and one lumped that are respectively HBV, HEC-HMS and HyMoLAP is used for simulating peak flow in Ouémé catchment in Benin Republic.

Furthermore, comparison studies conducted on various components of both HEC-HMS and SWAT such as governing equations, hydrological processes, minimum data required to run the model and spatial and temporal scale concluded about the best efficiency and lightness of HEC-HMS [76,77] as summarized in Table 1. HEC-HMS is mostly used in order to account for land use and cover aspects as well as soil types that are important in model humid area like Deltas.

Table 1.Characteristics comparison between SWAT and HEC-HMS.

Hydrological components	HEC-HMS	SWAT
Hydrological process	Precipitation, Runoff Volume (loss modelling), Direct runoff (overland flow and interflow), Baseflow, Flow routing, Infiltration, Evapotranspiration, Snow accumulation and melt runoff	Runoff, weather, sediment yield, snowmelt, soil temperature, crop growth, nutrients, pesticides, agricultural management, channel and reservoir routing, water transfer
Governing equations	Precipitation (Gridded precipitation or Inverse distance squared weighting), Direct runoff (Clark's UH, Kinematic wave, Modclark, SCS UH, Snyder's UH, User specified S-graph, and User specified UH), Base flow (Bounded recession, constant monthly, Linear reservoir, and Non- linear Boussinesq recession), snow accumulation and melt (temperature index method), Evapotranspiration (Monthly average, New Priestly Tailor & Gridded Priestly-Tailor), Loss rate (Deficit & Constant rate (DC), Initial & Constant rate, Exponential, Green & Ampt, SCS-CN, Smith Parlange, and Soil moisture accounting), Canopy interception (Simple canopy or Gridded simply canopy), Flow routing (Kinematic wave, lag, Modified Puls, Muskingum, Muskingum-Cunge, Straddle stagger method)	Runoff volume (Modified SCS-Curve Number or Green and & Ampt infiltration method), Peak runoff rate (Modified rational formula or the SCS TR-55 method, Lateral sub-surface flow & percolation (Kinematic storage routine (Sloan et al., 1983), Potential evapotranspiration (Hargreaves, Priestley-Taylor and Penman-Monteith equations), Snow melt (degree-day based method), Sediment yield (Modified Universal Soil Loss Equation (MUSLE)), Water routing (Variable storage coefficient method or Muskingum routing method & Manning's equation to define flow)
Input data	DEM, Soil information, topographic data, land use, daily precipitation, and daily observed runoff data	DEM, land use/land cover, soils, daily precipitation, max. and min. temperature, solar radiation, relative humidity, wind speed, daily discharge, sediment, nutrient delivery, fertilizer and pesticides application data, point source of pollution and management practices
Simulation capabilities	Continuous and forecast	Continuous

1.2.4. Hydrodynamic modeling and flood mapping in Ouémé Delta

The estimation of flood extent through early warning is essential for disaster alleviation. In fact, Benin disposed of an early warning system that is not yet automated. Actually, the existing system was built in 2014 and financed by the United Nation Development Program (UNDP). It is based on a statistical interrelationship of water level at the 3 mains hydrometric stations that are in Ouémé river outlet at Bétérou, Savè and Bonou. Thus, once water level is known in Bétérou that of Savè and Bonou are deducted as well [78]. From this point, a color code is made using green, yellow, orange and red meaning respectively to describe normal situation, moderate, moderately high and high risk of catastrophe. In addition, based on the water level at Bonou and previous studies, previsions are made for Ouémé Delta based on the previous color code. Consequently, Ouémé Delta is respectively in yellow, orange and red situation when water level reaches 5.5 m, 7 m and 8 m at Bonou station [78]. This way, there is no detailed information about area to be flooded, during how much time and at what time in the entire Delta.

Hydrodynamic model is implemented for flow propagation in order to predict the occurrence of flood at different scales. In practice, the calibration of hydrodynamic models aims to search the best possible parameters for the representation of the natural flow propagation. During the recent decades, the calibration of hydrodynamic models was more actual and faster due to advanced earth observation products and computer based optimization techniques [79–82]. Some hydrodynamic models are HEC-RAS, MIKE 21, TUFLOW, DELFT, TELEMAC and RIVER 2D [18,83–85]. These models are all based on Saint Venant equation discretization using implicit finite volume. However, HEC-RAS offers the possibility of using diffusion wave model which mathematical description is detailed in the methodology, instead of the complete Saint Venant equation as in others [81,86–88]. This is preferable when simulating long established flood event in comparison with flash flood. As consequences, simulation time is shorter in HEC-RAS than others. In addition, HEC-RAS is an open source tool.

In order to run such models, some key data are required. Topography, land use and cover and bathymetry data are needed for the model mesh. In addition, upstream and downstream forcing data are compulsory for boundary conditions. Then, calibration data has to be used for the model calibration and validation. However, all of those data listed above has to be collected taking into account resolution aspects for the model outputs precision.

In order to validate hydrodynamic model, flood maps are needed. However, in developing countries like Benin flood records are hardly found. Thus, validation of flood map is quite difficult since there is no memory record of past events. Remote sensing is a key approach through satellite imagery analysis using recent development of technologies, for event records. In fact, combination of remote sensing to hydrodynamic modeling makes valuable inputs in flood management process[89,90]. The use of SAR (Synthetic Aperture Radar) data offers a lot of applications not only in land and water resources management but also in flood monitoring [81,89,91–93]. The European Space Agency (ESA) Earth Observation Missions are made of ten recent missions from October 2013 which are Aeolus, Sentinel5P, Sentinel3, Sentinel2, Sentinel1, Swarm, ProbaV, CryoSat, SMOS and GOCE. Before these 10 missions, there were three missions such as Envisat, Proba1 and ERS missions which data series ended in 2012. More details are found at the following link: https://sentinel.esa.int/web/sentinel/missions. Each mission is designed for specific objectives. For instance, Sentinel2 objectives are land, vegetation, soil and coastal areas monitoring which is composed of two polar-orbiting satellites based on high-resolution optical imagery. Sentinel1 objectives are land and Ocean monitoring, and composed of two polar-orbiting satellites (A and B) operating day and night based on Radar imagery. Sentinel1 was launched in April 2014 whereas Sentinel2 in June 2015. These data are all available and free of charge on the ESA Copernicus platform. Sentinel1 data are free images available almost everywhere in the globe with 12 days frequency in Africa with a shifting of six days between the constellation satellite A and B. Therefore, considering the both, image frequency is days instead of 12 days. Unfortunately, the available Sentinel1B scene does not cover the entire Ouémé Delta. Thus only Sentinel1A is the one used in this work. Moreover, the heaviness of the scene makes difficult the download especially in developing countries. Therefore there is a need to look for simple approach like color composition for visualizing flood extent instead of downloading the image for classification process. Visio terra platform is found to be an easy, simple and free tool to that end with no download. In fact, on this platform, images are stored with preprocessing and processing availability.

1.3. Research questions

This research work is based on the following research questions:

- What is the current trend in climatic patterns in Ouémé Delta?
- What will be the future variability and trend of Ouémé River discharge till 2050?

- How can flood events be simply mapped in Ouémé Delta?
- How will Ouémé Delta hydrodynamic be influenced under the effects of climate change and hydraulic infrastructure projects?

1.4. Thesis objectives

1.4.1. Main objective

The general objective of this work is to quantify impacts of climate change on hydrodynamic functioning of Ouémé Delta in Benin.

1.4.2. Specific objectives

Specifically, this work aims to:

- assess current trend of extreme event in Ouémé Delta;
- quantify impact of climate change on Ouémé River discharge at Bonou outlet from 1971 to 2050 and improve Ouémé River peak flow simulation;
- design simple flood mapping process for Ouémé Delta;
- model Ouémé Delta hydrodynamic under climate change effect and dam construction scenario.

1.5. Hypothesis

Hypothesis that underlie this work are as followed:

- Extreme events tend to increase due to climate variability in Ouémé Delta.
- Ouémé River discharge will decrease under climate change effects at 2050 horizon.
- Early warning system in Ouémé Delta could be improved using combination of remote sensing, hydrologic and hydrodynamic tools.
- Dam construction on Ouémé catchment could drastically reduce discharge at Bonou outlet.

1.6. Novelty

Spatial averaged data using kriging method in Ouémé catchment is made available for future use. The efficiency of HEC-HMS model over Ouémé catchment hereby proved has not been done before. Furthermore, the mapping methodology exposed here based on Sentinel 1A data was not experienced before. Ouémé delta hydrodynamic model set up using HEC-RAS is

a new tool ever developed in Ouémé Delta. Since, the model informs on water level and flow at any point in the Delta, rating curve could then be updated.

1.7. Scope of the thesis

This work focuses on describing the current state of climate extremes especially flood in Ouémé Delta, quantifying climate change impacts on Ouémé River discharge at Bonou outlet as well as modeling Ouémé Delta hydrodynamic functioning. To this end, multiple hydrological models were run for ensemble model approach in order to simulate daily and peak discharge of Ouémé catchment at Bonou outlet. This discharge data represents the upstream forcing of the Ouémé Delta hydrodynamic model.

The hydrological modeling run hereby takes into account 2 kilometers resolution land use and land cover map using HEC-HMS with satisfactory results. However, future work should look for more details land use and cover map in order to reduce uncertainties at smaller scale. Moreover, the hydrodynamic model HEC-RAS applied also exhibits good results and gives inputs to improvements of the existing early warning system in Ouémé Delta. As the current model is based on 30 meters resolution digital elevation model, a perspective is the use of smaller resolution for more accuracy.

1.8. Expected results and benefits

The main result expected is an accurate hydrodynamic model for Ouémé Delta. It is the basis of not only an automatic early warning system settlement but also future projection of Ouémé Delta status for socio economic benefits. In fact, the knowledge of water availability and climate extremes trend in the Delta will help in sharpening more realistic resources management for sustainability. As Benin economy is rainfed agriculture based, the knowledge about current and future water resources state informs in resources availability. Such information is an input for designing climate adaptation strategies in order to reducing climate change impacts on the Ouémé Delta which the food basket of the southern Benin. Moreover, the early warning contributes to human life and infrastructures preservation against climate extremes consequences in terms of damages and losses.

1.9. Outline of the thesis

The thesis is structured as followed:

- Chapter one gives a general view of the problem followed by the state of the art about the different concepts addressed in the thesis. In addition, research question, main and specific objectives, research hypothesis and novelty, as well as thesis scope with expected results and benefits are detailed.
- Chapter two describes the study area. It contents the localization, relief, vegetation, climate, hydrography, soil, land use and demography of the study area.
- Chapter three accounts for overall data, materials and method used.
- Chapter four, five, six, seven and eight content each specific objective result.
- Chapter nine presents the general conclusion and perspectives.

Chapter 2: Study area

Chapter 2 presents the study area. Its geographic localization, relief and vegetation cover are respectively describes in Section 2.1, 2.2 and 2.3. In addition, climate, hydrography, soil and land use as well as demography of the study area are respectively presents in Section 2.4, 2.5, 2.6 and 2.7.

2.1. Localization

This work is conducted over the Ouémé Delta area which is feed in water by the Ouémé catchment. Figure 2 shows the complex of Ouémé catchment and Delta where Ouémé Delta is downward in purple color. Due to the fact that the hydrologic modeling is processed over Ouémé catchment, it is also described for better understanding.

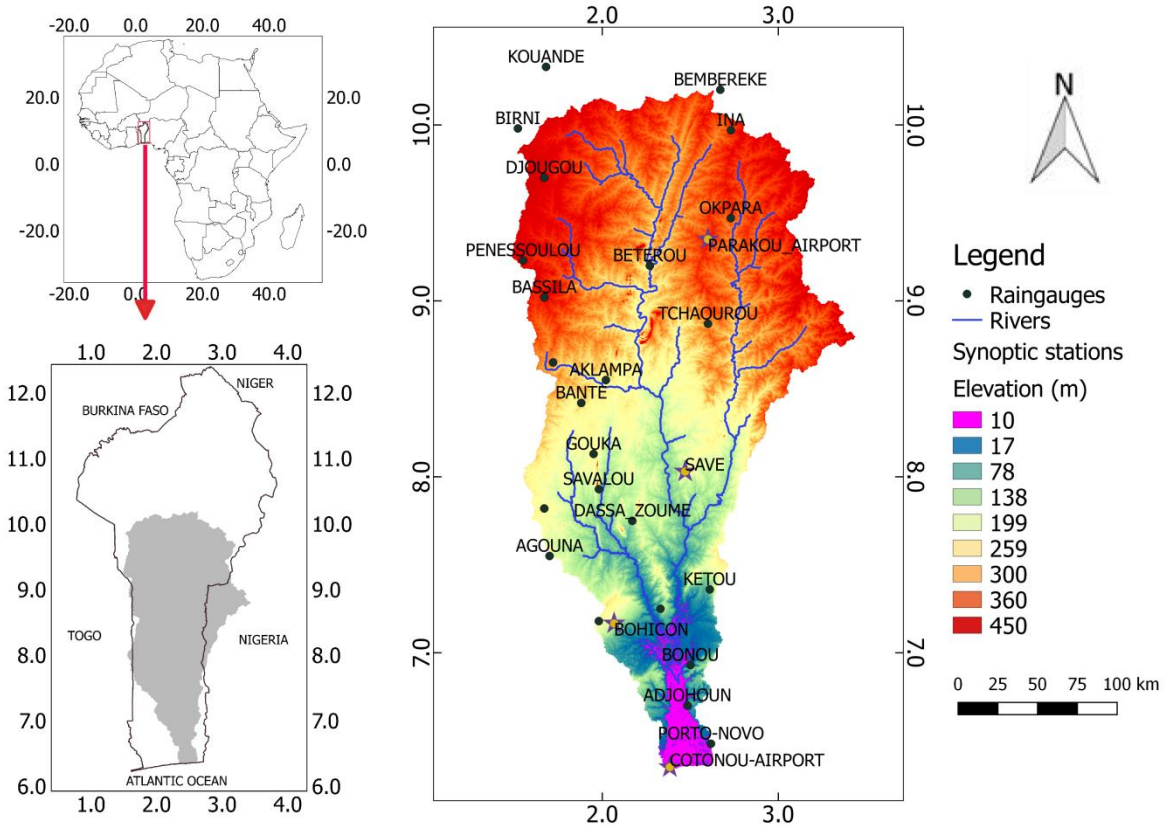

Figure 2. Ouémé catchment and Delta complex geographical position.

The Ouémé catchment and Delta complex is located between 6.3° and 10.3° latitudes, and 1.5° and 3.5° longitudes in West Africa. Benin is boarded in West by Togo, by Nigeria in the East, by Niger in the North, by Burkina Faso in Western North and Atlantic Ocean in the South.

Ouémé catchment area is about 50,000 km^2 with 0.1% of this in Togo and 8% in Nigeria [94]. It is positioned between 6.9° and 10.3° latitudes, and 1.5° and 3.5° longitudes (Figure 2). Ouémé catchment is under tropical climate with three climate zones from the subequatorial climate to sudanian climate northward. Ouémé catchment receives annually between 724 and 1396 mm rainfall [4].

Ouémé Delta actually is the depression between Benin littoral coast till Zagnanado latitude [6] with altitude varying from 0 to 15 m as shown on Figure 2. However, due to data availability, we choose to take into account here the area of the actual Delta that entrance is situated at Bonou station. Therefore the Ouémé Delta hereby considered is the depression area of 10 m altitude (Figure 2). It is positioned between 6.30° and 6.90° North and between 2.35° and 2.7° East. It covers the municipalities of Bonou, Adjohoun, Dangbo, Akpro-Missérété, Abomey-Calavi, Aguégué, Porto Novo, Sêmé Kpodji and Cotonou (Figure 3).

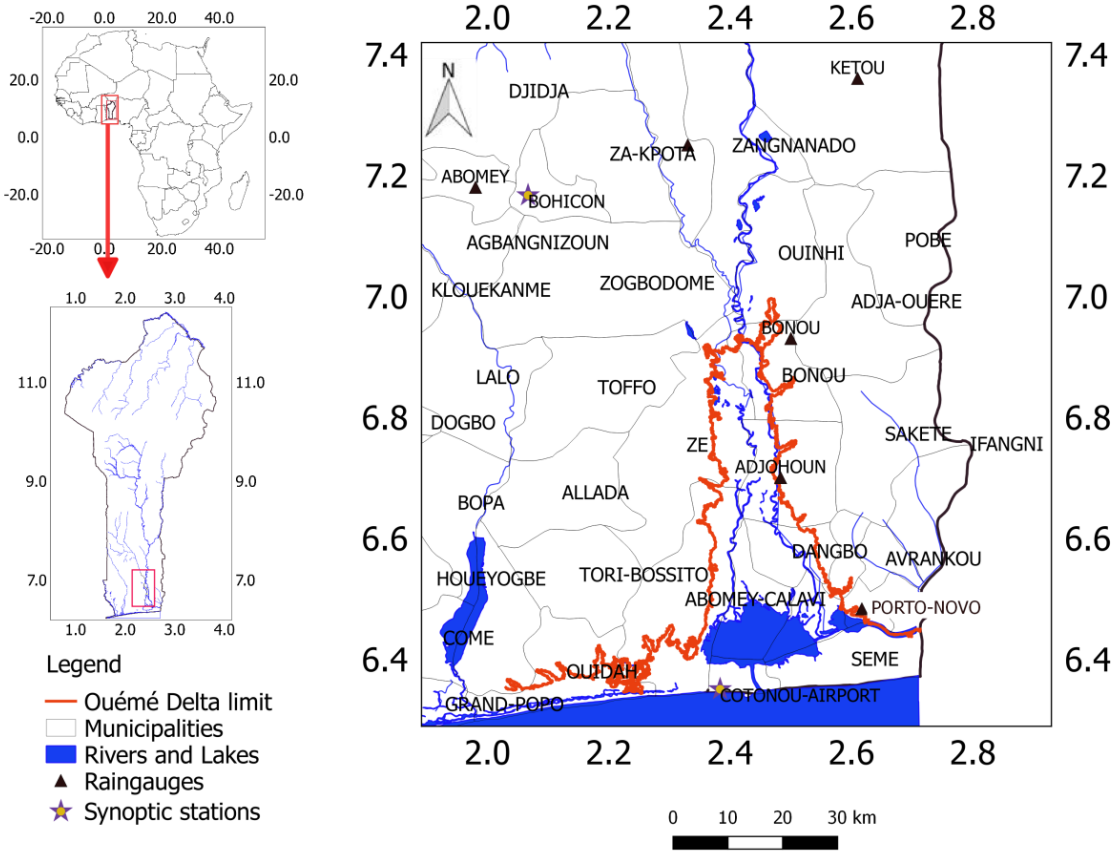

Figure 3. Ouémé Delta geographical position.

With a drainage area of about 5000 km^2 it is a very rich humid zone, that offers home to large number of ecological species [6,68]. It is an area well suited not only for agriculture

due to nutrients deposit but also for fishery and fluvial transactions. It also gives shelters to considerable number of human being who depends on these resources especially those living on Nokoué Lake as well as those along Ouémé and Sô rivers in the Delta. Nokoué Lake, the biggest in Bénin is the buffer zone of Ouémé Delta.

Nokoué Lake is positioned between 6.40° and 6.50° North and between 2.35° and 2.50° East. It is large of 20 km in East-West direction and long of 11 km from North to South [6,7,68]. It covers 150 km^2 in low water and could increase over 450 km^2 in high water [6,7,68]. It is limited in West by Abomey-Calavi's plateau, in East by Porto Novo's Lagoon, in North by the flood plain of Ouémé and So Rivers and in South by Cotonou city. Cotonou and Totchè channels connect it respectively to the Atlantic Ocean and to the Porto Novo's Lagoon [7].

2.2. Relief

Ouémé catchment is characterized by an abrupt relief where the altitude varies from more than 450 m to 30 m downward. Some mountains in the central region of Savè where the altitude is of almost 300 m are observed. In addition, there are hills in the area of Dassa-Zoumé where the altitude falls at 138 m. Ouémé Delta is made of depression area of maximum 10 m altitude. It is a flat area of alluviums that serves as floodplain of Ouémé catchment water.

2.3. Vegetation

The vegetation in Ouémé Delta is characterized by tree cover, crop lands, shrubs and grass land in the floodplain with aquatic vegetation along the rivers' banks. The tree cover is mainly made of palm oil tree, Acacia and teck. Most aquatic vegetation is located in swamps. They are mostly made of Paspalum vaginatym which root net is immerged about 1 meter deep. This type of vegetation constitutes a kind of water reservoir that gives shelters to a lot of species like fishes of calm water for instance *Heterotis niloticus*.

2.4. Climate

2.4.1. Rainfall

Because of its geographical position and the Inter-Tropical Convergence Zone circulation over Bénin, Ouémé Delta is under subequatorial climate with a bimodal rainfall

regime [6,68]. This area is characterized by two rainy seasons (April to July and September to October) and two dry seasons (November to March and the month of August) (Figure 4). Over the period 1971 – 2016, annual rainfall amount is between 719 mm and 2470 mm at station point.

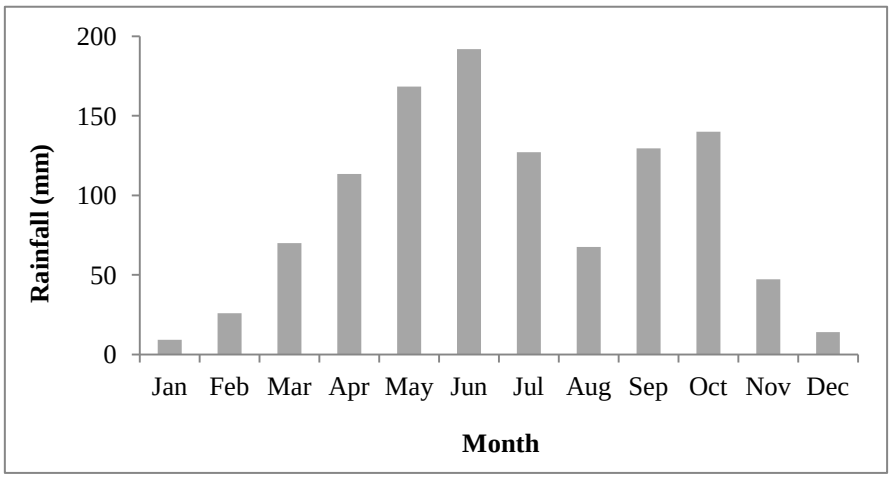

Figure 4. Monthly mean rainfall in Ouémé Delta from 1971 to 2016.

2.4.2. Temperature

Seasonal change in rainy and dry seasons induces temperature variation. The highest values are observed in dry season whereas the lowest are noticed in rainy season. Daily temperature varies from 17.2 °C to 39 °C over the period 1971 to 2016 (Figure 5.a). In average, monthly mean temperature varies from 25 °C to 30 °C (Figure 5.b).

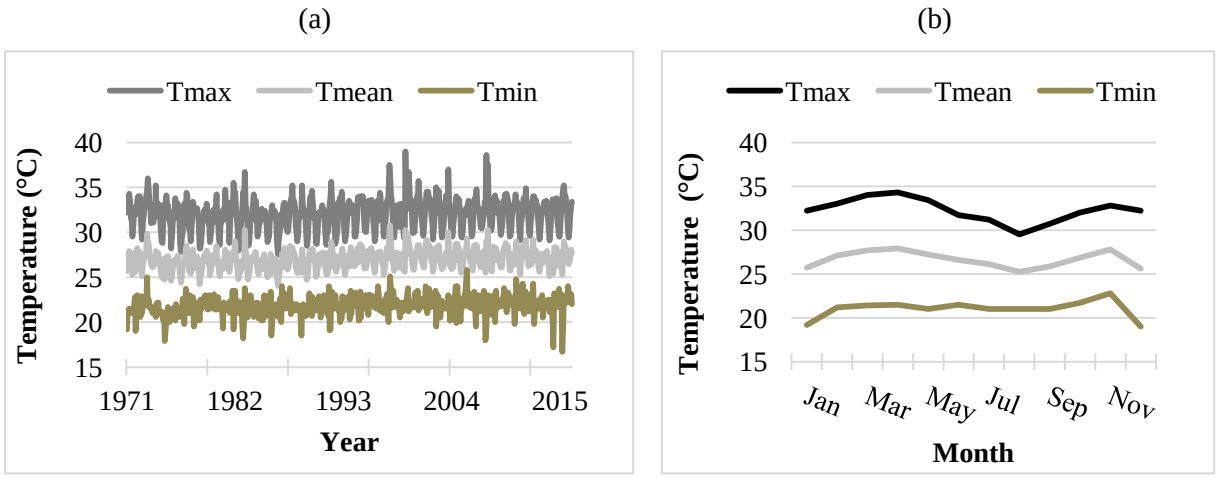

Figure 5. Daily (a) and monthly mean (b) temperature variation in Ouémé Delta.

2.4.3. Relative Humidity

The daily maximal humidity is about 100 % whereas the daily minimal humidity varies between 10 and 65 % from 1971 to 2016 (Figure 6.a). In average, monthly mean humidity varies between 60 and 83 %. The lower values are reached in the months of January and December (Figure 6.b). Monthly maximum relative humidity is about 100 % whereas monthly minimum relative humidity varies from 20 to 65 %.

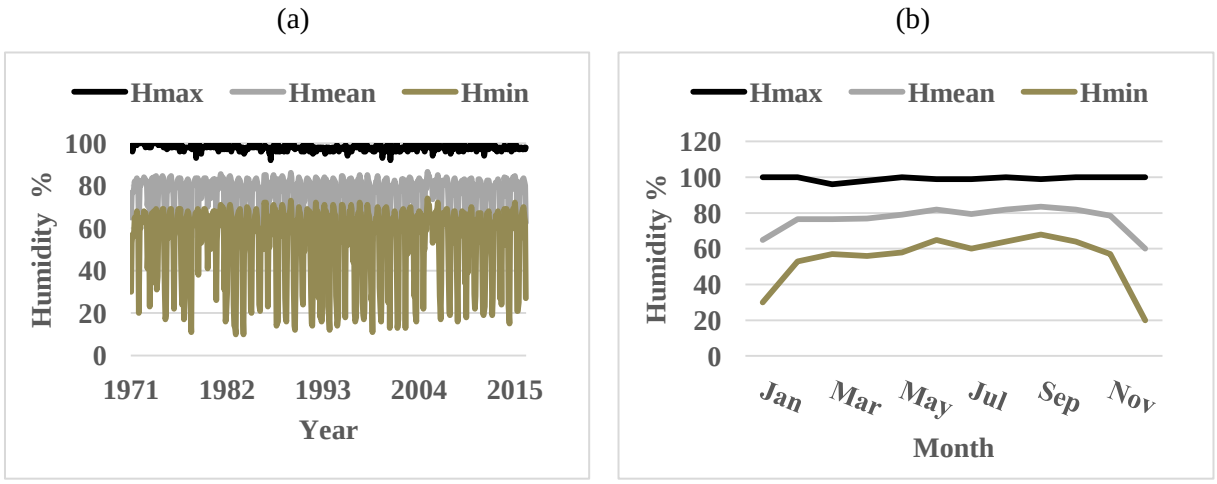

Figure 6. Daily (a) and monthly mean (b) relative humidity variation.

2.4.4. Pan evaporation

The minimum and maximum daily pan evaporation is respectively 1.4 and 7 mm from 1971 to 2016 (Figure 7.a). During the wet months of March and April, the monthly maximum pan evaporation is more than 4.5 mm (Figure 7.b) whereas it remains below 4.5 mm within the remaining months of the year.

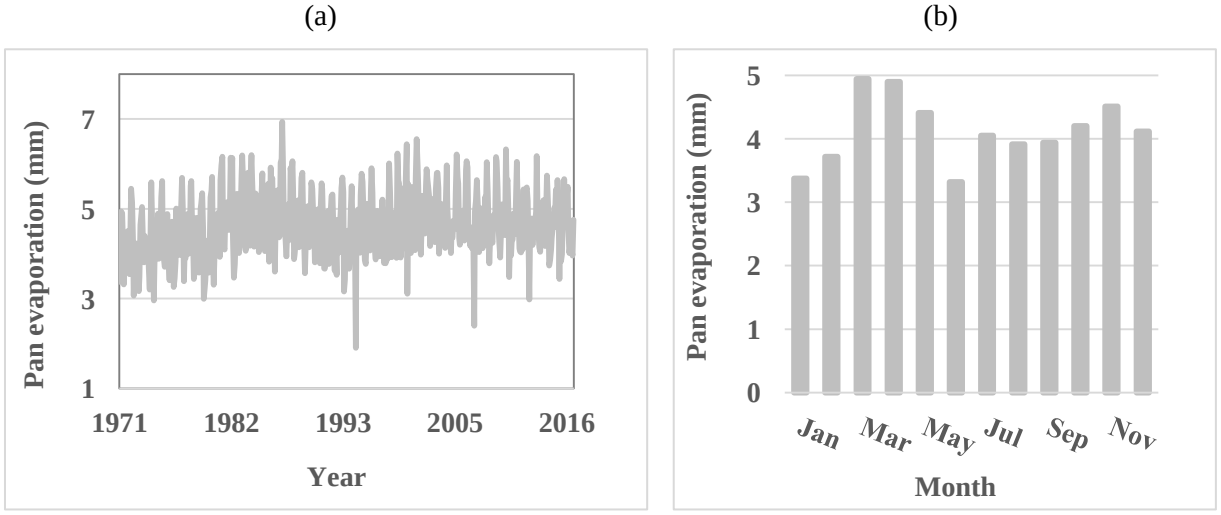

Figure 7. Daily (a) and monthly mean (b) pan evaporation variation.

2.4.5. Wind speed

Daily wind speed varies between 2.2 and 6 m/s from 1971 to 2016 (Figure 8.a). The maximum monthly mean wind speed is observed in the month of July whereas the minimum is reached in January (Figure 8.b).

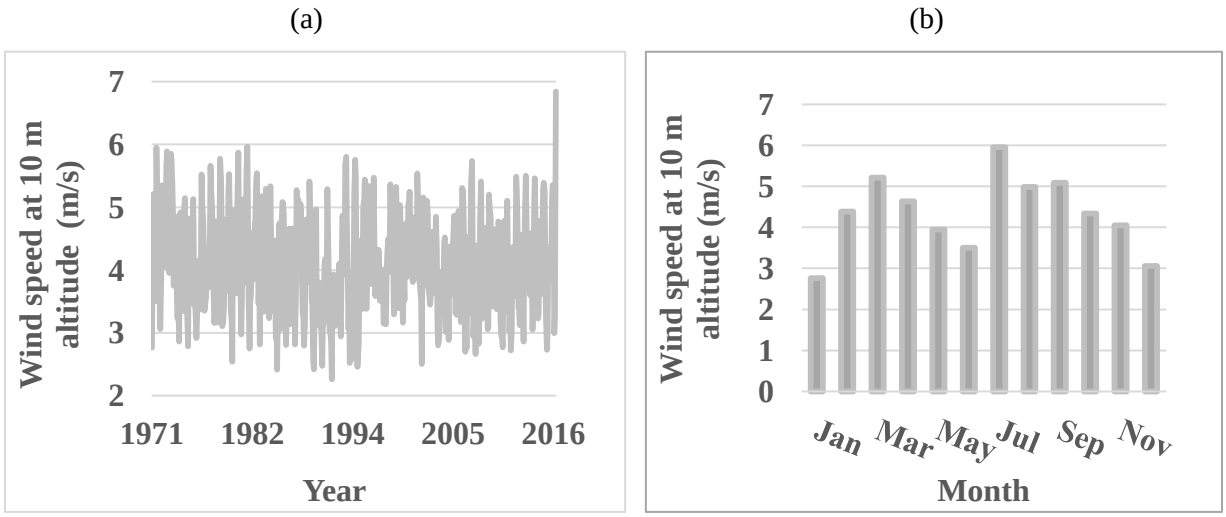

Figure 8. Daily (a) and monthly mean (b) wind speed variation.

2.5. Hydrography

Ouémé Delta hydrography is made of two main composed which are: Ouémé River and Sô River (Figure 9). Within the Delta area, they are roughly long of 90 km. These rivers are almost parallel in configuration and joined by four small rivers that Zouga (18.7 km) and Agbagbé (9.5 km) Ouovi (5 km) and Zouvi (3.5 km) through which they feed each other during high water. Nokoué Lake is the Ouémé Delta buffer zone that connects with Atlantic Ocean through Cotonou channel and Porto-Novo Lagoon through Totchè channel.

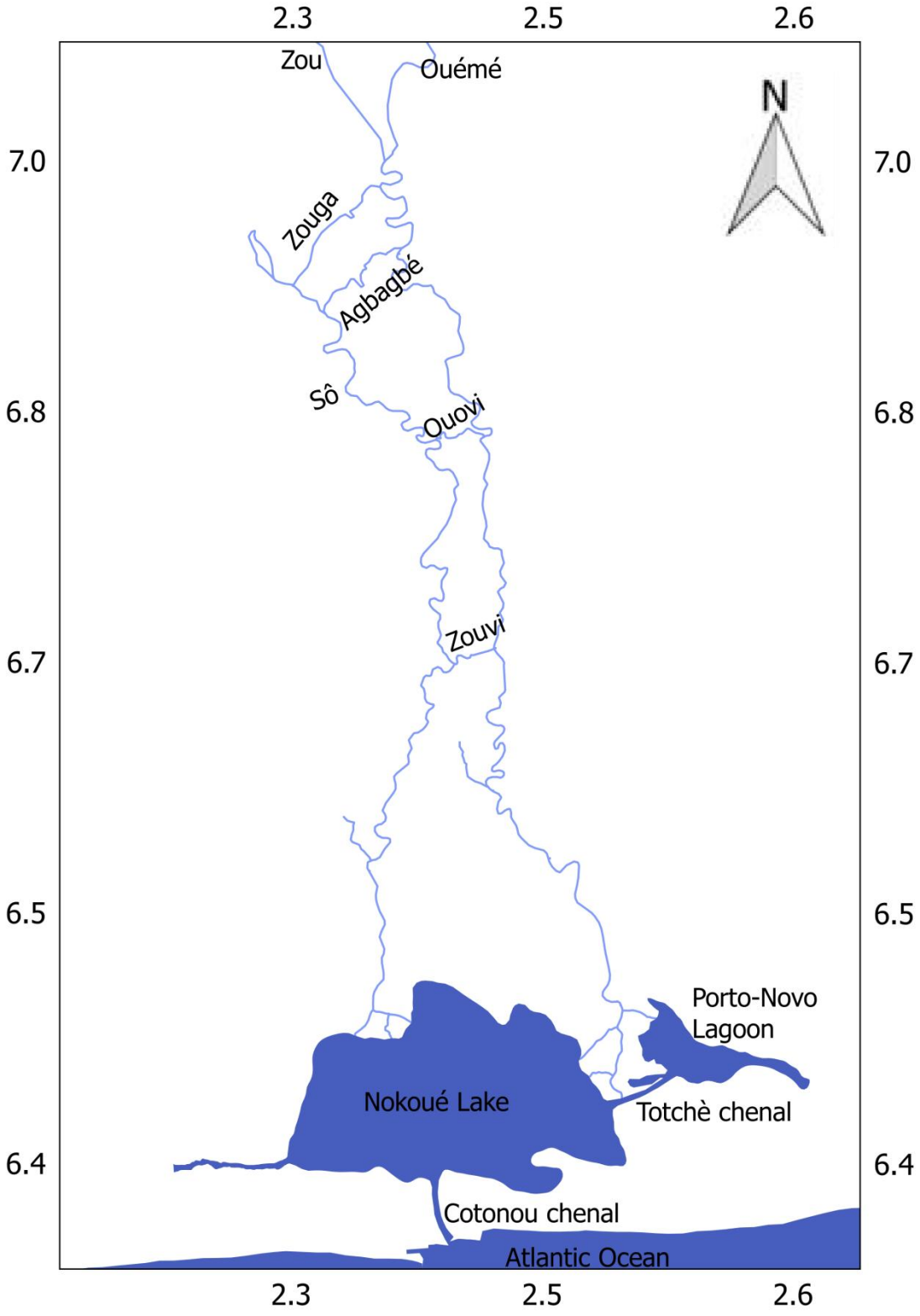

Figure 9. Ouémé Delta hydrography

2.6. Soil, land use and cover

2.6.1. Soil

Soil types and textures of Ouémé catchment and Delta complex based on the Harmonized World Soil Database (HWSD) [44] are shown on Figure 10.a and 10.b.

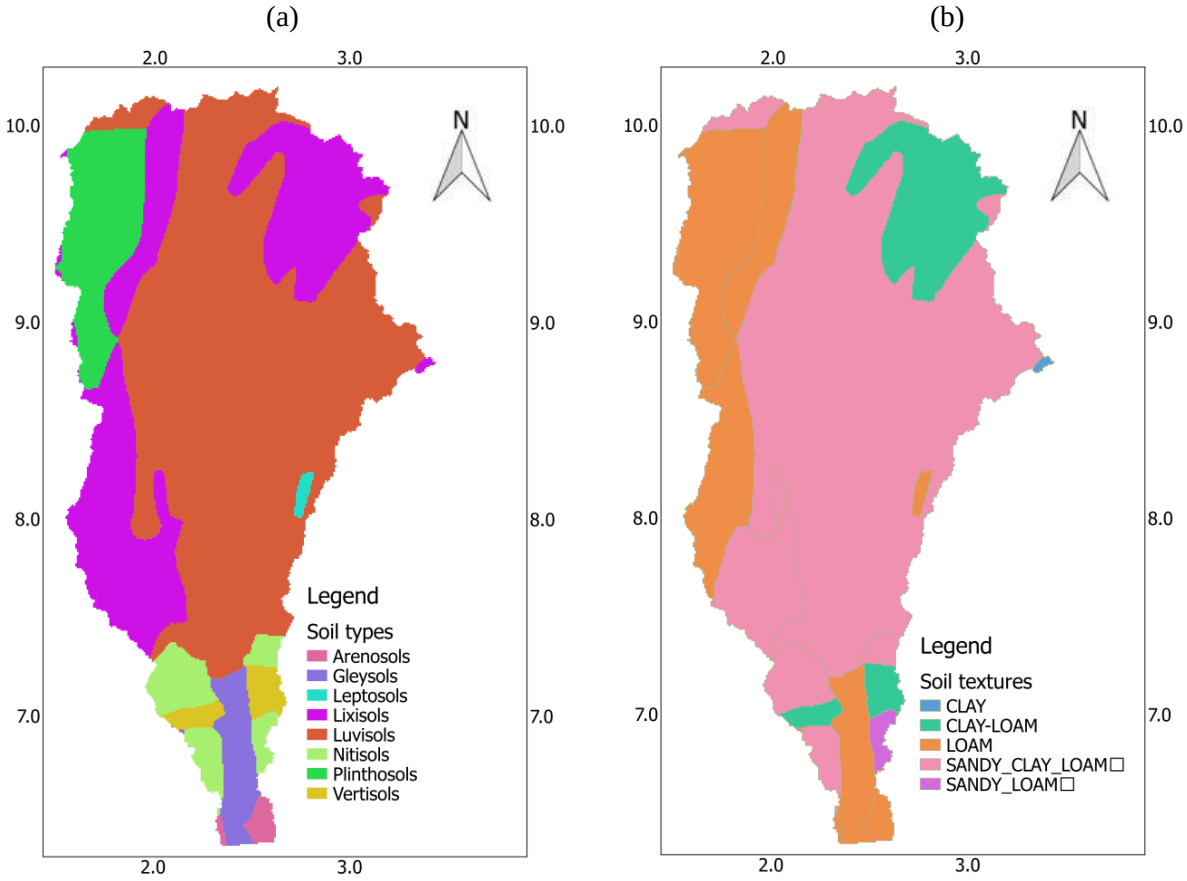

Figure 10. Ouémé delta complex soil types (a) and textures (b)

Luvisols are the dominant soil type in Ouémé catchment, reflecting stable geological conditions with high activity of clay throughout followed by lixisols (Figure 10.a). Moreover, productive nitisols are developed on the alluvium of the coastal region. On the sandbars and lagoons in the coastal region, there are gleysols. The vertisols lay on Zagnanado plateau within the Lama depression. In addition, 5% of the area is recovered with plinthosols. The texture of the various soil types encountered is mainly composed of loam, clay, clay-loam, sandy-loam and sandy-clay-loam as illustrated in Figure 10.b.

2.6.2. Land use and cover

The land use and cover map of the years 1975, 2000 and 2013 of the Ouémé catchment extracted from the West African land use and cover map provided by Tappan et al [95] is illustrated on Figure 11. Land use and cover degradation is observed in the complex. In fact, from 1975 to 2013 savanna represents respectively 77.01 % in 1975, 64 % in 2000 and 60 % in 2013 of Ouémé catchment as shown in Table 2. In addition, agriculture occupied 7.1, 23.1 and 31.4 % of the catchment area respectively in 1975, 2000 and 2013.

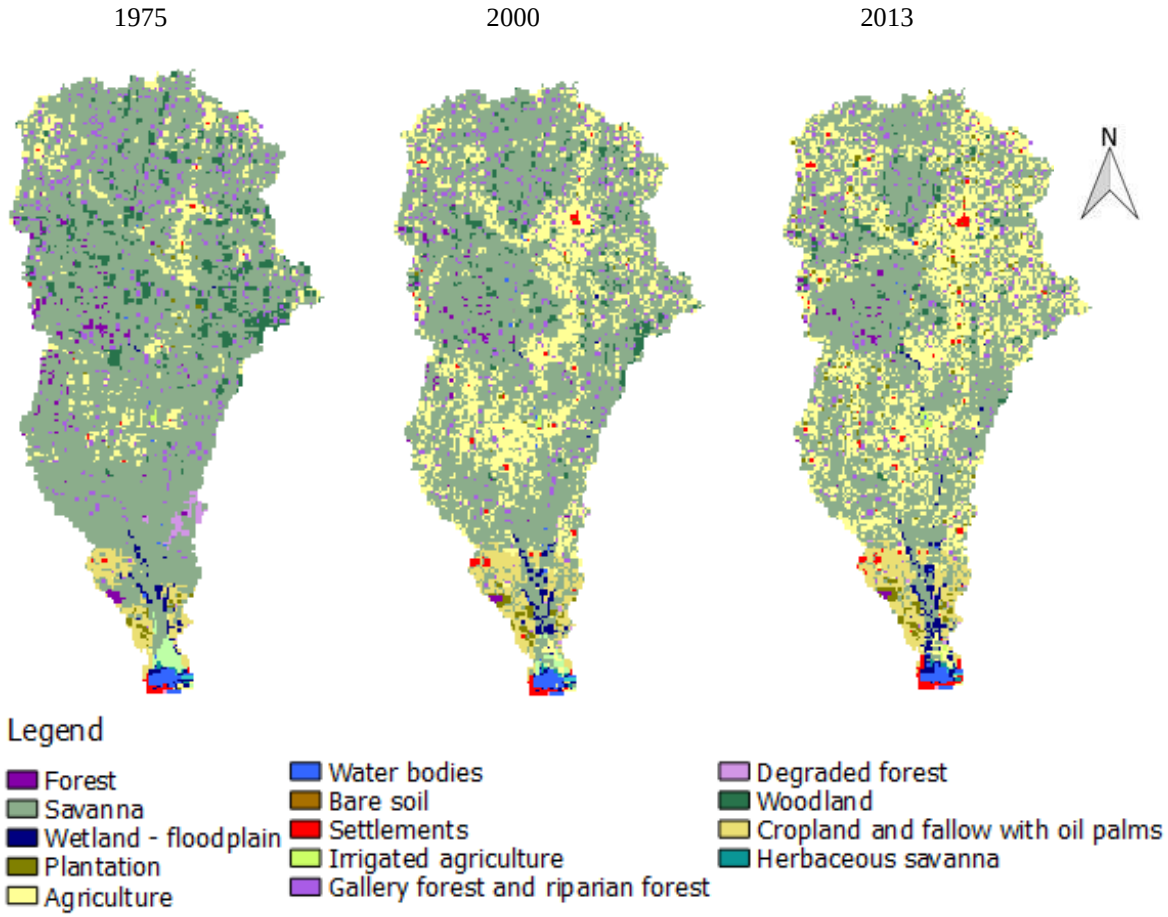

Figure 11. Land use and cover change from the years 1975, 2000 and 2013.

Thus, savanna has decreased over the years to the benefit of agriculture. Percentage of change in each land use and cover classes are computed and shown in Table 2.

Table 2. Percentage of change in land use and land cover within 1975 – 2000 and 2000 – 2013.

Land use types	Area percentage			Percentage of change	
	1975	2000	2013	1975-2000	2000-2013
Forest	1.2	0.7	0.6	-0.5	-0.2
Savanna	77.0	64.6	60.4	-12.4	-4.2

Wetland—flood plain	0.4	0.6	0.8	0.2	0.2
Plantation	0.3	0.4	1.8	0.1	1.3
Agriculture	7.1	23.1	31.4	16.0	8.3
Water bodies	0.1	0.1	0.1	0.0	0.0
Settlements	0.2	0.5	0.9	0.3	0.4
Irrigated agriculture	0.0	0.0	0.2	0.0	0.1
Gallery forest	5.1	4.7	4.1	-0.4	-0.6
Degraded forest	0.7	0.1	0.2	-0.6	0.1
Woodland	6.4	3.0	1.9	-3.4	-1.0
Cropland and fallow with oil palms	1.5	2.4	2.8	0.9	0.5

This land cover degradation may induce more runoff with a lot of sediment transport due to soil erosion. As consequence, Ouémé Delta Rivers may get filled up and loose part of their previous volume capacities. In such situation, water availability issues may increase. Therefore, precaution has to be taken in order to reduce land cover degradation for protection Ouémé catchment and Delta complex resources.

2.7. Demography

Municipalities closer to the Ouémé Delta with at least 50% of their area cover by the Delta are the following one: Bonou, Adjohoun, Dangbo, So-Ava, Aguégué, Porto Novo, Sêmé-Kpodji and Cotonou (Figure 12). Demography, population density and growth percentage of these municipalities are respectively shown on Figure 13, 14 and 15.

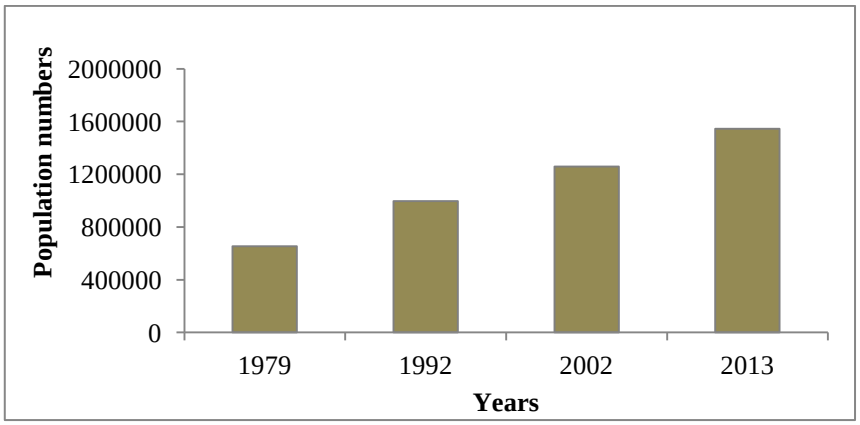

Figure 12. Ouémé Delta population effectif variation.

The increasing population growth over Ouémé Delta is observed on Figure 13 where the population numbers vary from almost 600,000 to 1,500,000 habitants respectively from 1979 to 2013 with a slope of almost 30,000 inhabitants per year. Therefore, population number has double over these 35 years period. In the case this trend is maintained, the population number will be more than 3 million inhabitants in the Delta in 2050.

In addition, population density is higher mostly in Cotonou and Porto-Novo. From 1979 to 2013, the density increased from 4055 to 8593 inhabitants per kilometer square in Cotonou and from 2663 to 5272 inhabitants per kilometer square in Porto-Novo.

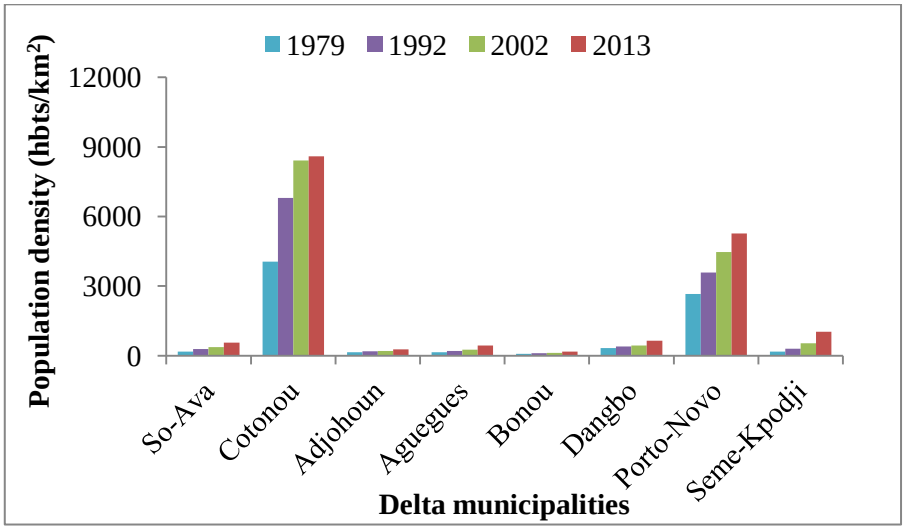

Figure 13. Ouémé Delta municipalities' population density variation from 1979 to 2013.

The increase in population density in Cotonou and Porto-Novo is attributable to the status of those two towns which are respectively the economical and administrative capitals of Benin. In addition, population growth rate decreases from the period 1979-1992 to the period 1992-2002 in So-Ava, Cotonou, Adjohoun, Aguégués Bonou and Dangbo (Figure 14). This may be due to the population migration from rural to urban areas because of job or commerce transaction.

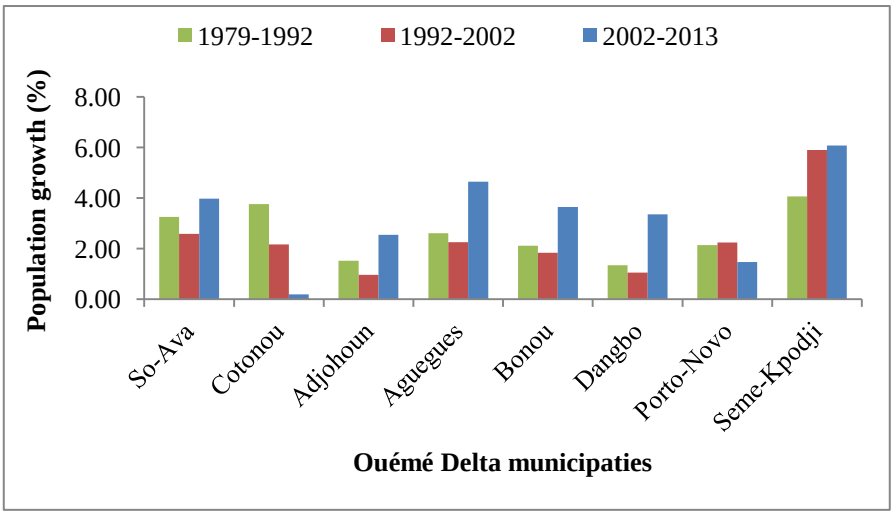

Figure 14. Ouémé Delta municipalities' population growth variation from 1979 to 2013.

However, during 1979 to 2013, population growth has increased in the overall municipalities except Cotonou and Porto-Novo where it is still decreasing. In Cotonou, the growth rate has drastically decreased from almost 4 to 2% since 2002 in favor of the surrounding municipalities especially the dormitory towns like Sêmé-Kpodji.

2.8. Partial conclusion

Ouémé Delta is the Ouémé catchment buffer zone that is localized between 6.30° and 6.90° North and between 2.35° and 2.7° East. The relief varies from 0 to 450 m altitude in the Ouémé catchment and Delta complex whereas in the Delta the highest elevation is of 15 m. the vegetation is made of crop and shrub lands with some forest and forest plantation. The study area is under bimodal regime. Annual rainfall varies between 719 mm and 2470 mm at station point over the period 1971 to 2016. Daily temperature varies from 17.2 °C to 39 °C during the same period. The daily maximal humidity is about 100 % whereas the daily minimal humidity varies between 10 and 65 %. The minimum and maximum daily pan evaporation is respectively 1.4 and 7 mm. Daily wind speed varies between 2.2 and 6 m/s. Ouémé Delta hydrography is mainly made of Sô and Ouémé Rivers as well as Nokoué Lake and Porto-Novo lagoon. The Delta's soil is mostly composed with gleysol which texture is made of loam, clay, clay-loam, sandy-loam and sandy-clay-loam. In addition, land use and cover degradation is noticed in the study area because of the anthropogenic activities due to the increasing population growth. In fact, the population number has tend to double in 35 years.

Chapter 3: Data, materials and methods

Chapter 3 provides data, materials and methods in Section 3.1, 3.2 and 3.3. Each of these sections is detailed based on each objective. Missing data are identified and filled using the double mass cumulus method [96].

3.1. Data

3.1.1. Data for analysis of current climatic and hydro-meteorological state of Ouémé Delta

Daily data are collected from six (6) rain gauges and two (2) synoptic stations which details are shown in Table 3 and presented on Figure 2. These stations are those available inside or closer to the Ouémé Delta area. Data were collected over the period 1960-2016 from the national meteorological agency. At synoptic stations, daily rainfall (PRCP), daily minimum (TMin) and maximum (TMax) temperature, minimum (Hmin) and maximum (Hmax) relative humidity, as well as daily wind speed (WIND), sunshine duration (SUND) and pan evaporation (EVA) data are collected. Data quality control is processed using RClimpact tool [97]. Unreasonable values are highlighted and removed. These are daily maximum temperature less than daily minimum temperature and daily minimum temperature higher than daily maximum. Outliers in daily maximum and minimum temperature are also identified and removed.

Table 3. Summary of available stations over Ouémé Delta with latitude and longitude.

Station Name	Acronyms	Longitude (degree)	Latitude (degree)
Abomey	ABO	1.98	7.18
Adjohoun	ADJ	2.48	6.70
Bohicon	BOH	2.07	7.17
Bonou	BON	2.50	6.93
Cotonou Airport	COT	2.38	6.35
Ketou	KET	2.61	7.36
Porto Novo	POR	2.62	6.48
Zagnanado	ZAG	2.33	7.25

In order to improve early warning system, risk management, and adaptation to both climate change and variability over large space and time scales, the World Meteorological

Organization (WMO), through the Commission for Climatology (CCl) Expert Team on Climate Risk and Sector-specific Indices (ET CRSCI), has recently defined, based on rainfall and temperature, 34 extreme indices with nine additional others, to achieve high level of climate knowledge. More detail is given at: http://www.wmo.int/pages/prog/wcp/ccl/opace/opace4/expertteam.php. The analysis of these extreme indices facilitates access to information and products for decision making. In this work, eight temperature based indices and fifteen rainfall based indices from WMO core set were computed. A summary of the chosen indices is presented in Table 4. Threshold based indices are computed using the baseline period 1981–2010. User-friendly R-based software (ClimPACT) was used to compute the indices.

Table 4 : Indices of Expert Team on Climate Risk and Sector-specific Indices (ET CRSCI) core indices where TN = minimum temperature and TX = maximum temperature, p = daily precipitation, and prcp = annual total precipitation [98].

ID	Indicator Name	Definitions	UNITS
TXx	Max TX	Monthly maximum value of daily TX	ºC
TNn	Min TN	Monthly minimum value of daily TN	ºC
TNx	Max Tmin	Monthly maximum value of daily min temperature	ºC
TXn	Min Tmax	Monthly minimum value of daily max temperature	ºC
WSDI2	Warm spell duration Indicator	Annual count of days with at least 2 consecutive days when TX>90th percentile	Days
TX95t	Very warm day Threshold	Value of 95th percentile of TX	ºC
TN95t	Very cold day Threshold	Value of 95th percentile of TN	ºC
DTR	Diurnal Temperature range	Monthly mean difference between daily max and min temperature	ºC
SDII	Simple daily intensity index	The ratio of annual total precipitation to the number of wet days (> 1 mm)	mm/day
R10 mm	Number of heavy precipitation days	Annual count when precipitation > 10 mm	Days
R20 mm	Number of very heavy precipitation days	Annual count of days when P> = 20 mm	Days
CDD	Consecutive dry Days	Maximum number of consecutive days with P < 1mm	Days
CWD	Consecutive wet days	Maximum number of consecutive days when precipitation ≥ 1 mm	Days
R95pTOT	Contribution from very wet days	Annual percentage of RR > 95th percentile / PRCPTOT	%
R99pTOT	Contribution from extremely wet days	Annual percentage of P > 99th percentile / PRCPTOT	%
R95p	Very wet days	Annual total precipitation from days > 95th percentile	Mm

PRCPTOT	Annual total wet-day precipitation	PRCP from wet days (P> = 1mm)	Mm
R99p	Extremely wet days	Annual total precipitation from days > 99th percentile	Mm
RX1day	Max 1-day precipitation amount	Monthly maximum 1-day precipitation	Mm
RX2day	Max 2-day precipitation amount	Monthly maximum consecutive 2-day precipitation	Mm
RX3day	Max 3-days precipitation amount	Monthly maximum consecutive 3-days precipitation	mm
RX5day	Max 5-day precipitation amount	Monthly maximum consecutive 5-day precipitation	Mm
RX10day	Max 10-days precipitation amount	Monthly maximum consecutive 10 days precipitation	Mm

3.1.2. Data for assessment of climate change impact on Ouémé River discharge as well as peak flow simulation at Bonou outlet at 2050 horizon, under anthropogenic degradation

Data from twenty-five rain gauges among which are 3 synoptic stations were collected over Ouémé catchment. Details about geographical position of each station are found in Table 5.

Table 5. Rain gauges and synoptic stations geographical position details.

station name	Longitude (Degree)	Latitude (Degree)	station name	Longitude (Degree)	Latitude (Degree)
ABOMEY	1.98	7.18	INA	2.73	9.97
AGOUNA	1.7	7.55	KETOU	2.61	7.36
AKLAMPA	2.02	8.55	KOUANDE	1.68	10.33
BANTE	1.88	8.42	OKPARA	2.73	9.47
BASSILA	1.67	9.02	PARAKOU_AIRPORT**	2.6	9.35
BEMBEREKE	2.67	10.2	PENESSOULOU	1.55	9.23
BETEROU	2.27	9.2	PIRA	1.72	8.65
BIRNI	1.52	9.98	SAVALOU	1.98	7.93
BOHICON**	2.07	7.17	SAVE**	2.47	8.03
BONOU	2.5	6.93	TCHAOUROU	2.6	8.87
DASSA_ZOUME	2.17	7.75	TCHETTI	1.67	7.82
DJOUGOU	1.67	9.7	ZAGNANADO	2.33	7.25
GOUKA	1.95	8.13			

Station names with (**) represent names of synoptic stations

Rainfall data over the 25 rain gauges and temperature at the 3 synoptic stations are provided by the National Meteorological Agency of Benin from 1971 to 2010. Moreover, Ouémé River discharge at Bonou outlet is provided by the general Benin Directorate of water (DGEau). Observed data went through quality control where missing values are filled using double curve mass [96] apart from discharge data in the entire years 2006 and 2009, which are left unfilled. These observed data were also used for peak flow simulation at Bonou outlet. In addition for the impact assessment, the regional climate models (RCM) are extracted at the twenty-five stations points. The four RCM used for rainfall and temperature projection are shown in Table 6. The historical period considered is from 1971 to 2005 while future projection is taken from 2020 to 2050. Climate scenarios used were based on the Representative Concentration Pathways 4.5 and 8.5.

Table 6. Details of the regional climate models used.

Model name	Institute	Driven model
CanRCM4	Canadian Centre for Climate Modeling and Analysis	CCCma-CanESM2_CCCma
RACMO22T	Royal Netherlands Meteorological Institute, De Bilt, The Netherlands	ICHEC-EC-EARTH
HIRHAM5	Danish Meteorological Institute	NCC-NorESM1-M
REMO2009	Helmholtz-Zentrum Geesthacht, Climate Service Centre, Max Planck Institute for Meteorology	MPI-ESM-LR

3.1.3. Data for assessment of climate change impacts on hydrodynamic and flood event in Ouémé Delta

The hydrodynamic model inputs and boundary data are mainly: digital elevation data, tidal, water level, discharge and precipitation (Table 7). Digital elevation model (DEM) was collected from SRTM (Shuttle Radar Topography Mission) at 30 m resolution. The elevation data was fill using Wang and Liu method under Quantum Gegoraphical Information System (QGIS) [99].

Bathymetry data of Ouémé and Sô Rivers was taken on field in 2017. In addition, that of Nokoué Lake collected in 2014 was collected from DGEau. Moreover, Ouémé and Sô Rivers bed and bank topographic data from Le Barbée et al. [6], as illustrated on Figure 16 is also used as complementary data of the Ouémé Delta bathymetry.

Table 7. List of data used for the hydrodynamic model.

Data	Availability	Spatial resolution	Source	Usage
Rainfall and temperature observation	1971-2010, daily	25 rain gauges	ANM/ Benin	Hydrological model input
Rainfall and temperature from climate model data	2016, 2018	25 rain gauges	CORDEX	Hydrological model input
Discharge	1971 – 2010, daily	Ouémé River at Bonou Outlet	DGEau / Benin	Hydrological calibration and validation / Hydrodynamic upstream forcing
SRTM	2014	30m * 30m	NASA	Hydrodynamic model mesh
Tide	2008, 2010, 2016, 2018	Cotonou harbor	IRHOB / Benin	Hydrodynamic model calibration and validation
Water level	2008, 2010	Bonou	DGEau / Benin	Hydrodynamic model calibration and validation
	2008, 2010, 2016	So-Ava station		
	2016	Adjohoun and Hêtin-Sota station		
	2018	Nokoué Lake station		
ESA ENVISAT/ASAR/IMP	2010/10/18 at 22:00:45		NASA	Hydrodynamic model calibration and validation
S1A_IW_GRDH_1SDV	August 9th till November 13th, 2018	Orbit number : 018273	NASA	Hydrodynamic model calibration and validation

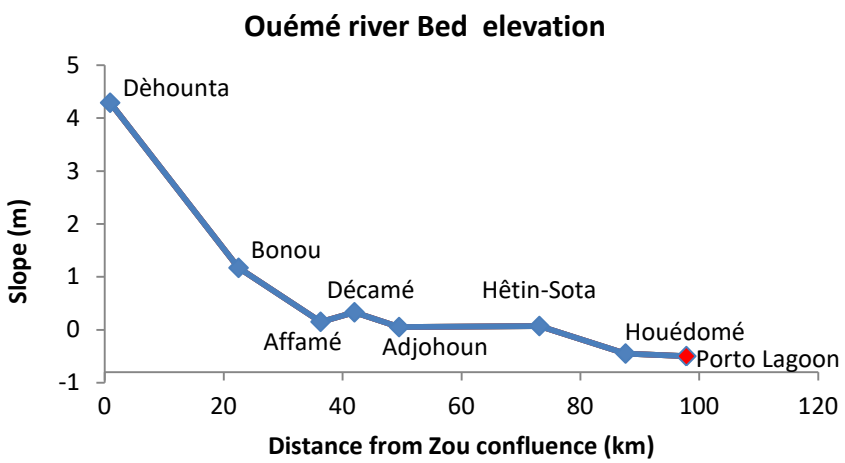

(a)

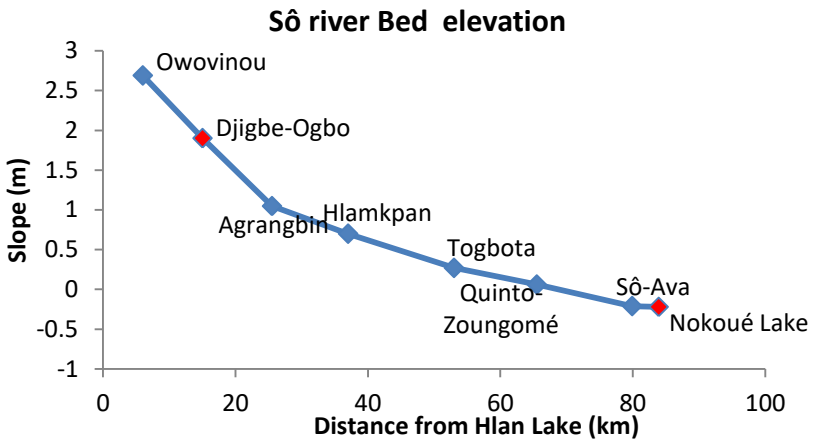

(c)

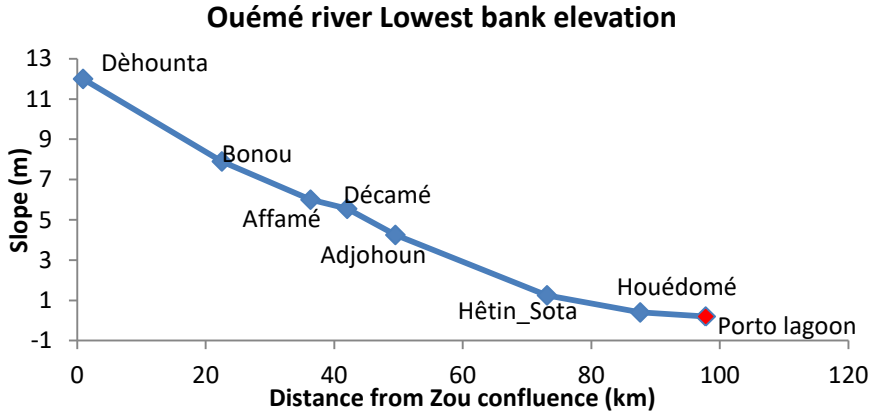

(b)

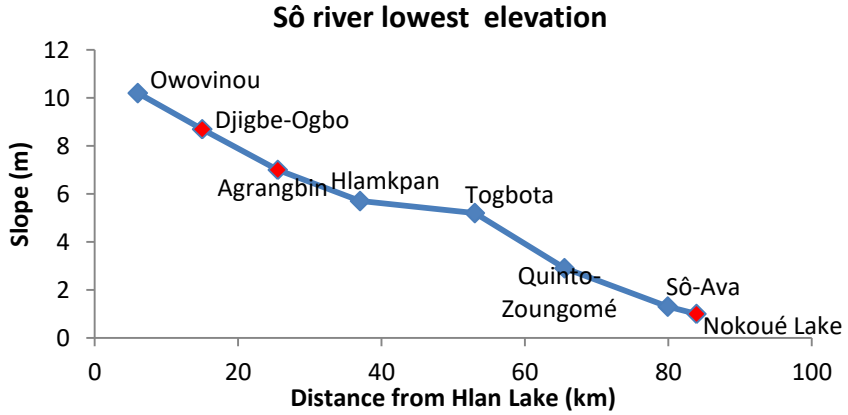

(d)

Figure 15. Bed and lowest bank elevation in Ouémé River (a) and (b), as well as Bed and lowest bank elevation in Sô River (c) and (d).

3.1.4. Ouémé Delta land use and flood event mapping

In order to validate the hydrodynamic model results, flood maps are needed. In the mapping process, Sentinel 1A images was collected over the period from 9th August to 7th December 2018 as well as Sentinel 2A from December 10, 2018 (Table 8).

Table 8. Sentinel 1A and 2 A data collected.

Sentinel 1A		**Sentinel 2A**	
Polarization	**VV/VH**		
Spatial resolution	20 x 22 m^2 (az. _ gr. range)	Spatial resolution	30 x 30 m^2
Pixel size	10 x 10 m^2 (az. _ gr. range)	Pixel size	
Swath width	250 km		
Incidence angle	36° – 42°		
Temporal resolution	12 days		
Equivalent Number of Looks	4.9		
Year	2018		2018
Dates	August 09, 21 September 02, 14, 26 October 08, 20 November 01,13 December 07	Dates	December10

2016 land use and cover map of Africa from the European Space Agency based on Sentinel2 data over the period of December 2015 to 2016 is used for class's confirmation. In addition, the satellite averaged rainfall records in 2018 from the NASA Global Precipitation Measurement (GPM) mission over Ouémé delta is used for correlation of flood extent and rainfall events.

3.2. Materials

3.2.1. ClimPACT

ClimPACT is an open source R software package that reads meteorological data (daily minimum and maximum temperatures, and precipitation) and calculates the frequency, duration and magnitude of various climate extremes directly relevant to sectors, at monthly and annual time scales. The climate extremes indices calculated by ClimPACT have been

recommended by the World Meteorological Organization in collaboration with the Expert Team on Climate Risk and Sector-specific Indices (ET-SCI). It currently calculates over 60 indices covering agriculture, water resources and health sectors, and more indices are being sought[9]. It is based on the R package RClimDEX but with some more flexibility [9]. It can easily be modified by R users in order to amend indices, to add more indices and to change language of Graphical User Interface. The software provides three methods for computing indices using text files containing station data: (i) Graphical User Interface; (ii) batch process of multiple station text files in parallel; and (iii) calculating indices using netCDF data [100]. The development and analyses of these ClimPACT sector specific indices have made a significant contribution to climate change discussions in the IPCC Assessment Reports [100].

3.2.2. CMhyd

Bias correction procedure is conducted in CMhyd (Climate Model data for hydrologic modeling). It is a tool that is used to extract and bias-correct data obtained from global and regional climate models. Furthermore, it is recommended when applying an ensemble approach to use bias-corrected data provided by several climate models and downscaling methods [101]. The flexibility that offers CMHyd facilitates climate model analysis [102]. As bias correction aims at minimizing the discrepancy between observed and simulated climate variables, corrected data should reasonably match observed ones. CMHyd has the ability to better reproduce observation. The bias correction process is summarized in the diagram on Figure 16.

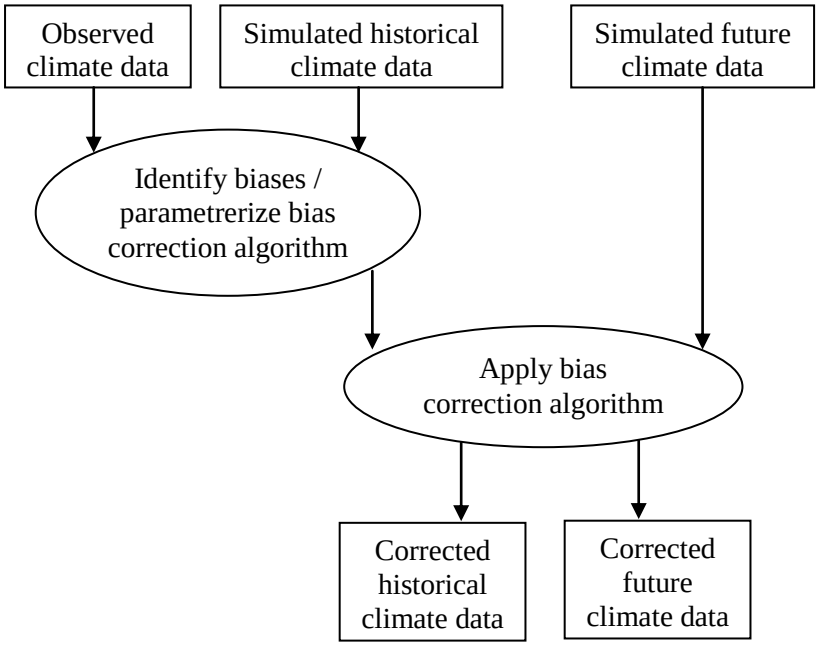

Figure 16. Bias correction framework.

Biases of nudging are identified from comparison between observations and historical climate model data for correction. The transfer function set up during correction is transposed over future data for their correction.

3.2.3. Hydrological models

Three hydrological models namely HEC-HMS, HBV and HyMoLAP are used. HEC-HMS and HBV are semi-distributed models while HyMoLAP is a lumped model.

HBV (Hydrologiska Byråns Vattenbalansavdelning) has been developed by the SMHI (Swedish Meteorological and Hydrological Institute). The structure of HBV components is as followed (Figure 17). Over each catchment or sub-catchment, losses are removed from precipitation and transform through the soil moisture routine function into runoff.

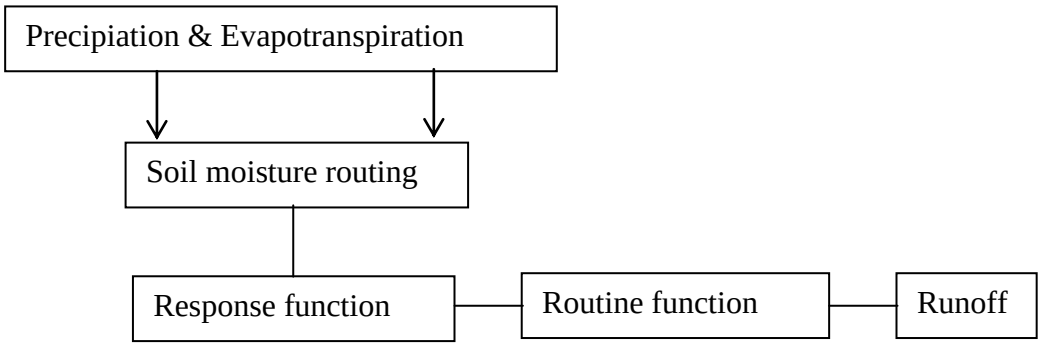

Figure 17. HBV model components structure.

HEC-HMS stands for Hydrologic Engineering Center (HEC) Hydrologic modeling system (HMS). It is a semi-distributed hydrologic model developed by the US Army Corps of Engineers to simulate the hydrologic response of a watershed subject to a given hydro-meteorological input (Figure 18).

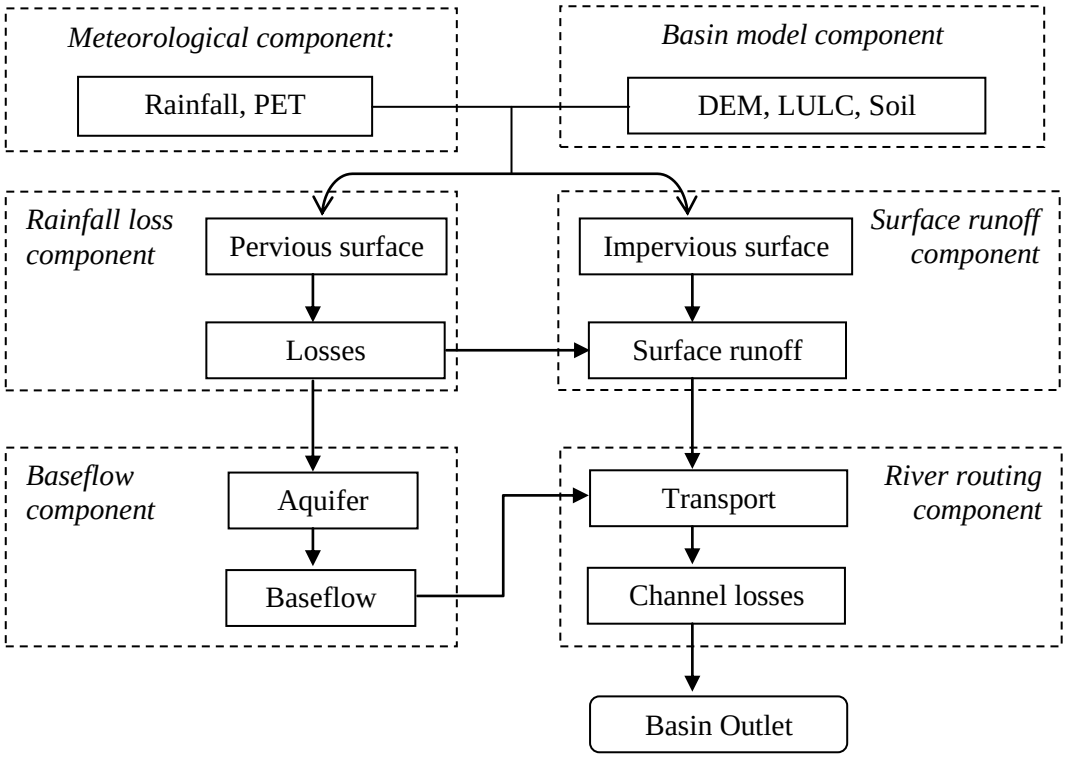

Figure 18. Schema of rainfall runoff modeling in HEC-HMS.

Like HBV, HEC-HMS inputs are rainfall and potential evapotranspiration. The model uses DEM information to partition the basin into sub-watersheds. In addition, it includes land use and covers data as well as soil data using the curve number loss method.

HyMoLAP (Hydrological Model based on the Least Action Principle) is developed in the University of Abomey-Calavi in Benin [103,104]. This model unlike the previous ones lacks the canopy and surface storage reservoirs (Figure 19). It is a lumped and semi-distributed model.

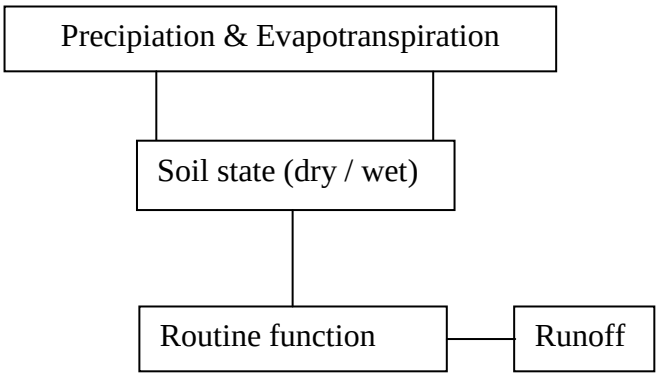

Figure 19. HyMoLAP model components structure.

3.2.4. HEC-RAS

Water level and flow simulation in Ouémé Delta is done using the physical hydrodynamic model HEC-RAS. It is mainly composed of three components namely: the geometry, the plan and the run. These components are interconnected as shown on Figure 20. The process used in this work is the unsteady flow analysis.

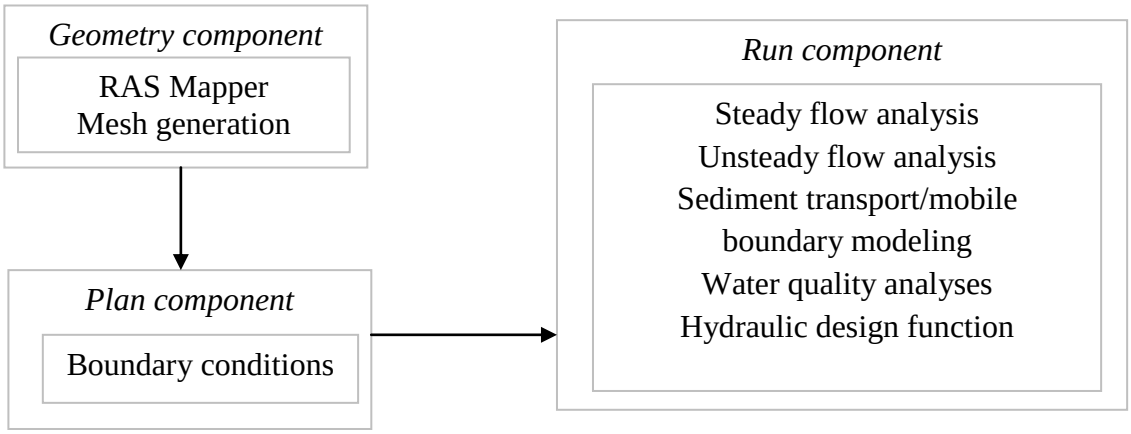

Figure 20. HEC-RAS model components.

3.3. Methods

3.3.1. Analysis of current climatic and hydro-meteorological state of Ouémé Delta

3.3.1.1. Trends analysis

Trend analysis is conducted at annual scale on each of the eight temperature based indices as well as the 15 rainfall based indices. In addition, trend in maximum consecutive 1, 2, 3, 5, and 10 days precipitation are computed at a monthly scale within the high water period in Ouémé Delta. We focused more on heavy rainfall during the high water period to assess its impacts on flood events. High water in the Delta area occurs essentially from September to November. This period represents the second rainy season in that area. In addition, relative humidity and wind speed are computed at annual scale taking into account the mean, minimum, and maximum at the two synoptic stations that fall in the Delta area. Sunshine and pan evaporation were computed at annual as well as monthly scale. Trends are detected using Mann–Kendall test, developed by Mann [105] and Kendall [106], and a prewhitened Mann–Kendall test at 0.05 confidence level by Brien [107], as shown on Figure 21.

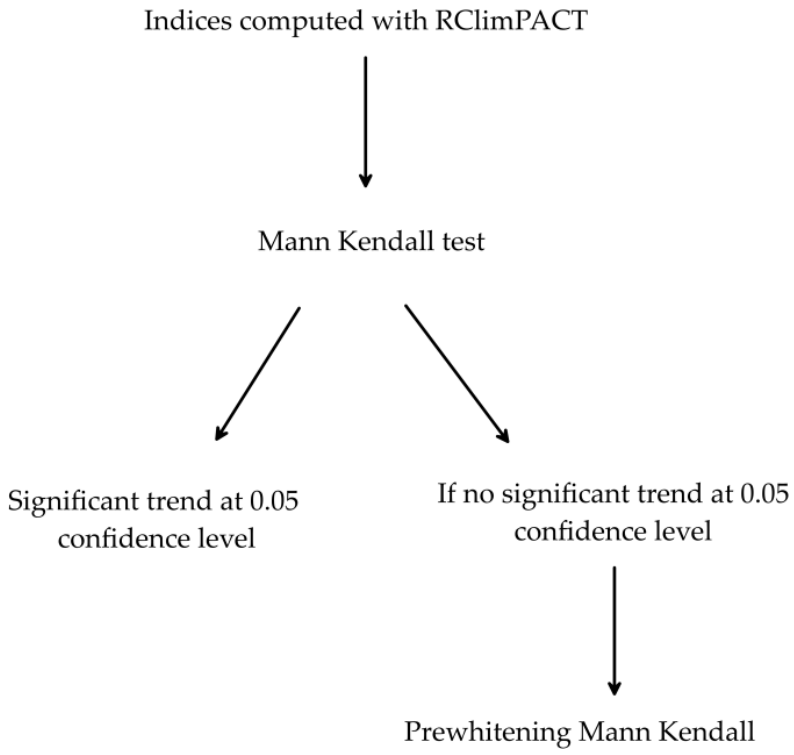

Figure 21: Trend analysis process sketch.

3.3.1.2. Mann–Kendall Test

The well-known Mann–Kendall test is a non-parametric test that is commonly applied for monotonic trend analysis in series of environmental data, climate data, or hydrological data. This test assesses the existence of a monotonic upward or downward trend of the variable of interest over time. A monotonic upward (downward) trend of a variable means its consistent increase (decrease) through time; moreover, the trend may or may not be linear. Thus, the Mann–Kendall test is preferably used instead of a parametric linear regression analysis, to enable the detection of a non-linear trend. This test does not require data to be normally distributed. Furthermore, it is not sensitive to abrupt breaks due to non homogeneous time series [108]. However, Thiel Sen's slope method that uses a linear model to estimate the slope of the trend and the variance of the residuals should be constant in time [109].

The null hypothesis of the Mann–Kendall test, H0, is that data come from a population with independent realizations with identical distribution. The alternative hypothesis, H1, is that data follows a monotonic trend. In this work, the trend was detected at 0.05 confidence level using Mann–Kendall test package in R [107]' where Tau is the correlation rank strength, Sen slope the magnitude, and p value the probability.

3.3.1.3. Prewhitened Mann–Kendall Test

In the case that the Mann–Kendall test detects no trend, prewhitening Mann–Kendall test was used to detect a probable trend covered by internal serial correlation. In fact, prewhitening is processed to remove serial correlation in the data set [110]. The presence of serial correlation in hydro meteorological time series often makes the detection of fake deterministic gradual or abrupt changes with tests such as Mann–Kendall (MK) [53]. Though, Mann Kendal test has shown a strong performance in trend detection, there are some limitation due to its own null hypothesis based on the assumption that data are independently and identically distributed [111]. Serial correlation increases the variance of the test statistic. As consequence, it increases the rejection rate of the null hypothesis. Then, the prewhitening procedure decreases the inflation of the variance of the test statistic due to serial correlation and reduces the rate of rejection below the rate before prewhitening [112]. Therefore, it is important to prewritten when there is no trend. Moreover, Yue et al. [113] stated that prewhitening is not suitable for eliminating the effect of serial correlation on the Mann–

Kendall test when trend exists in a time series, because it removes a portion (equal to the lag-one autocorrelation coefficient) of trend and hence reduces the probability of rejecting the null hypothesis when it is false.

3.3.1.4. Pan Evaporation influence on Ouémé Delta

In order to determine the main explanatory variables of pan evaporation, partial correlation and stepwise regression is used. Partial correlation is used in the case of one variable being partially correlated with some other independent ones. Thus, each partial correlation coefficient obtained represents the contribution of each independent variable to the dependent one. In fact, it is shown that pan evaporation is governed by three conditions: thermal, turbulent, and vapor conditions, each of which is influenced by group of pan evaporation explanatory variables, as shown by Liu et al. [114]. In addition, stepwise regression is used to quantify the relative weight of each variable to the dependent [39]. Thus, stepwise regression is used to further the partial the correlation results. In this study, the correlation coefficient is determined at daily scale between pan evaporation and each of the nine (9) following variables: rainfall, minimum and maximum temperature, mean temperature, minimum and maximum relative humidity, mean relative humidity, wind speed, and sunshine. Stepwise regression is a variable selection procedure for selecting the fewest most useful independent variables that are believed to be the most essential in the final prediction equation, which is as followed:

$$Y = \beta_0 + \beta_1 X_1 + \beta_2 X_2 + ... + \beta_n X_n \quad (1)$$

Where Y is the dependent variable, $X_{1,.....,n}$ the n independent explanatory variables, β_0 is the y-intercept, and $\beta_{1,.....,n}$ are the estimate of model parameters relatively to each dependent variable. The selection consists of a series of step to find the most significant independent variable to be included in the final regression model based on a set criterion, which is here the t-statistic. At each step of the regression, the independent variable retained is the one with the highest absolute t-value with p value being considered at the α confidence level.

3.3.2. Assessing climate change impact on Ouémé River discharge at Bonou outlet at 2050 horizon, under anthropogenic degradation

Impacts of climate change over streamflow in Ouémé River at Bonou outlet is quantified using the following steps. First of all, regional climate model bias correction is done. In addition, rainfall over the catchment is averaged using the robust and non biased kriging method [115] while temperature was averaged using the mean value of the three synoptic stations.

Then, rainfall runoff simulation is done using the semi distributed model HEC-HMS based on the curve number loss method in order to take into account land use and land cover change. In order to improve high flow simulation in Ouémé catchment using HEC-HMS, the soil moisture accounting (SMA) method is applied to account for long term catchment response to wet or dry condition. Furthermore, for model performance comparison purpose, HBV is run based one soil moisture accounting (SMA) method. The lumped model HyMoLAP based on least action principle was also run. Overall three hydrological models are used for model comparison namely HEC-HMS, HBV and HyMoLAP.

The calibration period is 1971 – 1990 and the validation period is 1991 – 2010. The future stream flow is projected over the period 2020 – 2050. Change in Ouémé River peak discharge is quantified using flow duration curve.

3.3.2.1. Climate models bias correction

Climate projection data are corrected using quantile mapping bias correction method. Comparing different bias correction methods such as delta change method, linear scaling and empirical quantile mapping over Ouémé catchment M'Po [62] proved that the empirical quantile mapping performed better than others in correcting biases of daily precipitation. Details of mathematical equations are found in [62,72]. Models bias correction efficiency is measured using two efficiency coefficients: the Kling-Gupta Efficiency (KGE) coefficient and the percentage of bias (PBIAS) as detailed in Table 9. The Kling-Gupta Efficiency ($0 \leq KGE \leq 1$) has the advantages of taking into account the Nash-Sutcliffe Efficiency (NSE) as well as the correlation coefficient [116]. In addition, the PBIAS is used to quantify the overall difference between observation and simulation.

Table 9. Model performance criteria.

Efficiency coefficient	Definition and utility	Optimal value	Expression
Nash-Sutcliffe Efficiency (NSE) [117]	NSE is a normalized statistic that determines the relative magnitude of the residual variance or noise compared to measured data variance. It runs from -inf to 1.	Value of 1	$NSE = 1 - \frac{\sum_{i=1}^{N}(S_i - O_i)^2}{\sum_{i=1}^{N}(O_i - \overline{O})^2}$
rPearson (r) [118]	*rPearson* estimates the degree to which two series are correlated and runs from 0 to 1	Value of 1	$r = \frac{\sum_{i=1}^{N} O_i S_i - N\,\overline{O_i}\,\overline{S_i}}{\sqrt{\left(\sum O_i^{\,2} - N\,\overline{O_i}^{\,2}\right)}\sqrt{\left(\sum S_i^{\,2} - N\,\overline{S_i}^{\,2}\right)}}$
Mean absolute error (MAE) [116]	MAE returns the mean absolute difference between simulated and observed data and runs from 0 to +inf.	Lower value	$MAE = \frac{1}{N}\sum_{i=1}^{N}\lvert S_i - O_i\rvert$
Percent bias (PBIAS) [119]	Percent bias (PBIAS) measures the average tendency of the simulated values to be larger or smaller than their observed ones. Positive values indicate overestimation bias, whereas negative values indicate underestimation bias.	Value of 0	$PBIAS = 100\frac{\sum_{i=1}^{N}(S_i - O_i)}{\sum_{i=1}^{N} O_i}$
Kling Gupta Efficiency (KGE) [120]	KGE provides a diagnostically interesting decomposition of the Nash-Sutcliffe efficiency which facilitates the analysis of the relative importance of its different components such as correlation, bias and variability in the context of hydrological modeling	Value of 1	$KGE = 1 - \sqrt{(r-1)^2 + (\alpha - 1)^2 + (\beta - 1)^2}$ where r = rPearson, α is the ratio between of simulated variance and observed variance, and β is the bias (the ratio between simulated mean and observed mean)

Where S_i simulated discharge, O_i observed discharge, N sample size

3.3.2.2. Hydrological modeling

The main components encountered in the various hydrological models used are detailed in Table 7.

Table 10. Hydrological modeling processing

Elements	Components	Data / method
Model types	Basin model	DEM for watershed delineation
Hydrological process	Precipitation (specified hyetograph)	Averaged precipitation using kriging method
	Potential evaporation	Mean temperature using Hamon method [121]
	Direct runoff	Soil Conservation Service Unit Hydrograph (SCS-UH)
	Base flow	Recession constant
	Loss rate	• Soil Conservation Service method using Curve Number (SCS-CN) • Soil moisture accounting method (SMA)
	Canopy interception	Simple canopy
	Surface method	Simple surface

Canopy-interception represents precipitation that is captured on trees, shrubs, and grasses. When precipitation occurs, it first fills canopy storage. Only after this storage is filled that precipitation become available for filling other storage volumes. Water in canopy interception storage is held until it is removed by evaporation.

In the loss method, infiltration rate is considered through curve number as well as the percentage of impervious area of the basin. In this method, it is considered that all land and water in a watershed can be categorized as either: directly-connected impervious surface or pervious surface. Directly-connected impervious surface in a watershed is that portion of the watershed on which all contributing precipitation runs off with no infiltration, evaporation, or other volume losses. Precipitation on the pervious surfaces is subject to losses. Impervious area percentage is catchment characteristics estimated using soil type and land use and cover data. In this work, the following two loss method types are processed: the curve number method (CN) and the soil moisture accounting (SMA) method.

a. Curve number method

The soil conservation service method based on curve number (SCS-CN) model estimates precipitation excess as a function of cumulative precipitation, soil cover, land use, and antecedent moisture, using the following equation:

$$P_e = \frac{\left(P - I_a\right)^2}{P - I_a + S} \tag{2}$$

where Pe is the accumulated precipitation excess; P, the accumulated rainfall depth; I_a is the initial abstraction; and S is the potential maximum retention which is a measure of the ability of a watershed to abstract and retain storm precipitation. Till the accumulated rainfall exceeds the initial abstraction, the precipitation excess, and hence the runoff, will be zero.

Based on the analysis of results from numerous small experimental watersheds, the SCS developed an empirical relationship of I_a and S:

$$I_a = 0.2S \tag{3}$$

Therefore, the cumulative excess at time t is:

$$P_e = \frac{\left(P - 0.2S\right)^2}{P + 0.8S} \tag{4}$$

Incremental excess for a time interval is computed as the difference between the accumulated excess at the end of and beginning of the period. The maximum retention, S, and watershed characteristics are related through an intermediate parameter, the curve number (commonly abbreviated CN) as:

$$S = \begin{cases} \dfrac{100 - 10CN}{CN} & (\textit{foot, pound system}) \\ \dfrac{25400 - 254CN}{CN} & \textit{SI} \end{cases} \tag{5}$$

CN values range from approximately 30 for permeable soils with high infiltration rates to 100 (for water bodies). Further background and details on use of the CN model are found in the Soil Conservation Service publications [122].

The CN for a watershed can be estimated as a function of land use, soil type, and antecedent watershed moisture, using tables published by the SCS. For convenience, Appendix A of this document includes CN tables developed by the SCS and published in Technical Report 55 (commonly referred to as TR-55) [122]. With these tables and knowledge of the soil type and land use, the single-valued CN can be found. For example, for a watershed that consists of a tomato field on sandy loam near Davis, the CN shown in Table 2-2b of the TR-55 tables is 78 [122]. (This is the entry for straight row crop, good hydrologic condition, B hydrologic soil group.) This CN is entered directly in the appropriate HEC-HMS input form. For a watershed that consists of several soil types and land uses, a composite CN is calculated as:

$$CN_{composite} = \frac{\sum A_i CN_i}{\sum A_i} \tag{6}$$

in which $CN_{composite}$ represents the composite of CN used for the runoff volume computations in HEC-HMS; i is an index of watersheds subdivisions of uniform land use and soil type; CN = the CN for subdivision i; and A_i = the drainage area of subdivision i.

b. Soil moisture accounting method

The soil moisture accounting (SMA) method is designed to account for watershed's soil moisture balance over a long-term period. It is suitable for simulating daily, monthly, and seasonal streamflow in both HBV and HEC-HMS. The SMA process include all runoff components such as direct runoff (surface flow) and indirect runoff (interflow and groundwater flow) [122]. HEC-HMS requires inputs of daily rainfall, soil condition and evapotranspiration data. It subdivides the watershed with five storage layers canopy interception, surface depression, soil profile, groundwater storages (1 and 2) as shown in the Figure 22.a and involves twelve parameters. The list of these parameters are: canopy interception storage, surface depression storage, maximum infiltration rate, soil storage, tension zone storage and soil zone percolation rate and groundwater 1 and 2 storage depths, storage coefficients and percolation rates.

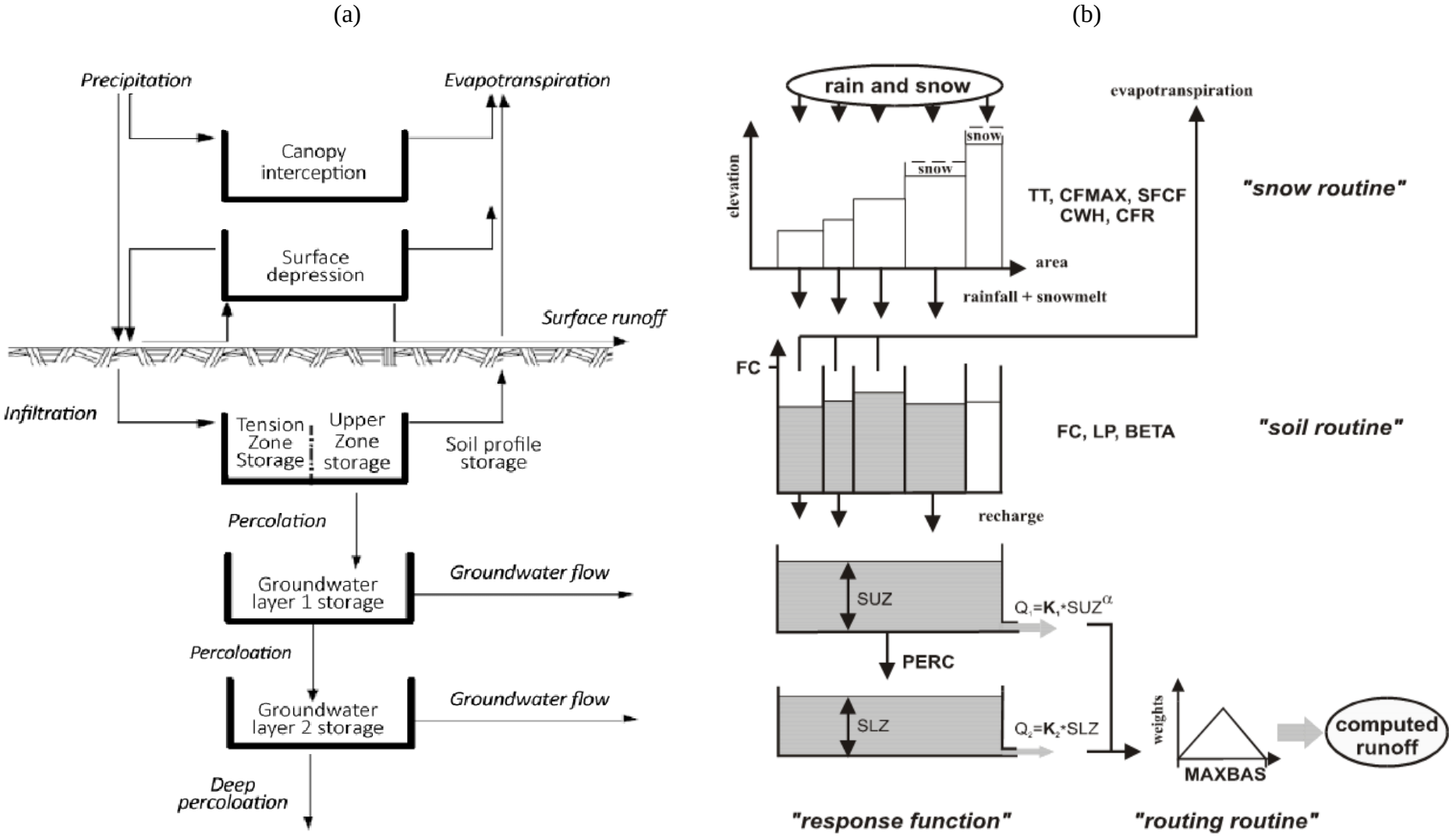

Figure 22. Structure of HEC-HMS (a) and HBV (b).

The soil moisture accounting method is used to facilitate comparison between HBV and HEC-HMS. HBV is a semi-distributed model as HEC-HMS. It is composed of two main components: precipitation accumulation and soil moisture accounting subroutines (Figure 22.b). HEC-HMS and HBV can divide a basin into sub-basins as primary hydrological units and an area-elevation distribution as well as crude classification of land use [123]. Then, they allow gridded data for precipitation, elevation and land use and cover [122]. Both models dispose of two groundwater reservoirs based on the soil moisture accounting method. Moreover, HEC-HMS takes a land surface component in which is incorporated canopy interception storage that does not exist in HBV. This storage capacity is filled before depression and other storage starts in HEC-HMS. HBV has 14 parameters among which are five snow routine parameters that are not applicable in Benin context in contrary to HEC-HMS which has more parameter especially in the soil moisture accounting method. HBV has proven efficiency around the world. In the review of applied methods in Europe for flood-frequency analysis in a changing environment, reported by the IPCC's Working Group 4 which focused on Flood frequency estimation methods and environmental change [124], there is a long list of works that used HBV in simulating discharge in various areas worldwide. Previous work using HEC-HMS are found in [125–131]. HyMoLAP is a lumped model with only two parameters λ and μ (Figure 23). It is based on the least action principle that is expressed by the following differential equation:

$$\frac{dQ}{dt} + \frac{\mu}{\lambda} Q^{(2\mu-1)} = \frac{X_t}{\lambda} q(t) \tag{7}$$

The numerical solution of Equation 7 is:

$$Q_t = Q_{t-1} - \frac{\mu}{\lambda} Q_{t-1}^{2\mu-1} + X_t \frac{q_{t-1}}{\lambda} \tag{8}$$

where :

Q_t is the discharge at the outlet at the time t.

Q_{t-1} represents discharge at the outlet at the time $t-1$.

X_t describes the state of the basin at the time

q_{t-1} = net rainfall of the time $t-1$ (= precipitation-ETP if precipitation> ETP)

Figure 23 describes mathematical structure of HyMoLAP.

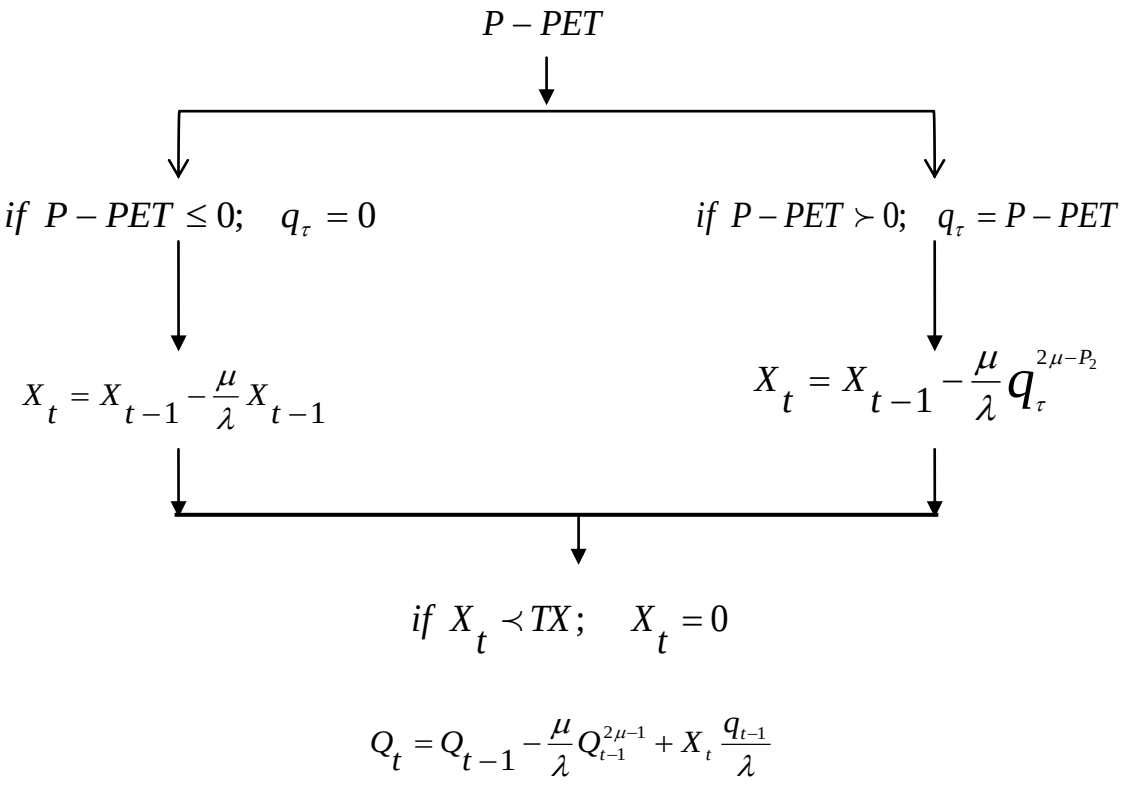

Figure 23. HyMoLAP structure.

On Figure 23, λ is the recession coefficient, μ describes non-linearity of the transformation of rainfall into runoff whereas X_t is infiltration parameter that accounts for the soil state [74,132]. The least action principle integrates the stochastic aspects of meteorological processes. Then, it account for the dynamic and the randomness in meteorological variables such as precipitation.

3.3.2.3. Quantifying climate change impacts on peak River discharge

Impact of climate change over stream flow in Ouémé catchment is quantified as change between observed and projected trend slope. This change is assessed in discharge,

rainfall, rainfall loss, potential evaporation and temperature, based on the Mann Kendall trend analysis [8].

3.3.3. Model comparison and ensemble model approach

HBV, HyMoLAP and HEC-HMS are the hydrological models used. The schematic structure of HBV and HyMoLAP are detailed in [74] while that of HMS is in [122]. Flow modeling is done using not only each models separately but also an ensemble approach. In ensemble approach, models were coupled and averaged as followed: HyMoLAP/HBV, HyMoLAP/HMS and HBV/HMS. In addition, all three models are averaged and named Ensemble_mean. Finally, there are 7 models that are assessed. Models' performances were measured using the three following steps: performance criteria method, quantile curve comparison method and peak flow trend comparison method [133].

3.3.3.1. Model performance criteria

Five model efficiency coefficients commonly used as detailed before in Table 9 are considered. Kling Gupta Efficiency (KGE) is an alternative solution that results from analysis of the decomposition of the Nash-Sutcliffe efficiency (NSE) in order to avoid problem like high sensitivity to extreme values and bias. Thus, it already accounts for the NSE, the correlation impacts and bias [133]. Consequently, assessment of model performance will mainly be based on KGE for measuring the match between observed and simulated data. In addition, MAE is used for quantifying the mean absolute error and the percentage of bias (PBias) to quantify overestimation or underestimation of observations.

3.3.3.2. Quantile curve comparison

After assessing the performance of day to day flow simulation, quantile interval analysis is implemented. Quantile method analysis is prominent in reproducing flow either in low or high flow for water resources management during drought and flood. Consequently, the best model should be as close as possible to observed quantile values. Observed flow duration curve is then drawn and compared with the corresponding

simulation output. Actually, intervals which serve as indicators of hydrologic conditions are derived from quantile curve analysis [133]. Quantile curve intervals could be subdivided into several groups. A standard approach is to divide the quantile curve into five classes: high flows (0–10%), moist flows (10–40%), mid-range flows (40–60%), dry conditions (60–90%), and low flows (90–100%) [133].

3.3.3.3. Peak flow trend comparison

As Ouémé Delta is a flood prone area due to flow coming from Ouémé catchment, high flow simulation is essential. In order to assess model performance in high flow, trend analysis of peak flow is done. Trend in observed annual peak flow is compared to that of each model simulation. The prewhitened Mann Kendall test is the one used [8]. The trend analysis is implemented to assess the conservation of peak flow trend from observed to simulated flow. Moreover, PBias between observed and simulated peak flow is computed for bias quantification.

3.3.4. Land cover and flood mapping

In order to assess flood extent in the Ouémé delta, satellite images, namely Sentinel 1A and Sentinel 2A were used. Sentinel1 are made of four polarizations outputs that are VV, VH, HV and HH where V stands for vertical polarization and H for horizontal polarization. Such polarization outputs need particular preprocessing and color composition in order to view them in RGB (Red Green Blue) format for any classification and mapping process. The most important calibrations are spatial and spectral as well as speckle filtration (Figure 24). All these processes are available in SNAP (Sentinel Application Platform) and can be batched [134]. Aside, python algorithm set up and implemented under Quantum GIS (QGIS) is also available for data preprocessing. Sentinel 2A are optical data that are similar to Landsat OLI made of eight band.

Because of their weights, downloading Sentinel images in developing countries is quite difficult. Therefore, possibility of analyzing them without downloading them would

be useful. This kind of shortcut is possible on Visio Terra platform where the available preprocessed images are color composed and thus, make it easy to distinguish between classes. Such images have already gone through the processes highlighted in the dashed box of Figure 24. From that point, only color composition is needed to visualize the three main classes (water, vegetation and built up). Therefore, from the differentiation, flood extent is observed.

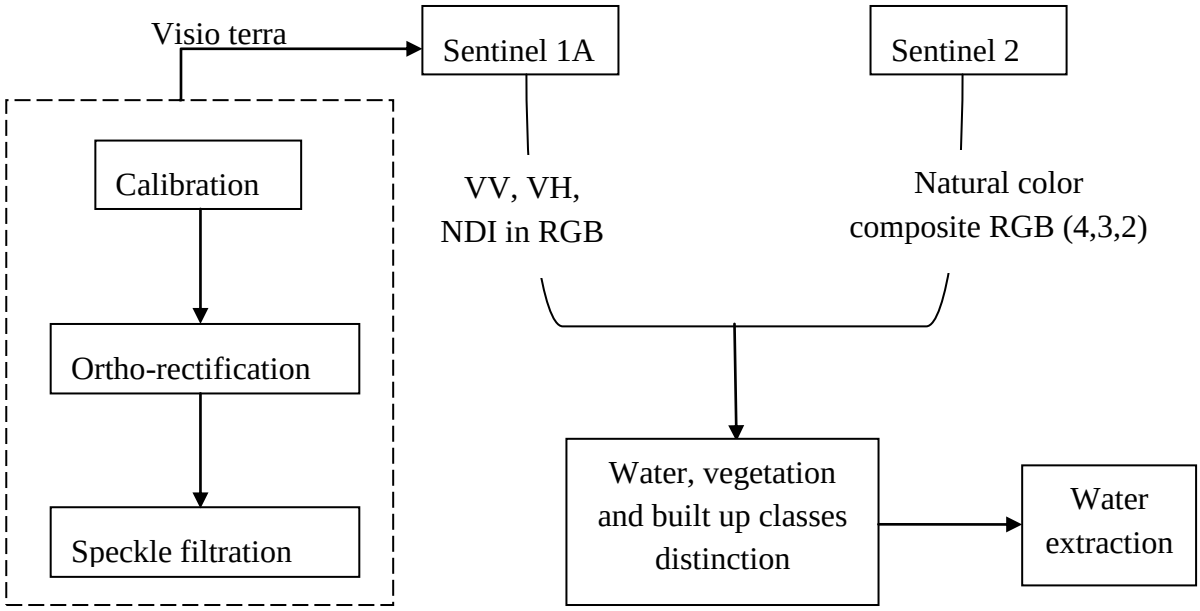

Figure 24. Image processing diagram.

Color composition of radar image Sentinel 1A of December 07, 2018 and optical image Sentinel 2A from December 10, 2010 are compared for calibration. Then validation is done using Sentinel 1A images over the period from August 9 till December 07, 2018. In fact, natural color composite (4-3-2) of Sentinel 2A image is done in order to distinguish between water, vegetation and soil. Such color composition show water in blue, vegetation in green, and soil in red. In order to put the radar image into the same color scale the following composition is processed: VV polarization is put in red, VH in green and NDI in blue. NDI stands for Normalized Deviation Index and is a standard index which expression is on Equation 7.

$$NDI = \frac{VV - VH}{VV + VH} \tag{9}$$

Consequently, due to backscatter effects, water and humid area appears in blue, vegetation in green and built up in yellowish and flooded vegetation in red. In order to confirm land use and cover classes, comparison is made between 2016 land use map from ESA and the proposed color composition result in December 2016. Moreover, rainfall occurrence influence over the pluvial flood mapping in 2018 is also analyzed based on Ouémé Delta average rainfall data from the Global Precipitation Measurement (GPM) data from the National Aeronautic and Space Administration (NASA).

3.3.5. Climate change impacts on Ouémé Delta hydrodynamic

3.3.5.1. Diffusion wave approach description

The complete Saint Venant equation system is as follow:

$$W_{,t} + F_1(W)_{,x} + F_2(W)_{,y} = S(W) \tag{10}$$

where

$$W = \begin{Bmatrix} h \\ hu \\ hv \end{Bmatrix} \tag{11}$$

$$F_1(W) = \begin{Bmatrix} hu \\ hu^2 + \frac{1}{2}gh^2 \\ huv \end{Bmatrix} \tag{12}$$

$$F_2(W) = \begin{Bmatrix} hv \\ huv \\ hv^2 + \frac{1}{2}gh^2 \end{Bmatrix} \tag{13}$$

$$S(W) = \begin{Bmatrix} q \\ -ghS_{fx} + gh\frac{\partial Z}{\partial x} + q\frac{u}{h} \\ -ghS_{fy} + gh\frac{\partial Z}{\partial y} + q\frac{v}{h} \end{Bmatrix} \tag{14}$$

with $h(x,y,t) \geq 0$ is water depth, $U(x,y,t) = (u,v)^T$ is water flow, S_{fx} and S_{fy} are friction slope in *x and y* directions. The friction slope, S_{fx} is given by

$$S_f = \frac{Q|Q|}{k^2} \tag{15}$$

where $k(x,y)$ is the conveyance. There are many common formulae for the conveyance, any of which may be used by the method described here, but here Manning's equation with $k = \frac{A^{5/3}}{nP^{2/3}}$ is used. $P(x,y)$ is the wetted perimeter and n is the Manning friction coefficient.

$Z = Z(x,y)$ accounts for bed level, in other word it is the channel bed elevation above some horizontal datum reference and g is the acceleration due to gravity.

q is the lateral inflow (that includes in our case: lateral river flow, rain, waste water, water withdrawals or other incompressible fluid due implications to anthropogenic impacts on the Delta. It is could be taken as followed: $q = q_n + q_l$ with q_n the net source term and q_l is every loss such evaporation, outtake of water from the lake. The inflow rate usually expressible in terms of rainfall is stochastic. Therefore, in order to consider its randomness, it can be represented as white noise process. In the frame of this work, we would leave the stochastic aspect that may a perspective for future work.

In addition, taking into account the overall distribution of peak discharge over time, water level rise in Ouémé delta couldn't be append to flash flood event. In fact, it is noticed in average, an increasing gradient that is about 100 m^3/s from June to July and 250 m^3/s from July to August while it is about 100 m^3/s from August to September considering daily discharge. Moreover, the annual peak stands from mid-September till mid-October where it starts decreasing weekly about 100 m^3/s till mid-November.

Thus, Ouémé Delta experiences well established flood with slow flow velocity instead of flash flood as in Netherland where flood occurs during a day. As consequences, the complete Saint Venant equations could be approximates with a diffusion wave equation

form, where inertial terms and velocity gradient within time are neglected whereas gravity and friction are preponderant. Therefore, the following terms $\frac{\partial u}{\partial t}$, $\frac{\partial v}{\partial t}$, $\frac{\partial u}{\partial x}$, $\frac{\partial v}{\partial x}$, $\frac{\partial u}{\partial y}$, $\frac{\partial v}{\partial y}$, $\frac{\partial(huv)}{\partial x}$ and $\frac{\partial(huv)}{\partial y}$ are negligible within the dynamic equation components from equations 10,11,12, 13 and 14.

3.3.5.2. Hydrodynamic modeling and robustness assessment

Daily propagation is simulated for the 365 days within a year to take into account seasonal variations. The calibration year is 2010 and the validation year is 2008 as detailed in Table 11 due to data availability. Based on the validated model, Bonou station discharge is reconstructed for the years 2016 and 2018.

Table 11. Hydrodynamic model simulation periods.

Model	Total Period	Calibration period	Validation period	Reconstruction and robustness assessment period
Hydrodynamic simulation	01/01/2008–31/12/2018	01/01/2010–31/12/2010	01/01/2008–31/12/2008	01/01/2016–31/12/2016 And 01/01/2018–31/12/2018

The hydrodynamic model calibration is done using the following schema (Figure 25).

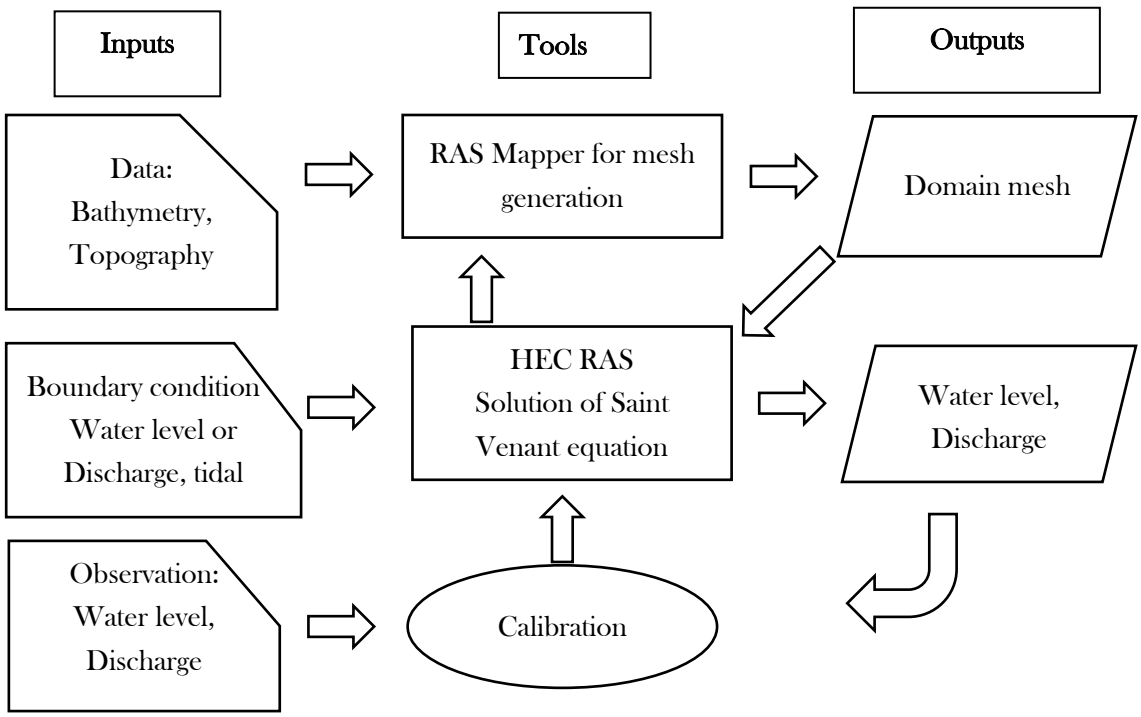

Figure 25. Hydrodynamic model calibration.

Once the model is calibrated, it is then used for validation. Based on the available data during the years 2016 (water level at Adjohoun, Hêtin-Sota and So-Ava stations) and 2018 (Nokoué Lake station) reconstruction is proceeded using respectively the interrelationship among stations and the hydrological model HEC-HMS outputs. In fact, interrelationship between water level at Bonou and Adjohoun is deducted based on the propagation of the average daily water level at Bonou from 1971 to 2010. Once this relationship is known, it is used to reconstruct water level at Bonou which is lacked in 2016. Then discharge from the hydrodynamic model is deducted at Bonou station. In order to assess the robustness of the hydrodynamic and the hydrologic model, discharge from both hydrodynamic model HEC-RAS and hydrologic model HEC-HMS is compared. Moreover, in the same line, 2018 discharge at Bonou is propagated in order to verify water level observation which is only at Nokoué Lake in that year.

3.3.5.3. Quantifying impacts of dam construction and climate change on Ouémé Delta hydrodynamic

Considering the governmental dam construction project, the projected volume that will be retained over Ouémé catchment at Bonou Outlet is roughly 3.5 billion of cubic meters [3]. In order to quantify impact of such huge retention on the Ouémé Delta functioning, the available water after construction is computed. In fact, average annual water volume which passes through Bonou station is computed based on the average discharge from 1971 to 2010. In addition, an equivalent hydrogram of the volume that is projected to be retained by the dam is deducted base on the average hydrogram profil. Available water hydrogram is then computed as the difference between the average hydrogram and the retention hydrogram. This available water hydrogram is propagated over the Delta to simulate Ouémé Delta average flood extent after dam construction. These impacts are analyzed taking into account the expected discharge reduction scenario at 2050 due to climate change impacts on Ouémé River discharge at Bonou outlet.

3.4. Partial conclusion

The overall data used are climatic and hydroclimatic such as: rainfall, temperature, relative humidity, wind speed and pan evaporation as well as water level and discharge. Moreover, satellite images like Sentinel 1A data are used for flood mapping The materials used are ClimPACT for extreme climatic indices computation and CMhyd for climate model data bias correction. Moreover, three hydrological models were tested: HBV, HEC-HMS and HyMoLAP. In addition, HEC-RAS is applied for the hydrodynamic modeling. Based on the available data and the materials used, trend analysis is done using the prewhitened Mann Kendall test. The empirical quantile mapping is the method used for climate model bias correction. Two loss methods are tested under the hydrological modeling: the curve number and the soil moisture accounting method. In order to well simulate peak flow an ensemble mean approach is adopted after comparison of the models separately using performance criteria and quantile curves. Land cover and flood mapping is

done using color composition to distinguish between classes. In the hydrodynamic model, the diffusion wave approximation is the method preferred because of its flexibility compared to the use of the entire Saint Venant equations.

Chapter 4: Change in Climate Extremes and Pan Evaporation Influencing Factors over Ouémé Delta in Bénin

Chapter 4 provides results of current climate extremes states in Ouémé Delta. Rainfall and temperature extremes indices analysis results are found in Section 4.1 and 4.2 respectively whereas Ouémé Delta climate drivers are detailed in Section 4.3. Discussion and partial conclusion are summarized in Section 4.3 and 4.4 respectively. These results are already published in MDPI Climate Journal [8] with the following doi: 10.3390/cli7010002. In this chapter, rainfall and temperature based indices, as well as maximum, minimum and mean of relative humidity, wind speed pan evaporation, and sunshine, are computed at annual scale. In addition, maximum Xday precipitation amount indices are computed at monthly scale to further understand extreme events in the Delta area. Moreover, monthly sunshine and pan evaporation trend is detected to assess their impact on water resources.

4.1. Rainfall trend analysis

The trend analysis results of rainfall in the Ouémé Delta are summarized below with numbers in bold indicating significant trend at 0.05 confidence level. Results show at annual scale that the prewhitening process did not add value to the trend analysis in the Ouémé Delta.

4.1.1 Trend analysis in annual precipitation

Results of rainfall intensity indices such as annual precipitation amount (PRCPTOT), numbers of heavy and very heavy precipitation days (R10mm, R20mm) as well as consecutive wet days (CWD), with significant trend, at least in one station are shown in Table 12.

Table 12. Annual rainfall intensity indices trends.

Stations	PRCPTOT			R10mm			R20mm			CWD		
	Tau	Sen Slope	*p* Value	Tau	Sen Slope	*p* Value	Tau	Sen Slope	*p* Value	Tau	Sen Slope	*p* Value
ABOMEY	−0.1	−1.8	0.6	−0.1	−0.1	0.4	−0.1	0.0	0.6	**–0.23**	**0**	**0.05**
ADJOHOUN	**0.3**	**8.4**	**0.0**	**0.3**	**0.3**	**0.0**	**0.3**	**0.2**	**0.0**	0.07	0	0.48
BOHICON	0.1	1.8	0.5	0.0	0.0	1.0	0.0	0.0	0.7	**–0.26**	**–0.02**	**0.01**
BONOU	**0.3**	**13.3**	**0.0**	**0.4**	**0.7**	**0.0**	**0.4**	**0.5**	**0.0**	–0.06	–0.01	0.63
COTONOU AIRPORT	0.0	0.0	1.0	0.0	0.0	0.6	0.0	0.0	0.8	**–0.20**	**–0.03**	**0.04**
KETOU	0.1	2.0	0.5	0.0	0.0	0.7	0.1	0.0	0.6	0.06	0	0.62
PORTO NOVO	**–0.2**	**–6.7**	**0.05**	**–0.3**	**–0.3**	**0.0**	–0.1	–0.1	0.4	**–0.45**	**–0.08**	**0**
ZAGNANADO	**0.3**	**10.3**	**0.0**	**0.3**	**0.4**	**0.0**	**0.3**	**0.2**	**0.0**	0.14	0.03	0.24

Rainfall intensity indices trend results showed in Table 12 are plotted on Figure 26.

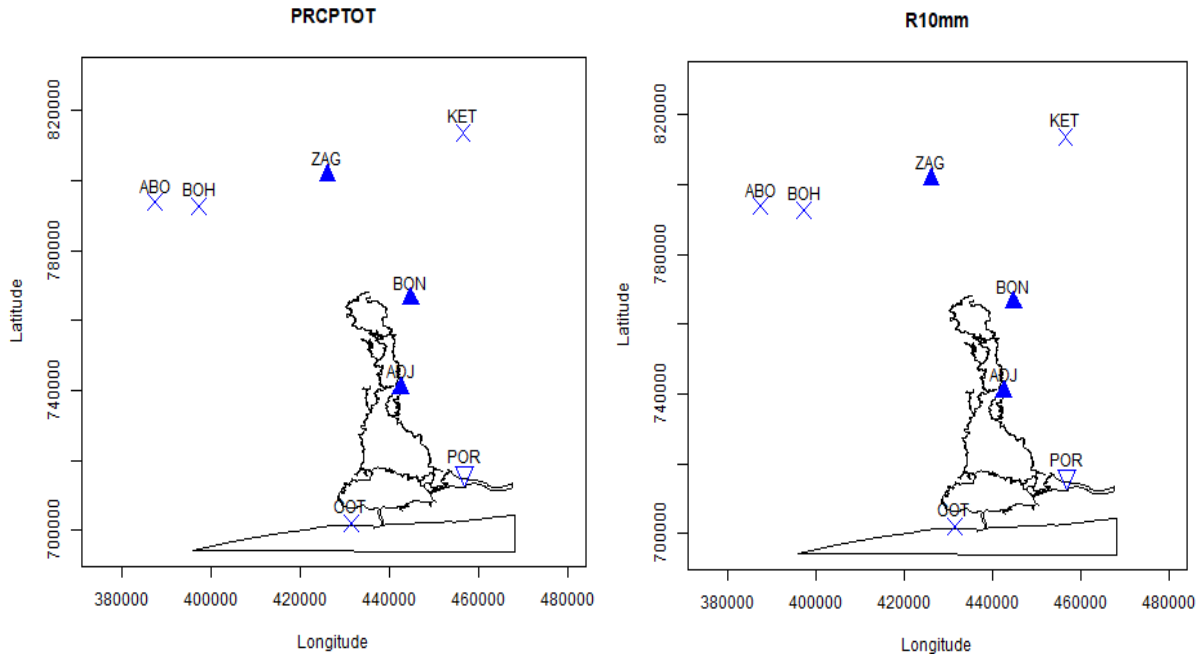

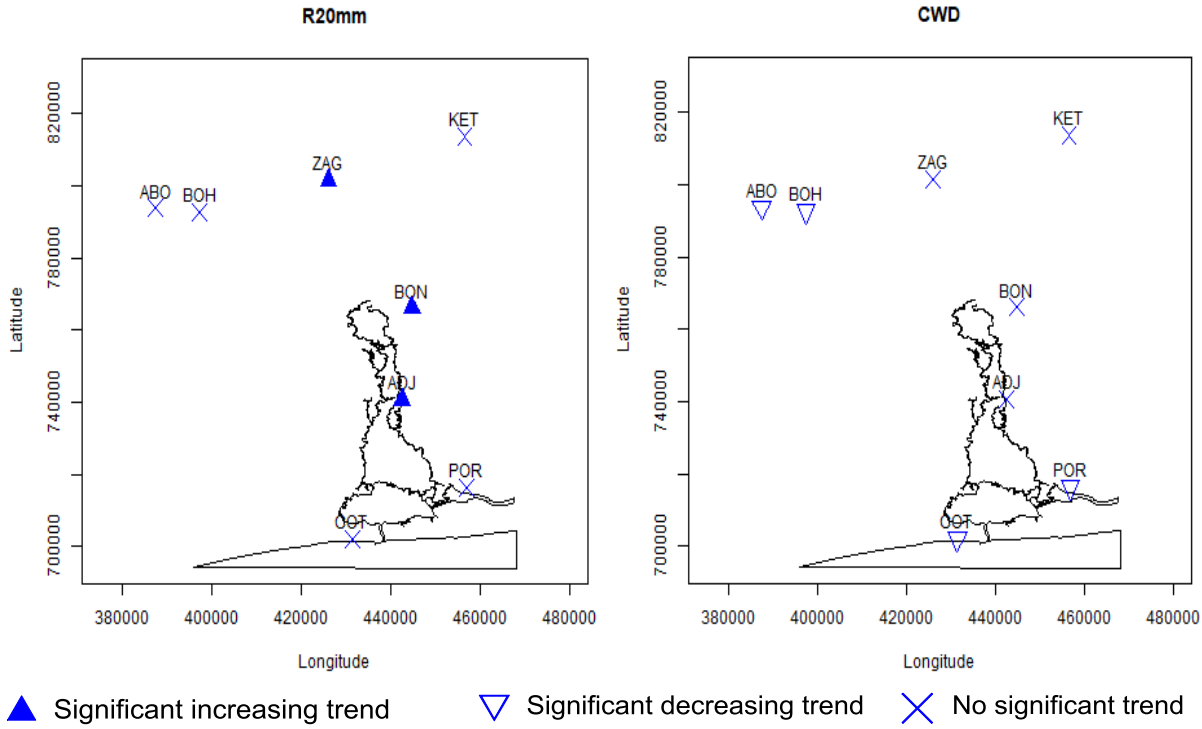

Figure 26. Plot of Annual total precipitation (PRCPTOT), R10mm, R20mm trend, and consecutive wet day (CWD) over Ouémé Delta.

Results of rainfall frequency indices like Simple daily intensity index (SDII), contribution from very wet days (R95pTOT**)** and contribution from extremely wet days (R99pTOT), with significant trend, at least in one station are shown in Table 13.

Table 13. Significant trend results of annual rainfall frequency indices.

Stations	SDII			R95pTOT			R99pTOT		
	Tau	Sen Slope	*p* Palue	Tau	Sen Slope	*p* Value	Tau	Sen Slope	*p* Value
ABOMEY	0.2	0.0	0.1	0.12	0	0.48	0.03	0	0.89
ADJOHOUN	**0.2**	**0.1**	**0.0**	–0.31	–0.01	0.06	**–0.37**	**0**	**0.02**
BOHICON	**0.2**	**0.0**	**0.0**	0.16	0	0.21	0.08	0	0.57
BONOU	**0.6**	**0.3**	**0.0**	–0.28	–0.01	0.35	0.11	0.01	0.75
COTONOU AIRPORT	0.0	0.0	0.6	0.26	0	0.08	0.15	0	0.33
KETOU	0.0	0.0	0.9	**–0.39**	**–0.01**	**0.018**	–0.04	0	0.83
PORTO NOVO	**0.3**	**0.1**	**0.0**	**0.33**	**0.01**	**0.048**	–0.24	0	0.16
ZAGNANADO	0.2	0.1	0.2	0.12	0	0.63	0.152	0	0.54

Rainfall frequency indices trend results showed in Table 13 are plotted on Figure 27.

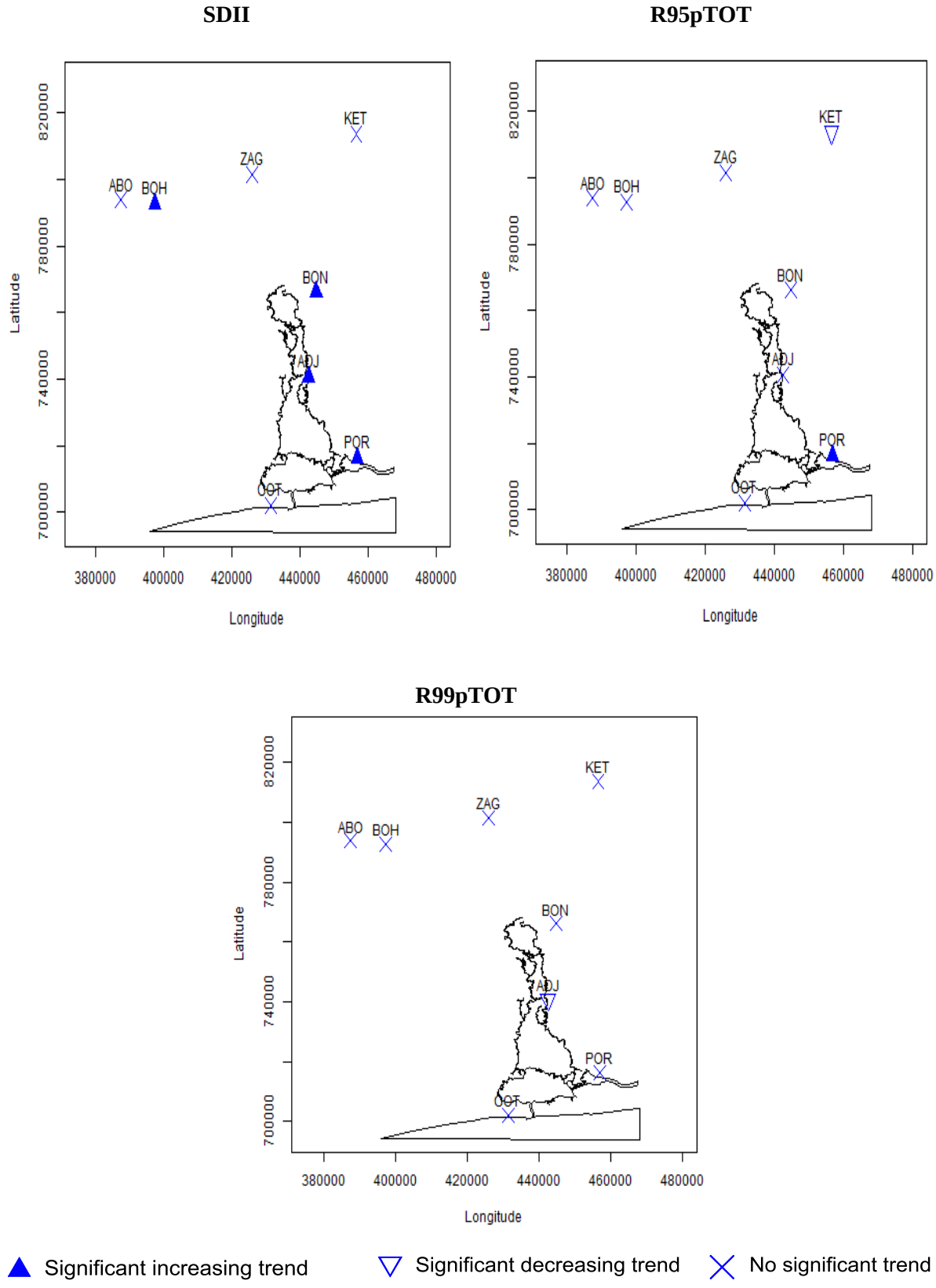

Figure 27. Plot of Simple daily intensity index (SDII), very wet day (R95pTOT), and extremely wet days (R99pTOT) trend over Ouémé Delta.

Rainfall indices with no significant trend are summarized in Table 14 and 15. At annual scale, no significant trend is detected for maximum one-day precipitation amount (RX1day) and maximum consecutive two-day precipitation amount (RX2day) over the entire Ouémé Delta as shown in Table 14. In addition, maximum consecutive three-day precipitation amount (RX3day) and maximum consecutive five-day precipitation amount (RX5day) also shows no significant trend over the entire study area, as shown in Table 14.

Table 14. Annual rainfall intensity indices with no trend.

Stations	RX1day			RX2day			RX3day			RX5day		
	Tau	Sen Slope	*p* Value	Tau	Sen Slope	*p* Value	Tau	Sen Slope	*p* Value	Tau	Sen Slope	*p* Value
ABOMEY	0.1	0.1	0.6	0.1	0.2	0.4	0.1	0.3	0.3	0.0	0.1	0.8
ADJOHOUN	0.1	0.1	0.6	0.0	0.0	1.0	0.1	0.3	0.4	0.1	0.2	0.6
BOHICON	0.1	0.1	0.4	0.2	0.4	0.1	0.1	0.2	0.3	0.0	0.1	0.7
BONOU	0.0	0.0	1.0	0.0	-0.1	0.8	0.0	–0.2	0.7	0.1	0.4	0.6
COTONOU AIRPORT	–0.1	–0.4	0.3	–0.1	–0.4	0.2	–0.1	–0.5	0.3	–0.1	–0.8	0.2
KETOU	0.0	0.0	1.0	0.1	0.3	0.4	0.1	0.2	0.5	0.1	0.5	0.2
PORTO NOVO	–0.1	–0.2	0.4	–0.1	–0.3	0.4	0.0	–0.3	0.7	–0.1	–0.7	0.3
ZAGNANADO	0.2	0.4	0.2	0.1	0.5	0.3	0.1	0.3	0.5	0.0	0.1	0.8

Similarly, intensity indices such as maximum consecutive 10-day precipitation amount (RX10day), annual total precipitation from very wet days (R95p), and annual total precipitation from extremely wet days (R99p) show no significant trend over the entire study area (Table 15).

Table 15. Annual consecutive dry day (CDD), very wet day (R95p), and extremely wet day (R99p) indices trend with no trend

Stations	RX10day			R95p			R99p			CDD		
	Tau	Sen Slope	*p* Value	Tau	Sen Slope	*p* Value	Tau	Sen Slope	*p* Value	Tau	Sen Slope	*p* Value
ABOMEY	–0.1	–0.2	0.6	0.1	1.3	0.3	0.1	0.0	0.6	0.014	0.043	0.895
ADJOHOUN	0.1	0.3	0.5	0.0	0.6	0.7	0.0	0.0	0.9	–0.11	–0.265	0.298
BOHICON	0.1	0.3	0.4	0.1	1.3	0.2	0.0	0.0	0.7	0.083	0.229	0.369
BONOU	0.1	1.0	0.4	0.0	–0.5	0.8	0.0	0.0	0.7	0.123	0.564	0.321
COTONOU AIRPORT	–0.1	–0.7	0.2	–0.1	–0.9	0.5	–0.1	0.0	0.5	0.081	0.141	0.381
KETOU	0.0	0.1	0.9	0.0	0.0	1.0	0.0	0.0	0.7	0.198	0.811	0.077
PORTO NOVO	–0.1	–0.5	0.5	–0.1	–1.4	0.5	–0.1	0.0	0.3	0.073	0.179	0.474
ZAGNANADO	0.1	0.4	0.4	0.1	2.4	0.4	0.1	0.0	0.4	0.146	0.668	0.222

Annual total precipitation (PRCPTOT) shows a significant decreasing trend of about 6.7 mm/year at the southeast station Porto Novo, whereas from North to South, Zagnanado, Bonou, and Adjohoun show significant increasing trends (Figure 26), respectively, with slopes of 10.3, 13.3, and 8.4 mm/year.

Consecutive dry day (CDD) shows no significant trend over the entire area of study, as shown on Table 15. However, consecutive wet day (CWD) is significantly slightly decreasing at Abomey, Bohicon, Porto Novo, and Cotonou Airport as displayed by Figure 27. The number of heavy and very heavy precipitation days (R10mm, R20mm) increases at Zagnanado, Bonou, and Adjohoun (Figure 26). However, the number of heavy precipitation days decreases at Porto- Novo. Contribution from very wet days (R95pTOT) shows an increasing trend only at Porto Novo (Figure 27), whereas contribution from extremely wet days (R99pTOT) decreases at Adjohoun (Figure 27). Simple daily intensity index (SDII) increases at Adjohoun, Bonou, and Porto Novo (Figure 27), respectively, with slope of 0.1, 0.3 and 0.1.

Increase in annual total precipitation is due to more frequent heavy and very heavy rainfall event. This intensification in the frequency of extreme rainfall events will result in high peak flow and then more damageable flood events in the high water period. Moreover, the most impacted areas are going to be those closer to Ouémé Delta, since significant trends are detected at the closest stations.

4.1.2. Trend Analysis in Monthly Maximum Precipitation

In order to detect change in intense precipitation at short time scale, monthly trends have been assessed on maximum 1, 2, 3, 5, and 10 days precipitation at all stations. Results are shown below with numbers in bold showing significant trend at the 0.05 confidence level. Maximum 1 and 2 days precipitation results are shown in Table 16 whereas Maximum 3 and 5 days precipitation results are illustrated in Table 17.

Table 16. Monthly trend analysis of one-day precipitation amount (RX1day) and two-day precipitation amount (RX2day) during high water.

Stations	RX1day									RX2day								
	SEP			OCT			NOV			SEP			OCT			NOV		
station	Tau	Sen Slope	p Value	Tau	Sen Slope	p Value	Tau	Sen Slope	p Value	Tau	Sen Slope	p Value	Tau	Sen Slope	p Value	Tau	Sen Slope	p Value
ABOMEY	0.0	0.1	0.7	–0.1	–0.1	0.6	0.0	0.0	0.9	0.0	0.1	0.8	–0.1	–0.2	0.4	0.0	0.0	0.9
ADJOHOUN	0.0	0.0	0.9	0.2	0.2	0.1	**0.3**	**0.5**	**0.0**	0.0	0.0	1.0	**0.3**	**0.5**	**0.0**	**0.4**	**0.6**	**0.0**
BOHICON	0.1	0.2	0.2	0.1	0.2	0.3	0.1	0.1	0.4	0.2	0.3	0.1	0.1	0.1	0.5	0.2	0.2	0.1
BONOU	0.1	0.2	0.4	**0.3**	**0.4**	**0.0**	0.0	0.0	0.9	0.1	0.2	0.6	**0.3**	**0.5**	**0.0**	0.1	0.2	0.3
COTONOU AIRPORT	**0.2**	**0.4**	**0.0**	0.1	0.1	0.4	0.0	0.0	0.8	**0.2**	**0.4**	**0.0**	0.0	0.1	0.8	0.0	0.0	0.9
KETOU	0.1	0.1	0.6	**0.2**	**0.3**	**0.0**	0.1	0.1	0.3	0.0	0.1	0.8	**0.2**	**0.4**	**0.0**	0.1	0.1	0.3
PORTO NOVO	0.2	0.5	0.1	0.0	0.1	0.8	**–0.3**	**–0.4**	**0.0**	0.1	0.5	0.1	0.0	0.1	0.8	**–0.3**	**–0.4**	**0.0**
ZAGNANADO	0.1	0.3	0.5	0.1	0.3	0.3	0.0	0.0	0.9	0.1	0.5	0.2	0.1	0.2	0.5	0.0	0.0	1.0

Maximum 3 and 5 days precipitation results are shown in Table 17.

Table 17. Monthly trend analysis of three-day precipitation amount (RX3day) and five-day precipitation amount (RX5day) during high water.

Stations	RX3day									RX5day								
	SEP			OCT			NOV			SEP			OCT			NOV		
	Tau	Sen Slope	*p* Value	Tau	Sen Slope	*p* Value	Tau	Sen Slope	p Value	Tau	Sen Slope	*p* Value	Tau	Sen Slope	*p* Value	Tau	Sen Slope	*p* Value
ABOMEY	0.0	0.1	0.7	–0.1	–0.2	0.3	0.1	0.1	0.6	0.1	0.3	0.5	0.0	0.0	0.9	0.0	0.0	0.9
ADJOHOUN	0.0	0.1	0.7	**0.3**	**0.6**	**0.0**	**0.3**	**0.6**	**0.0**	0.1	0.4	0.5	**0.4**	**1.0**	**0.0**	**0.4**	**0.9**	**0.0**
BOHICON	0.2	0.4	0.1	0.1	0.2	0.5	0.1	0.2	0.1	**0.2**	**0.6**	**0.0**	0.1	0.3	0.3	0.1	0.2	0.2
BONOU	0.1	0.3	0.3	**0.3**	**0.6**	**0.0**	0.1	0.2	0.3	0.1	0.3	0.3	**0.3**	**0.9**	**0.0**	0.2	0.5	0.1
COTONOU AIRPORT	**0.2**	**0.5**	**0.0**	0.0	0.1	0.8	0.0	0.0	0.9	**0.2**	**0.6**	**0.0**	0.1	0.4	0.2	0.0	0.0	0.9
KETOU	0.1	0.2	0.4	0.1	0.3	0.3	0.1	0.2	0.2	0.1	0.3	0.4	**0.2**	**0.6**	**0.0**	0.2	0.3	0.2
PORTO NOVO	0.2	0.7	0.1	0.1	0.2	0.3	**–0.3**	**–0.4**	**0.0**	0.1	0.8	0.1	0.2	0.5	0.1	**–0.2**	**–0.5**	**0.0**
ZAGNANADO	**0.2**	**0.8**	**0.0**	0.1	0.3	0.4	0.0	0.0	1.0	**0.3**	**1.0**	**0.0**	**0.2**	**0.7**	**0.0**	0.0	0.0	0.8

Maximum 10 days precipitation results are shown in Table 18.

Table 18. Monthly trend analysis of ten-day precipitation amount (RX10day) during high water.

Stations	SEP			OCT			NOV		
	Tau	**Sen Slope**	***p* Value**	**Tau**	**Sen Slope**	***p* Value**	**Tau**	**Sen Slope**	***p* Value**
ABOMEY	0.1	0.5	0.3	0.0	0.0	0.9	0.0	0.0	0.9
ADJOHOUN	0.1	0.6	0.3	**0.3**	**1.4**	**0.0**	**0.4**	**1.4**	**0.0**
BOHICON	**0.2**	**0.8**	**0.0**	0.1	0.4	0.2	0.1	0.2	0.5
BONOU	**0.2**	**1.2**	**0.0**	**0.3**	**1.1**	**0.0**	0.0	0.1	0.8
COTONOU AIRPORT	**0.2**	**0.8**	**0.0**	**0.2**	**0.7**	**0.1**	0.0	0.0	0.9
KETOU	0.1	0.6	0.3	0.2	0.7	0.1	0.2	0.5	0.1
PORTO NOVO	0.1	0.8	0.2	**0.2**	**0.7**	**0.1**	**–0.3**	**–0.9**	**0.0**
ZAGNANADO	**0.3**	**1.8**	**0.0**	0.2	0.7	0.2	0.0	0.1	0.8

At monthly scale, maximum consecutive 1, 2, and 3-day precipitation amount showed significant increasing trend in Adjohoun in February (Table 17). In addition, maximum consecutive 10-day precipitation amount significantly decreased at Porto Novo in March. Maximum one-day precipitation increased significantly at Cotonou Airport in September. In October, maximum consecutive 10 days precipitation increased significantly at Cotonou Airport and Porto Novo. The trends listed above were detected only after prewhitening.

In April, Bonou station showed a significant decreasing trend for maximum consecutive 2, 3, and 5-day precipitation amount (Table 18). As consequence, water stress may probably impact on garden products yield in Bonou. In addition, maximum consecutive 5-day precipitation in Cotonou Airport decreased significantly for the same month. In contrary, Zagnanado showed significant increasing trend for maximum consecutive 2 and 3-day precipitation, whereas Adjohoun increased significantly only for maximum consecutive 3-day precipitation. In July, Bohicon and Zagnanado maximum 3 and 5-day increased significantly, while maximum consecutive 10-day significantly decreased at Porto Novo. It seems to be the most watered area during the first rainy season, which is from April to July. In August, maximum consecutive 2, 3, 5, and 10-day significantly increased only at Zagnanado. Thus, Agriculture at Zagnanado may less suffer from water stress, but may be susceptible to flood event.

In Ouémé Delta, high water period runs from September to November [6]. In September, maximum consecutive 1, 2, 3, 5, and 10-days precipitation exhibits a significant increasing trend at Cotonou Airport. Only Maximum consecutive 3, 5, and 10-days precipitation increased at Zagnanado. Maximum consecutive 5 and 10-days precipitation at Bohicon as well as maximum consecutive 10 days precipitation increased at Bonou. In October, maximum 1, 2, 3, 5, and 10-day precipitation increased significantly at Bonou. Maximum consecutive 1, 2, and 5-days precipitation increased significantly at Kétou. Maximum consecutive 2, 3 and 5 days precipitation increased significantly at Adjohoun. Only maximum consecutive 5 days precipitation increased significantly at Zagnanado. In November, maximum consecutive 1, 2, 3, 5, and 10-days precipitation increased significantly only at Adjohoun, but they all decreased significantly at Porto Novo.

In general, most of the stations showed increasing trend at least for one of the maximum 1, 2, 3, 5, and 10-days precipitation amount in the months of September, October, and November, except Porto Novo, which showed a decreasing trend for all of these indices in November. With these findings, more attention needs to be given and efforts have to be made for developing an early warning system in the Delta area in order to reduce the impacts on agriculture and on human livelihood.

4.1. Trend Analysis in Temperature, Relative Humidity, Pan Evaporation, Sunshine Duration and Wind Speed at 10m Altitude

The trend of each climatic variable, such as temperature, relative humidity, and wind speed in this section was computed at the annual scale taking into account the mean, minimum, and maximum at the two synoptic stations that fall in the Delta area. Sunshine and pan evaporation were computed at annual as well as monthly scale. Table 19 shows results of temperature based indices trend.

Table 19. Temperature based indices trend.

Stations	TXn			TXx			TNn			TNx		
	Tau	Sen Slope	*p* Value	Tau	Sen Slope	*p* Value	Tau	Sen Slope	*p* Value	Tau	Sen Slope	*p* Value
BOHICON	**0.22**	**0.03**	**0.01**	**0.22**	**0.02**	**0.01**	**0.2**	**0.04**	**0.03**	**0.4**	**0.02**	**0**
COTONOU AIRPORT	**0.40**	**0.04**	**0**	**0.22**	**0.02**	**0.02**	0.07	0.01	0.5	**0.4**	**0.03**	**0**
Stations	DTR			WSDI2			TX95t			TN95t		
	Tau	Sen Slope	*p* Value	Tau	Sen Slope	*p* Value	Tau	Sen Slope	*p* Value	Tau	Sen Slope	*p* Value
BOHICON	**–0.34**	**–0.01**	**0**	**0.26**	**0.248**	**0.01**	**–0.28**	**–0.01**	**0**	**–0.30**	**–0.01**	**0**
COTONOU AIRPORT	**–0.29**	**–0.01**	**0**	**0.3**	**0.38**	**0**	**–0.31**	**–0.01**	**0**	**–0.30**	**–0.01**	**0**

Table 20 shows results of minimum, maximum and mean value at annual scale for maximal relative humidity.

Table 20. Maxima relative humidity based on annual minimum, maximum, and mean.

Stations	Maximal Relative Humidity								
	Minimum			Maximum			Mean		
	Tau	Sen Slope	*p* Value	Tau	Sen Slope	*p* Value	Tau	Sen Slope	*p* Value
BOHICON	**-0.43**	**0**	**0**	**-0.3**	**-0.5**	**0.004**	**-0.34**	**-0.05**	**0.001**
COTONOU AIRPORT	**-0.29**	**0**	**0.02**	**-0.22**	**-0.12**	**0.04**	**-0.51**	**-0.06**	**0**

Table 21 shows results of minimum, maximum and mean value at annual scale for wind speed at 10 m altitude.

Table 21. Wind speed at 10 m altitude based on annual minimum, maximum, and mean

Stations	Wind Speed at 10 m Altitude								
	Minimum			Maximum			Mean		
	Tau	Sen Slope	*p* Value	Tau	Sen Slope	*p* Value	Tau	Sen Slope	*p* Value
BOHICON	**-0.32**	**-0.03**	**0.004**	0.17	0	0.17	**-0.26**	**-0.01**	**0.01**
COTONOU AIRPORT	-0.04	0	0.72	0.14	0.01	0.2	**-0.22**	**-0.01**	**0.03**

At annual scale, all temperature based indices considered show a significant increasing trend at the two synoptic stations except the diurnal temperature (DTR), very warm day (TX95t), and very cold day (TN95t) temperature thresholds that decreased about 0.01 °C in average, as shown in Table 10. In fact, annual minimum (TXn) and annual

maximum (TXx) of daily maximal temperature as well as annual minimum (TNn) and annual maximum (TNx) of daily minimal temperature showed significant increasing trends, respectively of 0.03 °C, 0.02 °C, 0.03 °C, and 0.03 °C in average, as shown in Table 19. In addition, two days warm spell duration (WSDI2) showed an increasing trend of 0.308 °C in average (Table 19). Annual mean of minimal relative humidity exhibits an increasing trend at Bohicon station, however annual minimum, maximum, and mean of relative humidity maxima show a decreasing trend running from 0.047 to 0.5 % (Table 20). Annual wind speed at 10 m altitude showed a slighter decreasing trend between 0.01 and 0.03 (Table 21).

Monthly and annual significant trend results for sunshine and pan evaporation are shown in Table 22.

Table 22. Monthly and annual significant trend for sunshine and pan evaporation.

	COTONOU AIRPORT						BOHICON					
	SUND			EVA			SUND			EVA		
Stations	**Tau**	**Sen Slope**	***p* Value**	**Tau**	**Sen Slope**	***p* Value**	**Tau**	**Sen Slope**	***p* Value**	**Tau**	**Sen Slope**	***p* Value**
January	**–0.33**	**–1.08**	**0.00**	**0.5**	**0.7**	**0**	–0.19	–0.58	0.08	0.3	0.9	0.1
February	**–0.27**	**–0.63**	**0.01**	0.2	0.4	0.1	–0.15	–0.22	0.27	–0.3	–0.4	0.1
March	–0.18	–0.52	0.09	**0.4**	**0.6**	**0**	0.02	0.03	0.88	–0.1	–0.1	0.7
April	**–0.28**	**–0.55**	**0.01**	0	0	0.9	–0.02	–0.03	0.85	0.1	0.3	0.5
May	**–0.27**	**–0.84**	**0.01**	**0.3**	**0.5**	**0**	–0.04	–0.05	0.70	0	–0.1	0.9
June	–0.17	–0.56	0.12	**0.3**	**0.6**	**0**	–0.19	–0.41	0.06	0	–0.1	0.9
July	–0.13	–0.48	0.22	**0.3**	**0.4**	**0**	0.11	0.23	0.29	**0.3**	**0.6**	**0**
August	–0.03	–0.08	0.80	0.1	0.2	0.2	0.1	0.18	0.36	0	0.2	0.8
September	–0.03	–0.05	0.79	0.1	0.2	0.3	0.15	0.34	0.14	0	0	1
October	**–0.21**	**–0.38**	**0.04**	0	0.1	0.8	0.16	0.4	0.14	0.1	0.3	0.3
November	–0.10	–0.22	0.34	0.1	0.2	0.2	0.17	0.26	0.09	0	–0.2	0.8
December	0.07	0.18	0.50	**0.5**	**0.8**	**0**	**0.29**	**0.68**	**0.01**	**0.3**	**1**	**0**
Annual	**–0.45**	**–5.28**	**0.00**	**0.3**	**4.4**	**0**	0.13	1.17	0.28	0.1	3.4	0.4

At annual scale, Sunshine duration decreased significantly, whereas evaporation increased over Ouémé Delta (Table 22). At monthly scale, sunshine decreases significantly in the month of January, February, April, May, and October in Cotonou. Pan evaporation increases significantly in the month of January, March, May, June, July, and September in Cotonou.

4.2. Ouémé Delta Climate Drivers

As shown in Table 23, the significant variables that positively influence pan evaporation are sunshine duration (SUND), precipitation (PRCP), wind speed (WIND), mean temperature (TMean), and maximum temperature (TMax), decreasingly based on the correlation coefficients. Relative humidity parameters (RH, Hmax, and Hmin) negatively influence pan evaporation in Ouémé Delta. Thus, an increase in relative humidity decrease pan evaporation and vice versa. Dominant climatic variables with more than 10% absolute value of correlation with pan evaporation are mean relative humidity (RH), maximum relative humidity (Hmax), mean temperature (Tmean), wind speed (WIND), precipitation (PRCP), and sunshine (SUND).

Table 23. Correlation coefficient of pan evaporation with mean relative humidity (RH), maximal relative humidity (Hmax), minimal relative humidity (Hmin), minimal temperature (Tmin), maximal temperature (Tmax), mean temperature (Tmean), wind speed at 10 m altitude (WIND), precipitation (PRCP), and sunshine duration (SUND).

Climate variables	COTONOU AIRPORT		BOHICON	
	Coef	P.Value	Coef	P.Value
RH	–0.23	0.00	-0.24	0.00
Hmax	–0.12	0.00	-0.13	0.00
Hmin	–0.07	0.00	-0.04	0.00
TMin	0.02	0.00	0.01	0.12
TMax	0.04	0.00	0.12	0.00
Tmean	0.12	0.00	0.21	0.00
WIND	0.23	0.00	0.19	0.00
PRCP	0.25	0.00	0.24	0.00
SUND	0.47	0.00	0.25	0.00

Table 24 showed the relative importance of these dominant climatic variables in pan evaporation. By considering the regression coefficients, mean temperature, sunshine duration, and wind speed have high relationship with pan evaporation at both stations at 0.001 level of confidence.

Table 24. Stepwise regression coefficient of pan evaporation and relative humidity (RH), mean temperature (Tmean), wind speed at 10 m altitude (WIND), precipitation (PRCP), and sunshine duration (SUND).

Climate variables	COTONOU AIRPORT					BOHICON			
	Coef	Std. Error	t value	Pr(> |t|)		Coef	Std. Error	t value	Pr(> |t|)
WIND	0.24	0.01	28.41	0***	WIND	0.26	0.01	20.46	0***
SUND	0.22	0.00	68.16	0***	SUND	0.14	0.00	31.60	0***
Tmean	0.14	0.01	19.83	0***	Tmean	0.25	0.01	29.59	0***
PRCP	0.03	0.00	33.17	0***	PRCP	0.03	0.00	26.25	0***
RH	–0.05	0.00	–24.53	0***	RH	–0.04	0.00	–17.01	0***

*** Significant at 0.001 level of confidence

At Cotonou Airport, mean temperature, sunshine duration, and wind speed, respectively, explained pan evaporation at 20, 22, and 33%, as shown on Figure 28. However, at Bohicon, sunshine duration, mean temperature, and wind speed explained pan evaporation, respectively, at 19, 33, and 35 %.

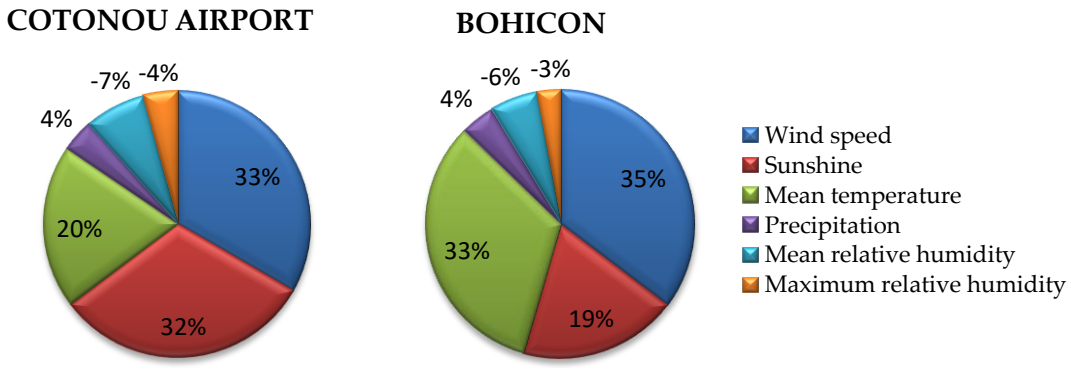

Figure 28. Plot of the percentage of pan evaporation variance hold in each of its explanatory variables**.**

4.3. Discussions

Increasing trends in heavy and very heavy rainfall extreme are in accordance with Hounkpè et al. [27], which noticed an East West gradient from negative to positive trend in interpolated change rainfall in lower Ouémé catchment. Moreover, decreasing trend in annual rainfall at Porto-Novo in the eastern part of the Delta is in line with regional trends as showed in Nigeria by Oguntunde et al. [40], Kabo-bah et al. [25] in Ghana hydropower dam, as well as in Ivory Coast by Soro et al. [23]. However, increase of Simple daily intensity index (SDII) with 0.11 slope demonstrates evidence of intensification of heavy rainfall, whereas the contribution from very wet day is almost constant. Even though,

annual total precipitation decreased, the amount of rainfall recorded occurs in short period as found by Panthou et al. [21] for West Africa semi-arid regions. This is more visible when trend analysis is conducted at monthly scale. Thus, the area is experiencing the erratic rainfall announced for the West African coastal area by the intergovernmental panel on climate change in the fifth report [14]. In September, November, and October, Maximum consecutive 10-days rainfall increased significantly, as evidence of rainfall intensification, especially in the high water period over the Delta, as shown by Hounkpè et al. [27] over Ouémé Basin. These changes in rainfall extreme indices trends will impact extreme events like flood occurrence, as noticed by Nka et al. [135] and Guhathakurta et al. [136]. In addition, the increasing trend in air temperature as a result of global warming experienced in Ouémé Delta was predicted by the Intergovernmental Panel on Climate Change, with impacts on irrigated land and then reducing agricultural yield that is sensitive to water availability [35]. Though, the change in temperature noticed in this dissertation are relatively slight, the overall country experienced an increase of 1.1 °C since 1960, as mentioned by Bodegom et al. [137]. Pan evaporation as key element in surface water resource management has been taken together with rainfall, sunshine duration, relative humidity, wind speed, as well as temperature to detect those to which it is sensitive. Results showed that most significant explainers of pan evaporation detected here are also found in Chinese Lower Yellow River Basin for the period 1961 to 2010 by Xing-Jie et al. [39]. In fact, combined effects of decrease in wind speed and sunshine duration with an increase in mean temperature are the main causes for decrease in pan evaporation in that area. Moreover, Sun radiation, wind speed, and vapor pressure deficit were found to be explanatory variables of pan evaporation in Ibadan in Nigeria over the period of 1973–2008 using principal component analysis for variable selection by Oguntunde et al. [40]. In fact, they showed that sun radiation, wind speed, and vapor pressure deficit, respectively, explained pan evaporation variance at 30, 15, and 6%. The main explanatory variables of pan evaporation found in this study are the same as those of Liu et al. [114]. In fact, they found daily temperature range, sunshine duration, and average wind speed to be the main influencing factors of pan evaporation, and even the determinative factors of its trend. However, air temperature and vapor pressure are the major factors impacting pan evaporation in Zoige Plateau alpine wetland of eastern Tibetan region, as reported by Zhao et al. [138]. Though vapor pressure was one of the main explanatory variables cited in some regions, they were not available in our study area. In addition, despite the difference in climate variables considered in searching for pan evaporation influencing factors, wind

speed, sunshine duration, and temperature are found to be the main drivers of pan evaporation. An increase in temperature and pan evaporation combined with decrease in wind speed could increase heat stress in plant, as shown by Hoffman et al. [139]. Consequently, such situation could favor livestock migration and then trigger conflict between farmers and herders, as observed in West African regions and reported by Touré et al. [35]. Furthermore, increase in temperature and flood event will also positively impact on the spread of infectious diseases, like malaria, which accounts for about 41% of all visits to health centers in Bénin [140]. In fact, more standing water will increase the habitats for malaria vectors that are mosquito, whereas increased temperatures and prolonged dry seasons will have the potential to extend the vector's seasonal window, exposing human population to the risk of this disease.

4.4. Partial conclusion

This work analyzed trends in rainfall and temperature extremes, as well as pan evaporation influencing factors over Ouémé Delta in Bénin. Fifteen rainfall based climate indices; eight temperature based indices as well as minimal relative humidity, maximal relative humidity, sunshine duration, wind speed at 10 m altitude, and pan evaporation at annual scale were computed at eight gauging stations (including two synoptic stations) from 1960 to 2016. Prewhitened Mann–Kendal method furthered trend detection over Ouémé Delta, especially at monthly scale, by removing the internal serial correlation. Results showed intensification in heavy rainfall frequency with increase in monthly maximum precipitation in the months of September, October, and November, which constitute the high water period in Ouémé Delta. As results showed a clear increase in extreme rainfall, especially heavy, very heavy rainfall, maximum consecutive 1, 2, 3, 5, and 10-day maximum, it will probably impact flood event in damages and losses in Ouémé Delta. Most impacted areas will be those with positive trends and are found to be the closest to Ouémé Delta. An increase in temperature as a consequence of global warming and a decrease in relative humidity are going to put stress on plants in terms of water availability. Water loss in rivers is basically measured using pan evaporation. Furthermore, explanatory climatic variables that influence pan evaporation in Ouémé Delta area are wind speed, mean temperature, and sunshine duration, with wind speed and sunshine explaining its variance at almost 50%. In this work, pan evaporation showed a significant increasing trend given evidence of an increase in surface water loss over Ouémé Delta River and ponds. Consequently, water availability issue is probably going to be problematic with rise

in conflicts between farmers and herders because of livestock migrations. In addition, a decrease in surface water combined with increasing temperature will result in the loss in biodiversity and ecosystem production function in Nokoué Lake. With an increase in frequent extreme rainfall events, an early warning system has to be well set for damages and losses prevention in Ouémé Delta, the food basket of Southern Bénin. Moreover, with an increase in surface water evaporation, actions have to be taken for efficient water usage. For instance, clipping dam in the upper stream of Ouémé Delta could help in overflow water storage for future use, like irrigation. In addition, health facilities should be developed and well equipped to cater for needs.

Chapter 5: Impact of climate change on Ouémé river discharge

Chapter 5 presents results from the regional climate model bias correction in Section 5.1, the runoff modeling using HEC-HMS based the curve number method in section 5.2 as well as the climate change impacts assessment in Section 5.3. Discussion and partial conclusion are presented in Section 5.4 and 5.5 respectively. These results are already published in MDPI Hydrology journal [5] with the following doi: 10.3390/hyd6030072.

5.1 Regional climate model bias correction

5.1.1 Rainfall

Result of catchment averaged rainfall after bias correction is shown on Figure 29. On graphical basis, seasonal regime of corrected models fits well that of observation.

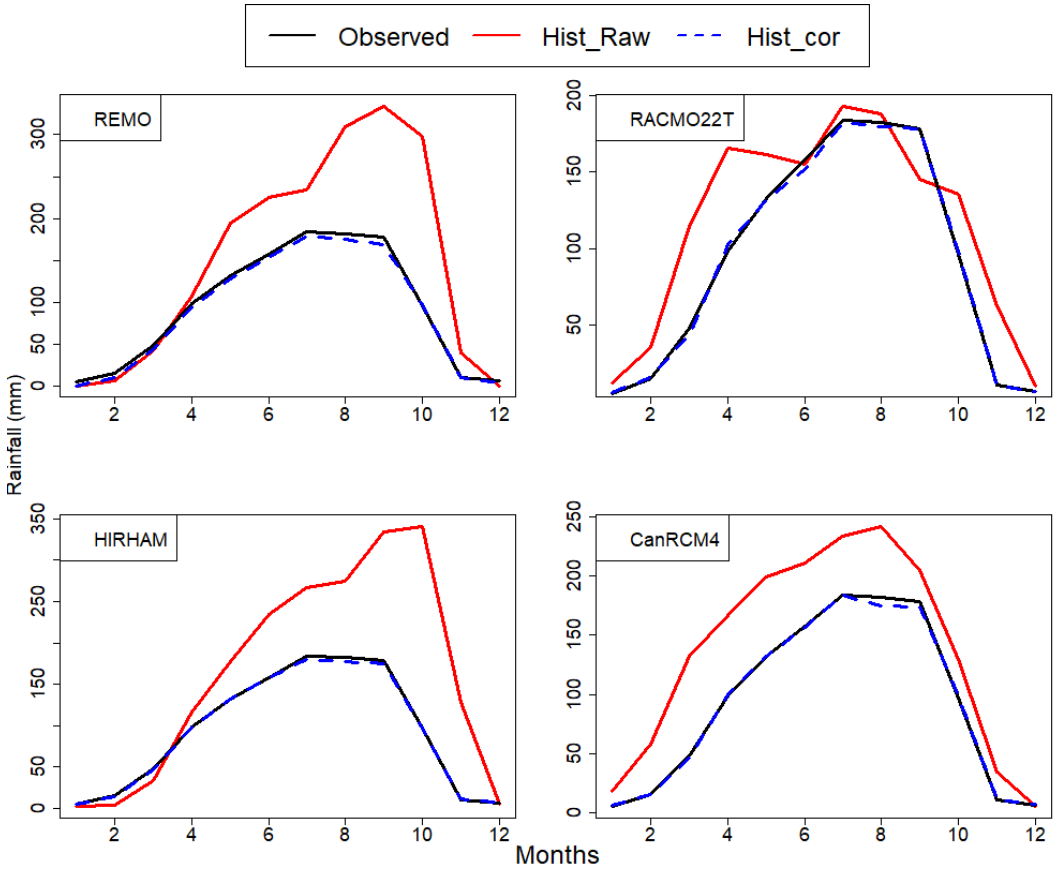

Figure 29. Comparison of raw and bias corrected rainfall with observation at seasonal scale over the historical period 1971 – 2005

The agreement between observed and corrected data is confirmed by the efficiency coefficients computed below. Bias correction performance is assessed using the KGE and the PBIAS and summarized in Table 25.

Table 25. Bias correction efficiency at seasonal scale

	KGE		PBias	
	Before correction	After correction	Before correction	After correction
REMO	0.01	0.95	60.7	-4.6
RACMO22T	0.73	0.99	23.6	-0.8
HIRHAM	-0.06	0.98	71.7	-1.6
CanRCM4	0.50	0.98	46.5	-1.1

After bias correction, KGE of all the models is equal or more than 0.95 with an absolute percentage of bias between 0.8 and 4.6. In average the quantile mapping method used here showed good performance at models' bias correction. However, RACMO22T is the best corrected with a KGE of 0.99 and 0.8% of underestimation of observation followed by CanRCM4 and HIRHAM, which KGE is 0.98 with respectively 1.1 and 1.6 of underestimation.

Result of bias correction at daily scale is shown on Figure 30. Bias corrected and observation superposed well.

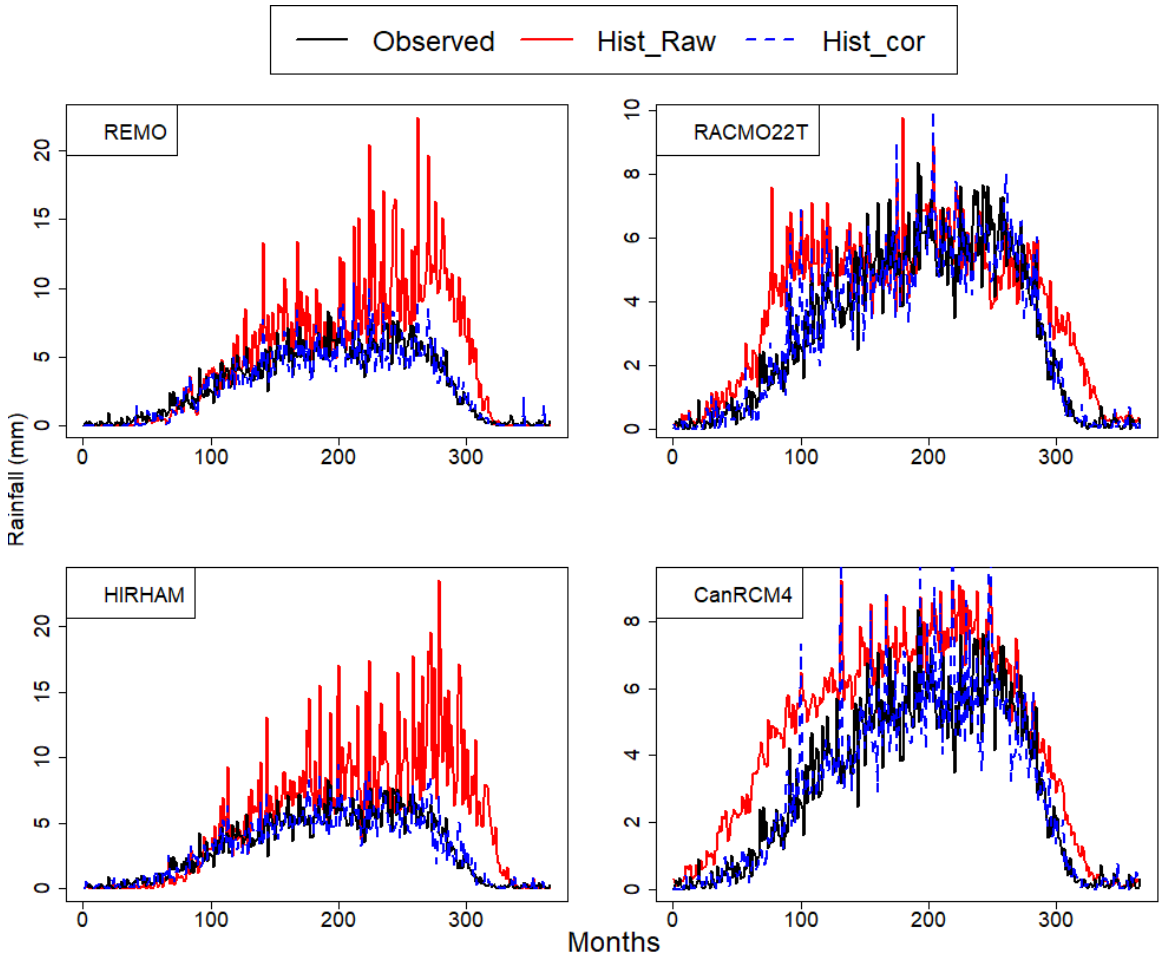

Figure 30. Comparison of raw and bias corrected rainfall with observation at daily scale over the historical period 1971 – 2005

Efficiency coefficients computed for the bias correction at daily scale is summarized in Table 26.

Table 26. Bias correction efficiency at daily scale

	KGE		PBias	
	Before correction	After correction	Before correction	After correction
REMO	-0.08	0.89	60.7	-4.6
RACMO22T	0.70	0.91	23.6	-0.8
HIRHAM	-0.22	0.89	71.7	-1.6
CanRCM4	0.50	0.88	46.5	-1.1

It is noticed that before bias correction, prediction of observations by CanRCM4 and RACMO22T was acceptable with KGE respectively of 0.5 and 0.7. Moreover, the percentage of bias was respectively 46.5 and 23.6. After correction, KGE is of 0.88 and 0.91 respectively for CanRCM4 and RACMO22T whereas it is 0.89 for both REMO and

HIRHAM. Furthermore, percentage of bias is 4.6, 1.6, 1.1 and 0.8 % of underestimation of observation respectively for REMO, HIRHAM, CanRCM4 and RACMO22T. Therefore, at daily scale, RACMO22T still remains the best corrected model.

The good agreement between observation and correction at seasonal scale compared to the daily is not surprising. In fact, the correction is made based on the conservation of observation quantile curve.

5.1.2. Temperature

Result of bias correction of averaged temperature is exhibited on Figure 31. As previously noticed, corrected data fits well observation. CanRCM4 raw data is closer to observation compared to others.

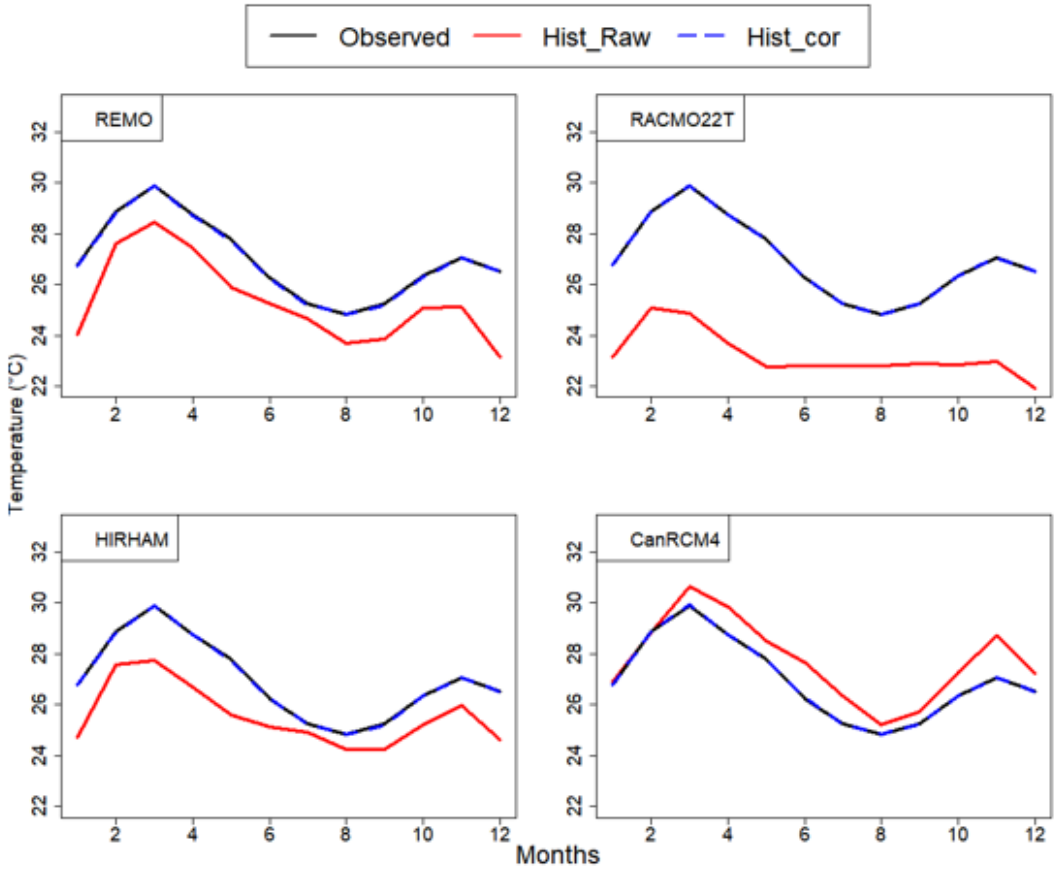

Figure 31. Comparison of raw and bias corrected temperature with observation at seasonal scale over the historical period 1971 – 2005

The efficiency coefficients of models before and after bias correction are summarized in Table 27.

Table 27. Efficiency of temperature bias correction

	KGE		PBias	
	Before correction	After correction	Before correction	After correction
REMO	0.86	0.98	-5.9	-0.1
RACMO22T	0.50	0.98	-13.9	-0.03
HIRHAM	0.74	0.99	-5.2	-0.1
CanRCM4	0.94	0.99	2.9	0.02

The KGE before correction is respectively of 0.5, 0.74, 0.86 and 0.94 for RACMO22T, HIRHAM, REMO and CanRCM4. In addition, the PBIAS is 13.9, 5.9 and 5.2 % of observation underestimation respectively for RACMO22T, REMO and HIRHAM whereas CanRCM4 overestimated observation of 2.6 %. After correction, the KGE of all four models is between 0.98 and 0.99 with absolute value of bias percentage between 0.02 and 0.1.

5.2. Runoff modeling with HEC-HMS using the curve number

5.2.1. Model calibration

In order to assess the impact of climate change on Ouémé river discharge at Bonou outlet, the rainfall-runoff model HEC-HMS is used and calibrated based on the curve number loss method. The model parameters optimization result is detailed in Table 28.

Table 28. Optimized model parameters

Parameter	Optimized value	Unit
Recession - Initial Discharge	31.373	m3/S
Recession Constant	0.9314	
Recession - Threshold Discharge	4.9428	m3/S
Curve Number	35.721	
Initial Abstraction	0	mm
Lag Time	23292	min
Simple Canopy - Initial Storage	1	%
Simple Canopy - Max Storage	116.93	mm
Simple Surface - Initial Storage	35	%
Simple Surface - Max Storage	598.6	mm

As presented on Figure 32, the model is found to be sensitive to three parameters: the lag time, the maximum canopy storage and the maximum surface storage, as showed by the dashed lines. In addition, the model is insensitive to the remaining parameters.

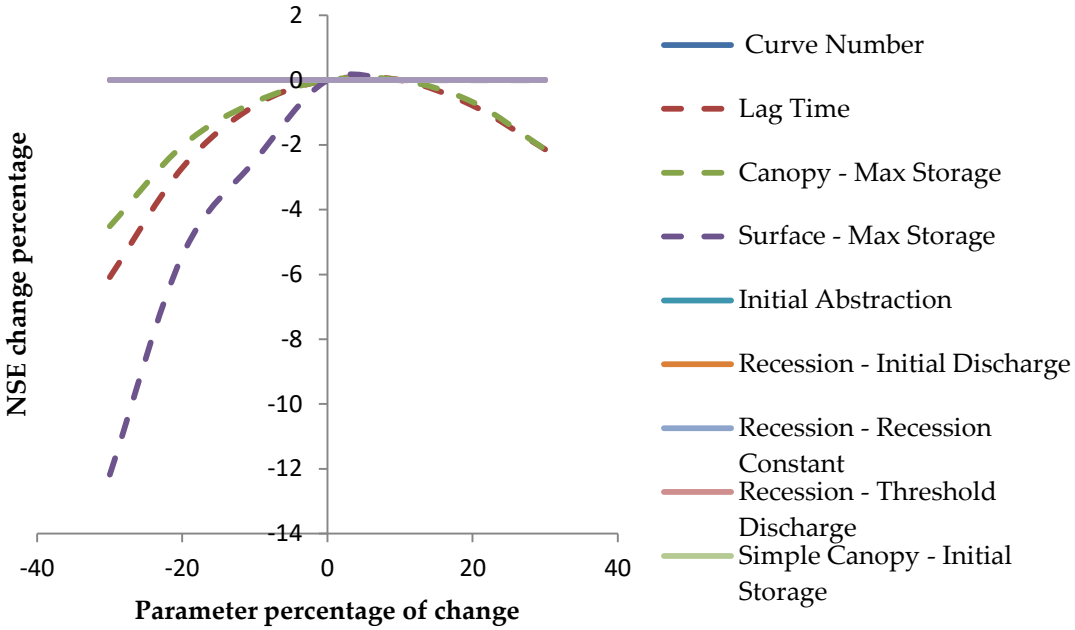

Figure 32. Model parameter sensitivity.

Moreover, the maximum surface storage (Surface – Max Storage) is revealed to be the most sensitive parameter followed by the lag time and the maximum canopy storage (Canopy – Max Storage) as illustrated on Figure 33.

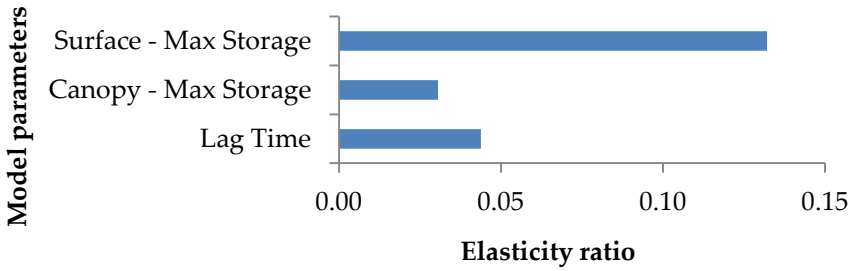

Figure 33. Model parameter elasticity ratio.

Results of statistics of the uncertainty analysis based on Monte Carlo are shown in Table 29. The average value of the Lag time, the maximum canopy storage and the maximum surface storage are respectively 23 286.6 min, 115.2 mm and 599.1 mm. These particular values of the sensitive parameters are then used to calibrate the HEC-HMS model

Table 29. Results of Monte Carlo Analysis with 500 Trials.

Statistique	Canopy - Max storage	Lag Time	Surface - Max storage
Mean	115.2	23286.6	599.1
Number of trials d'observations	500.0	500.0	500.0
Minimum	85.1	23091.0	571.0
Maximum	129.8	23487.0	630.9
Amplitude	44.7	396.0	59.9
1stQuartile	109.7	23251.8	592.7
Median	116.1	23286.0	598.7
3rd Quartile	122.0	23324.0	605.4
Mean	8.2	60.2	10.0
Standard deviation	0.1	0.0	0.0
Variation coefficient	0.1	0.1	0.1

5.2.2. Hydrological model performance

Results of HEC-HMS model calibration and validation of Ouémé River discharge at Bonou outlet are plotted respectively on Figure 34.a and Figure 34.b. In calibration, simulated discharge reproduces better observed with an efficiency of 0.94 based on the KGE and 7% overestimation based on the PBIAS. In validation, the efficiency was 0.91 based on the KGE with 1.3% of underestimation of observation. Therefore, we can conclude on the high performance of HEC-HMS over Ouémé catchment.

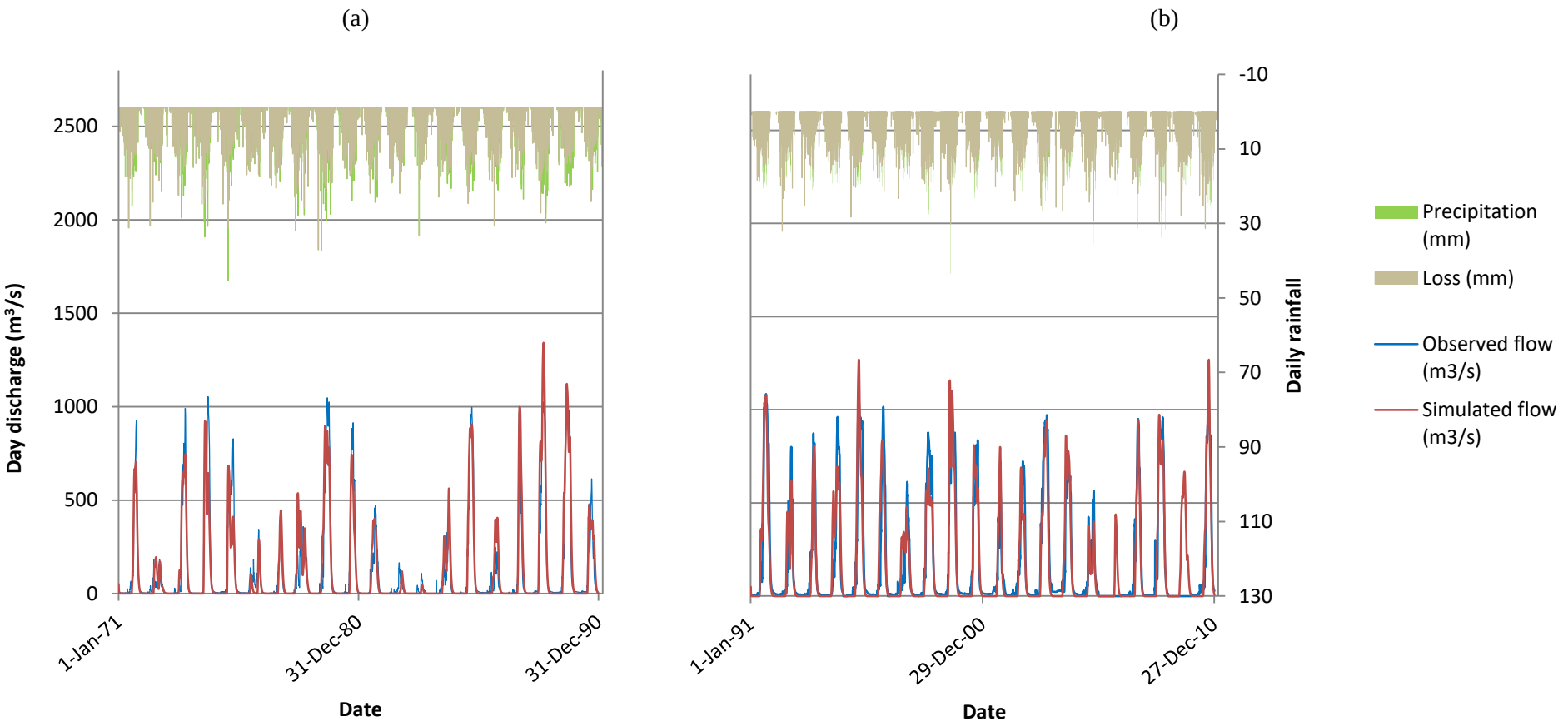

Figure 34. Hydrological model calibration from 1971 - 1990 (a) and validation over 1991 - 2010 (b) graph.

5.2.3. Comparison of observation and simulation flow duration curve

Calibrated and observed flow duration curve is compared according to the flow quantile values. Results are shown respectively on Figure 35.a and Figure 35.b. Assessment of model performance is based on the five standard classes: high flows (0–10%), moist flows (10–40%), mid-range flows (40–60%), dry conditions (60–90%), and low flows (90–100%).

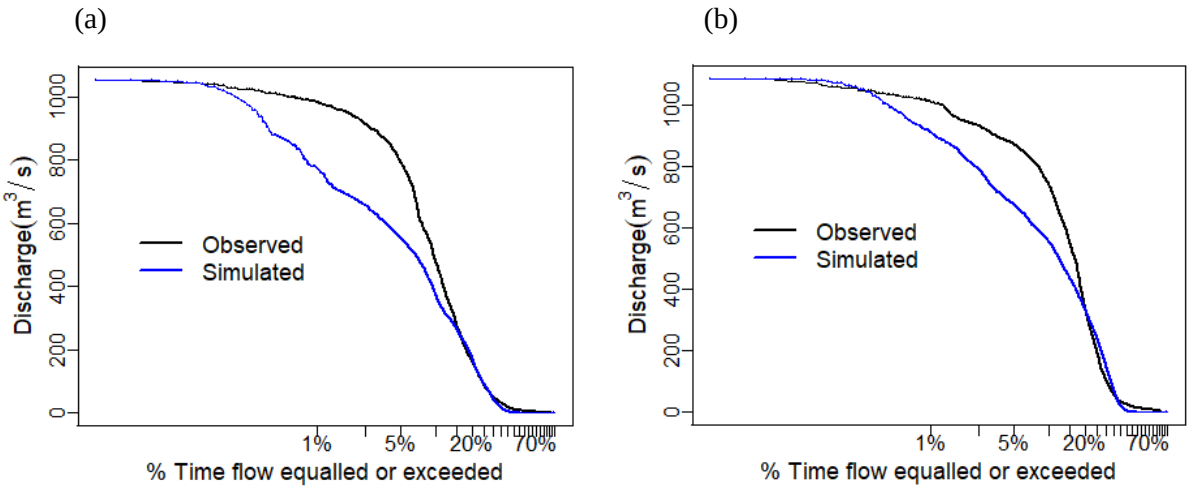

Figure 35. Flow duration curve of daily observed and simulated discharge in calibration over 1971 – 1990 (a) and validation over 1991 - 2010 (b).

During calibration and validation, high flow is mostly underestimated. In calibration (Figure 35.a) the underestimation is about 200 m^3/s whereas in validation (Figure 35.b) underestimation is about 100 m^3/s. However, simulated moist flow fits that of observed. Mid-range and dry flow are slightly underestimated whereas low flow is better simulated. Therefore, this underestimation has to be taken into account in designing hydraulic infrastructures for high flow attenuation.

5.3. Climate change impacts

At annual scale, change in annual rainfall, peak discharge, temperature and potential evapotranspiration from observation (1971 - 2010) to future projection (2020 to 2050) based on the RCP 4.5 and RCP 8.5 are illustrated on Figure 36. On visual basis, the four variables show an increasing trend during observation period. Considering RCP 4.5 projection, rainfall is expected to decrease whereas the trend stays constant for RCP85 (Figure 36.a). As results, peak discharge follows rainfall trend as shown on Figure 36.c. Moreover, temperature is projected to increase when comparing both RCP 4.5 and RCP 8.5 to observation (Figure

36.b). Consequently potential evapotranspiration also shows an increasing trend for both future scenarios (Figure 36.d).

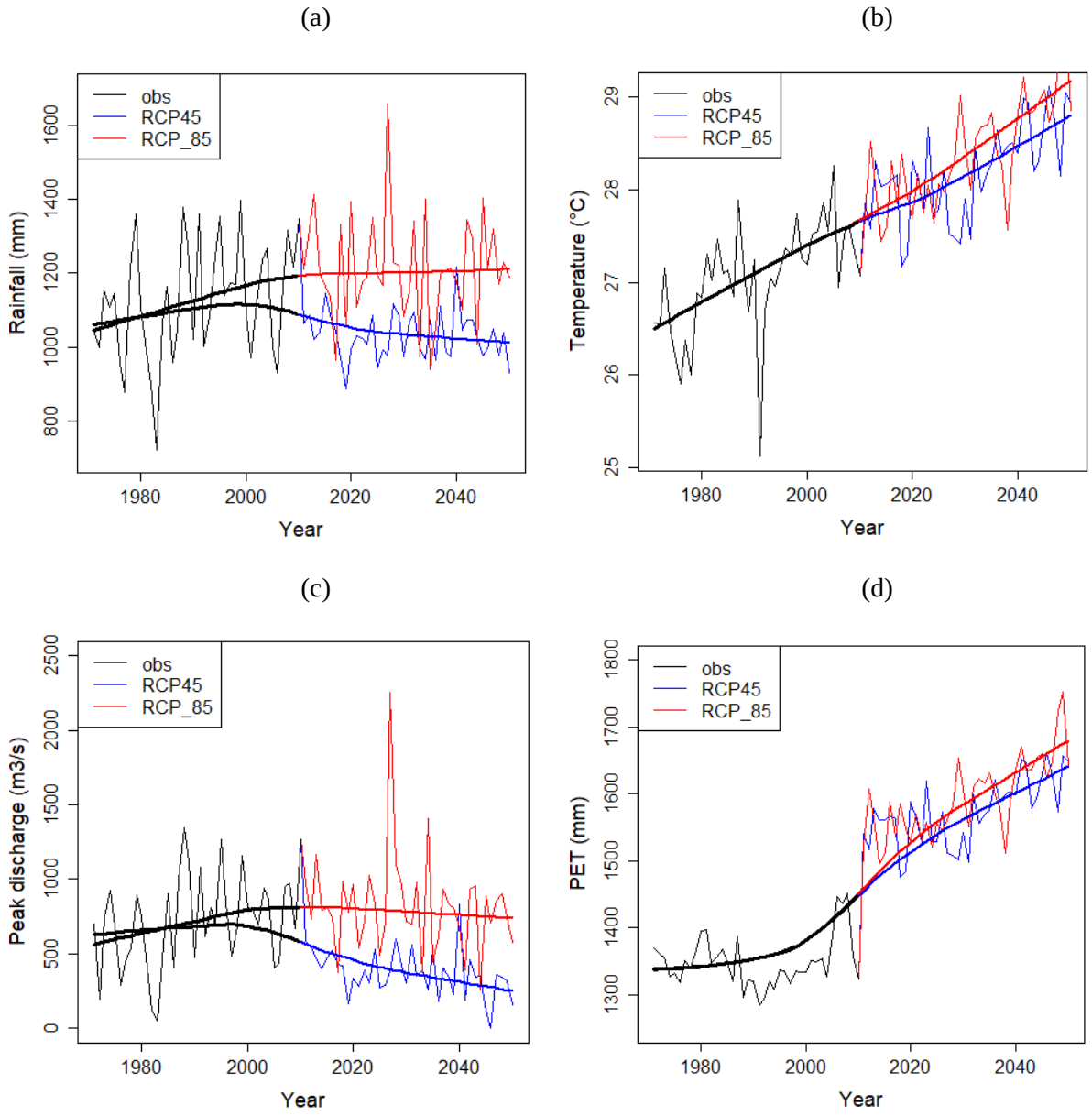

Figure 36. Change in annual rainfall (a), temperature (b), potential evapotranspiration (c) and peak flow (d) from observation to projection based on the RCP 4.5 and RCP 8.5 over the period 1971 – 2050.

Mann Kendall trend analysis results at 0.05 confidence level, during observation and projection periods over annual rainfall, peak discharge, temperature and potential evapotranspiration are summarized in Table 30. During observation period, there is significant yearly increase of 4.42 mm in rainfall, 9.56 m^3/s in discharge and 0.03 °C in temperature. No trend is observed in observed potential evapotranspiration. Moreover, there is significant

yearly increase of 0.04 °C and 0.05 °C respectively in the temperature projection based on RCP 4.5 and RCP 8.5. Similarly, potential evapotranspiration based on the RCP 4.5 and RCP 8.5 significantly increases respectively by 4.51 mm and 4.92 mm per year. Annual rainfall will decrease significantly by 1.33 mm per year according to RCP 4.5 whereas it will significantly increase by 1.89 mm per year based on RCP 8.5. As result, peak discharge significantly decreases by 6.58 m^3/s per year under RCP 4.5 and insignificantly increases by 1.59 m^3/s per year based on RCP 8.5.

Table 30. Trend in annual rainfall, discharge, temperature and potential evapotranspiration.

	Observed			RCP 4.5			RCP 8.5		
Variable	Tau	Sen's slope	p-value	Tau	Sen's slope	p-value	Tau	Sen's slope	p-value
Rainfall	**0.22**	**4.42**	**0.05**	**-0.18**	**-1.33**	**0.02**	**0.21**	**1.89**	**0.01**
Peak discharge	**0.22**	**9.56**	**0.05**	**-0.37**	**-6.58**	**0.00**	0.09	1.59	0.23
Temperature	**0.46**	**0.03**	**0.00**	**0.67**	**0.04**	**0.00**	**0.73**	**0.05**	**0.00**
PET	0.03	0.07	0.79	**0.63**	**4.51**	**0.00**	**0.66**	**4.92**	**0.00**

Apart from the significant decrease in peak discharge from 2020 to 2050 based on the RCP 4.5, there is also decrease in high flow whose probability of exceedance is less than 10% compared to observation (Figure 37). Similarly a decreasing trend is obtained considering discharge projection from 2020 to 2050 based on RCP 8.5. Moreover, there is less high flow in projected discharge under RCP 8.5 than that of RCP 4.5. However, more mid-range and low flow are observed according to RCP 8.5 than RCP 4.5 and observation.

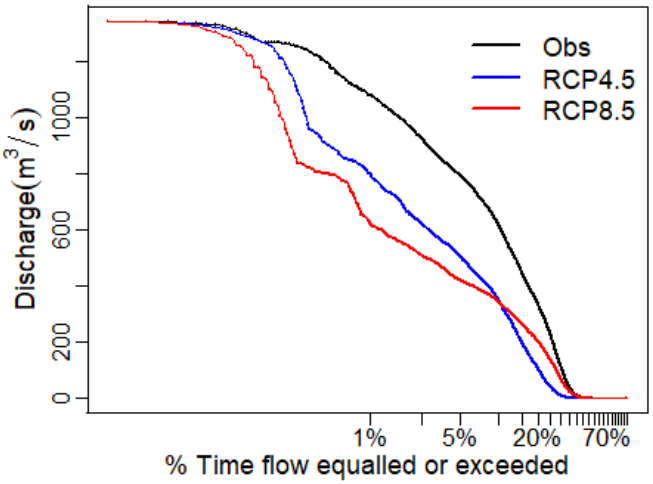

Figure 37. Flow duration curve comparison between observation, RCP 4.5 and RCP 8.5 discharge.

Consequently, water resource management has to be developed to encounter future water shortage in an increasing demand context.

5.4. Discussions

The efficiency of bias correction using quantile mapping method corroborates that of M'Po et al. [62] over Ouéme catchment, Obada et al. [61] in Mékrou catchment and Badou et al. [72] in Benin portion of the Niger River catchment. In addition, Ouémé River discharge modeling using HEC-HMS showed very good results in calibration and validation. However, it exhibits an overall underestimation of high discharge. This has to be taken into account in setting up a hydrodynamic model especially for flood forecasting as well as dam construction scenarios. In addition, a soil moisture accounting method may be a good option in taking groundwater flow into account using HEC-HMS over Ouémé catchment, rather than the curve number method in order to consider the eventual delayed flow due to surface storage.

Moreover, the increase in annual rainfall during the observed period 1971 – 2010 showed in this work is also noticed by Oyerinde et al. [59] in the Niger sahelian catchment for the near future term. Current results are also in accordance with that of Oyerinde et al. [59], Biao et al. [60] and M'Po et al. [62] and showed an increase in projected rainfall based on the RCP 8.5 and a decrease under the RCP 4.5. Moreover, the increase in temperature noted here is also reported by Oyerinde et al. [59], Biao et al. [60], M'Po et al. [62], Hounguè et al. [8] and Lawin et al. [115] as proof of global warming. Similarly, increase in potential evapotranspiration is also highlighted by Oyerinde et al. [59] and Biao et al. [60]. All of the changes impede on discharge. As results, decrease of about 6.58 m^3/s is observed in projected discharge based on the RCP 4.5 scenario and an insignificant increasing trend for the projected discharge based on the RCP 8.5 at mid-century term as obtained by Essou et al. [141] and Stanzel et al. [142]. These results are also in line with that of Benin country profile, which addressed climate change impacts on hydro-climatic variables based on projections made till year 2085 [19]. Therefore, it is essential, to take adaptation measures for preventing possible drought or flood in Ouémé catchment as consequences of climate change impacts on Ouémé River discharge.

5.5. Partial conclusion

This chapter was devoted to climate impact assessment in Ouémé catchment for the period 1971-2050 based on four regional climate models (RCM) as well as land use and land

cover change. From 1971 to 2010, simulation of Ouémé River discharge showed 0.94 and 0.91 of Kling-Gupta efficiency respectively in calibration and validation. Compared to previous works, HEC-HMS performed well and can be adopted in areas with limited soil data especially in developing countries. However, future studies should explore the option of using soil moisture accounting (SMA) method for losses processing while using HEC-HMS over Ouémé catchment, in order to evaluate whether the model could better simulate high flow than it did under the curve number (CN) loss method. Furthermore, underestimation of high flow should be taken into account in hydraulic scenario development. Moreover, in the next fifty years an increase in temperature is projected as proof of global warming. A significant decreasing trend is noticed in projected discharge based on the RCP 4.5 scenario with an insignificant increase in the projected discharge based on the RCP 8.5 at mid-century term. Thus resource planning has to be addressed in order to avoid potential future shortages.

Chapter 6: Ensemble model approach on peak flow simulation in Ouémé catchment at Bonou outlet in Benin

Chapter 6 provides results of the ensemble modeling approach based on the model HEC-HMS and HBV using the Soil Moisture Accounting (SMA) method as well as HyMoLAP which is based on the least action principle. Section 6.1 and 6.2 present results of each model performance and sensitivity respectively. The ensemble models performance and their quantile curve comparison are illustrated respectively in Section 6.3 and 6.4 whereas peak flow comparison results are detailed in Section 6.5. Discussion and partial conclusion are presented in Section 6.6 and 6.7 respectively.

6.1. One by one model performance

Performance of each of the three models taken separately is summarized in Table 31. Values in bold indicate highest performance based on each criterion. The models are calibrated over the period 1971-1990 whereas validation period is 1991-2010. Furthermore, it is worth noting that HEC-HMS is run this time using the soil moisture accounting (SMA) method.

Table 31. One by one model calibration and validation performance.

	HBV		HEC-HMS		HyMoLAP	
	Cal	Val	Cal	Val	Cal	Val
MAE	41.88	59.74	**41.39**	**58.03**	54.86	77.28
PBias	5.80	4.90	**2.10**	**1.90**	3.80	-10.60
KGE	0.90	0.90	**0.94**	**0.92**	0.86	0.78

Cal : Calibration, Val : Validation

The best model based on the KGE is HEC-HMS in both calibration and in validation. In addition, it holds the least percentage of bias in calibration and validation as well as the smaller mean absolute error in calibration and validations. However, HBV mean absolute error as well as KGE in calibration and validation is close to that of HEC-HMS. HyMoLAP show the lowest performance compared to others with the highest percentage of bias of about 10% of underestimation in validation period. So, coupling HBV and HEC-HMS may improve results because of inner performance and possible complementarities between them. Plots of simulated and observation of each model is shown on Figure 38.

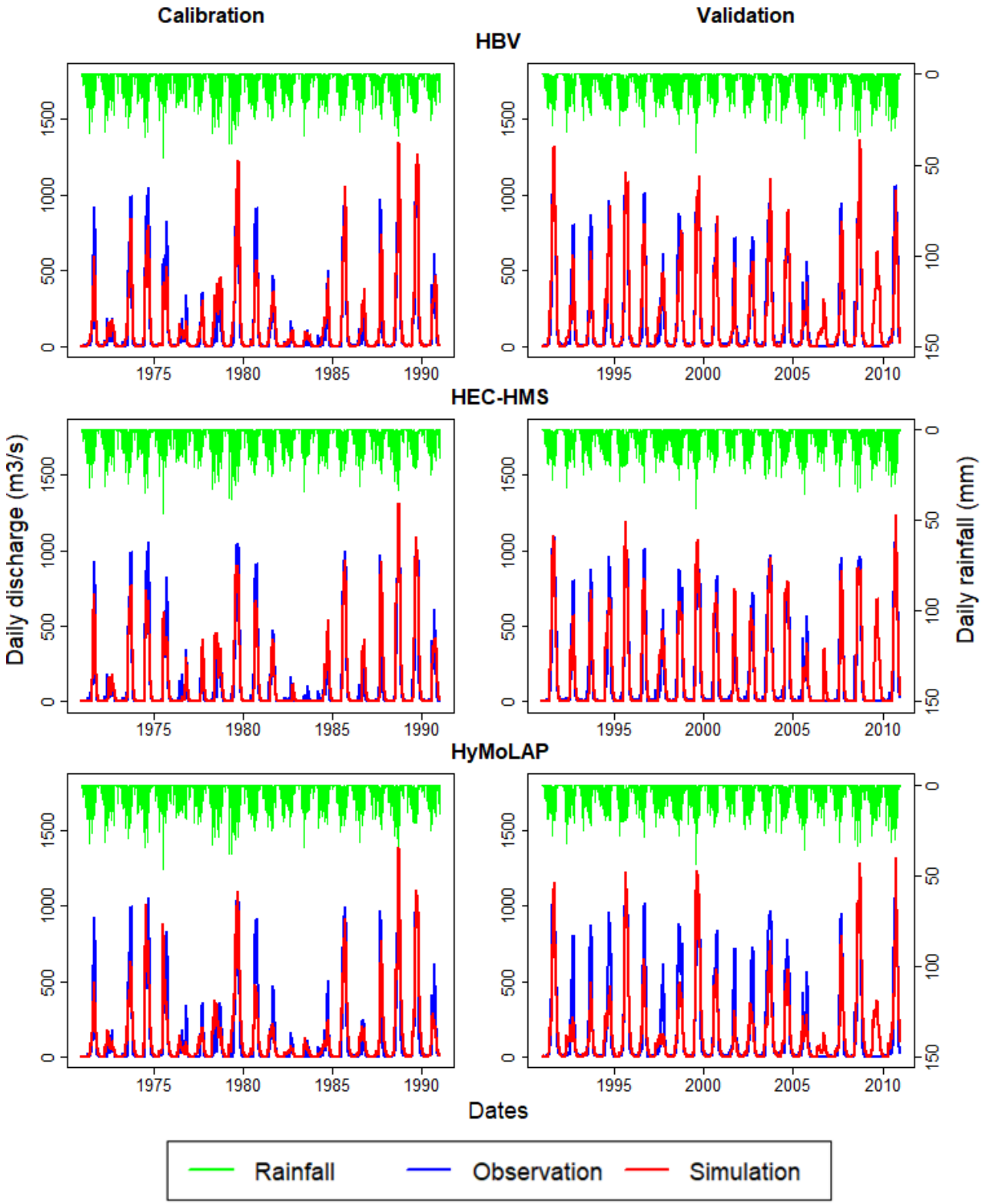

Figure 38. One by one model calibration and validation.

6.2. Model sensitivity analysis

The sensitivity analysis is done like in the previous chapter. The HBV and HEC-HMS change percentage graph as well as the elasticity ratio are illustrated hereby on Figure 39.

HEC-HMS

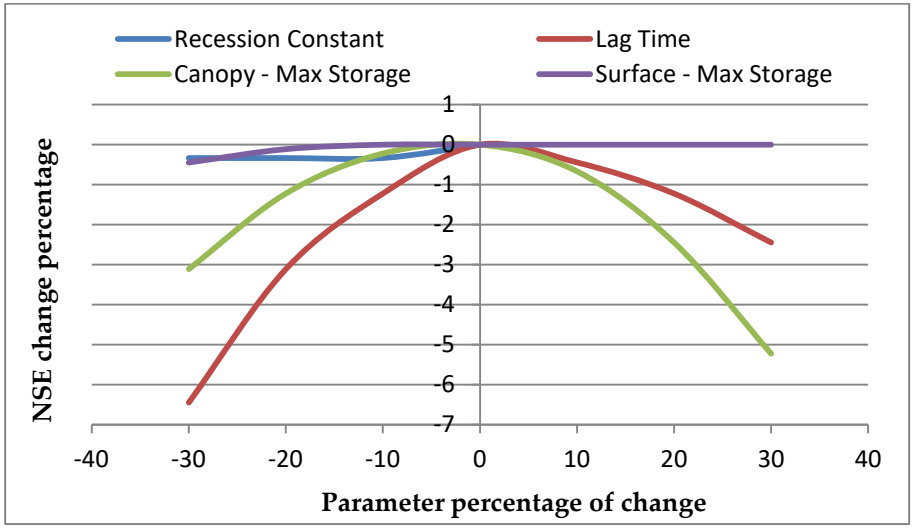

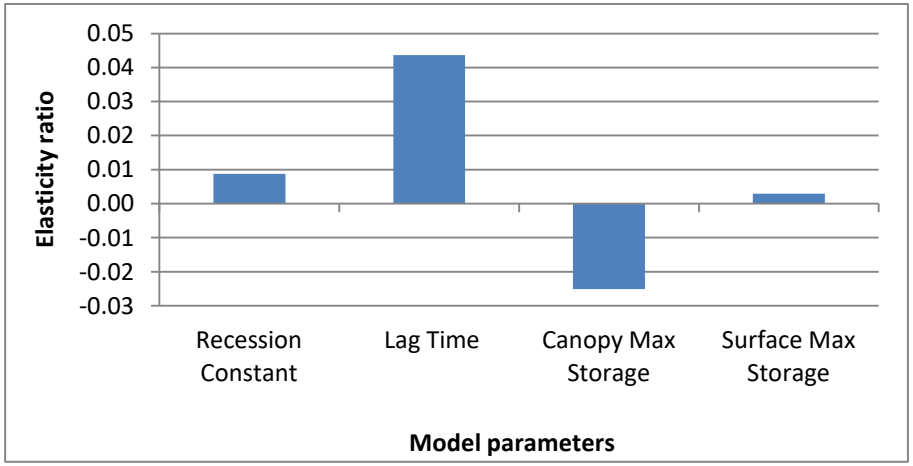

HBV

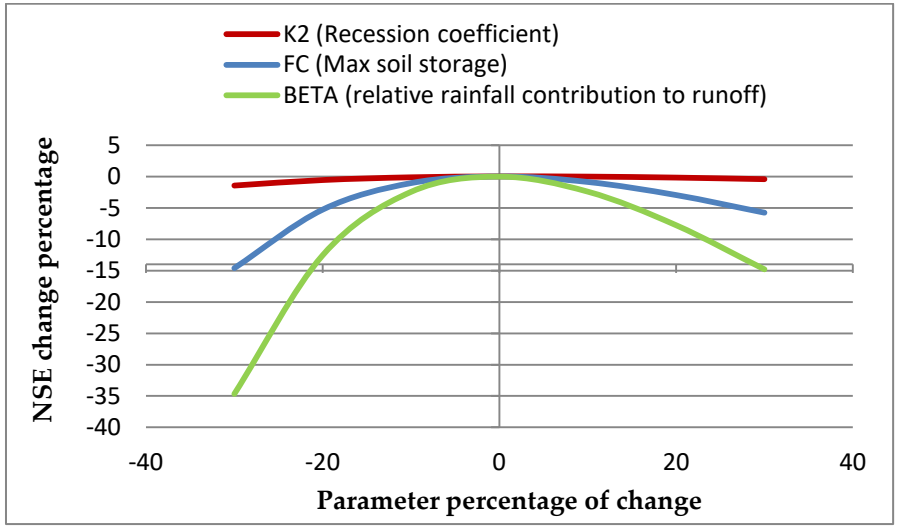

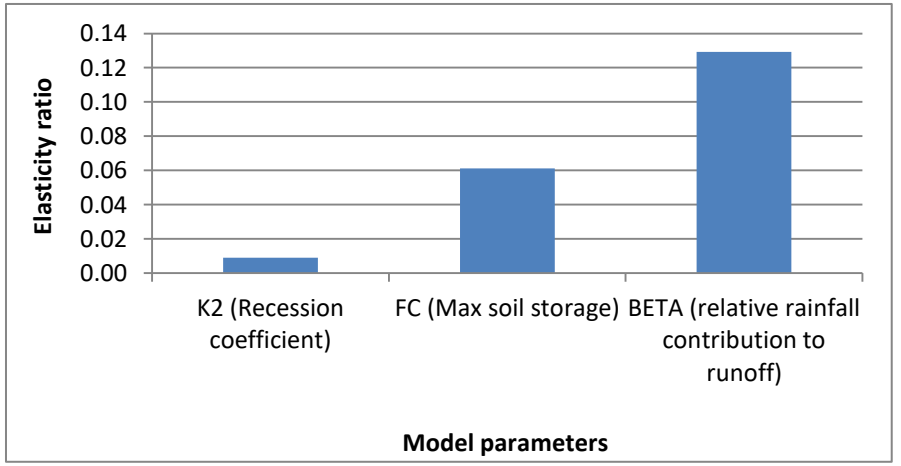

Figure 39. Sensitivity analysis of HEC-HMS and HBV

It is observed that both models are sensitive to recession coefficient, storage component as well as lag time. In fact, the relative contribution of rainfall to runoff is implicitly related to the lag time. Therefore, the hydrological modeling should care of these components especially with HBV which is highly sensitive to these parameters than HEC-HMS. HyMoLAP sensitivity analysis is not showed hereby because previous works revealed its high sensitivity to the parameter μ that expresses the non-linearity of flow [132,143].

6.3. Ensemble model performance

Ensemble models performance is shown in Table 32. Like in the previous table, bold figures indicate high performance.

Table 32. Ensemble models calibration and validation performance

	HyMoLAP/HBV		HyMoLAP/HEC-HMS		HBV/HEC-HMS		Ensemble_mean	
	Cal	Val	Cal	Val	Cal	Val	Cal	Val
MAE	44.61	63.23	41.87	60.44	**36.95**	**53.12**	39.59	57.01
PBias	4.80	-2.90	2.90	-4.40	**3.90**	**3.40**	3.90	-1.30
KGE	0.88	0.86	0.90	0.86	**0.92**	**0.91**	0.90	0.88

Cal : Calibration, Val : Validation

The performance criteria indicate that the coupled model HBV/HEC-HMS is the best one. In fact, based on the KGE and MAE, HBV/HEC-HMS showed high performance in calibration as well as validation. However, the ensemble mean of the three models showed good performance based on the percentage of bias in validation whereas the couple HyMoLAP/HEC-HMS was the one that less overestimates observation in calibration. The combinations HyMoLAP/HEC-HMS and HBV/HEC-HMS showed lowest performance compared to others. Though, it is noticed that HEC-HMS impacted more positively HyMoLAP than HBV during calibration.

As observed on Figure 40, the couple HBV/HEC-HMS which is the mean of the outputs from HBV and HEC-HMS simulates better observations than others couples.

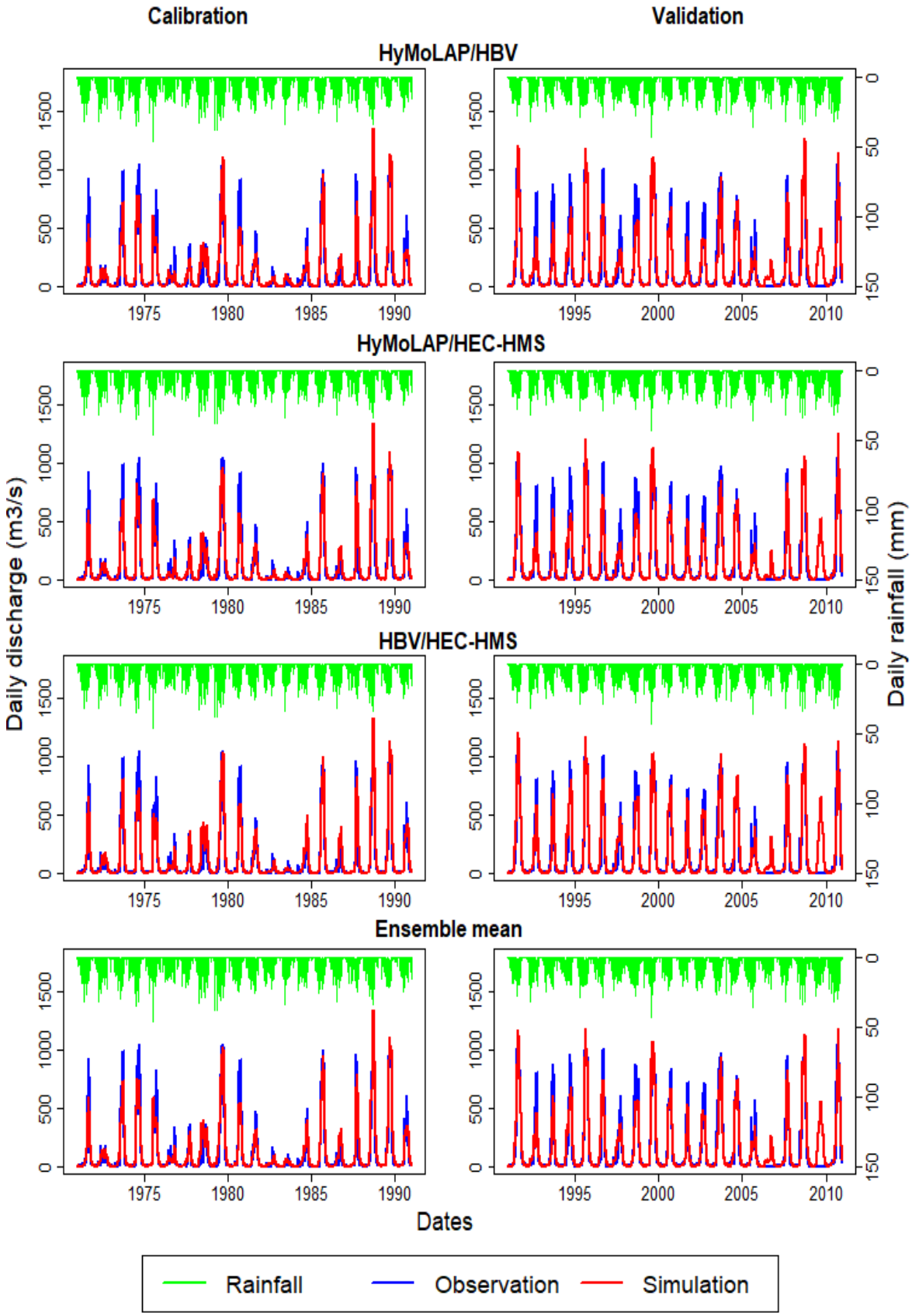

Figure 40. Ensemble models simulation.

6.4. Quantile curve method

Flow duration curves on Figure 41 show that HBV and HEC-HMS have good performance in high and low flow with underestimation of observations in both calibration and validation. HyMoLAP shows underestimation in high flow and good performance in dry period (60–90%) and low flow (90–100%). However, during moist flows (10–40%) and mid-range flows (40–60%) all models simulations do not suit well to observations. Nevertheless, during moist flows and mid-range flows HEC-HMS simulation is closer to observation than others as shown on Figure 41.a and Figure 41.b. Considering ensemble models during moist flows and mid-range flows, HBV/HEC-HMS is the closest among others followed by the ensemble mean of the three models as shown on Figure 41.c and Figure 41.d. Thus, there is a need to figure out whether peak flows that seems to be well simulated conserve observation trend.

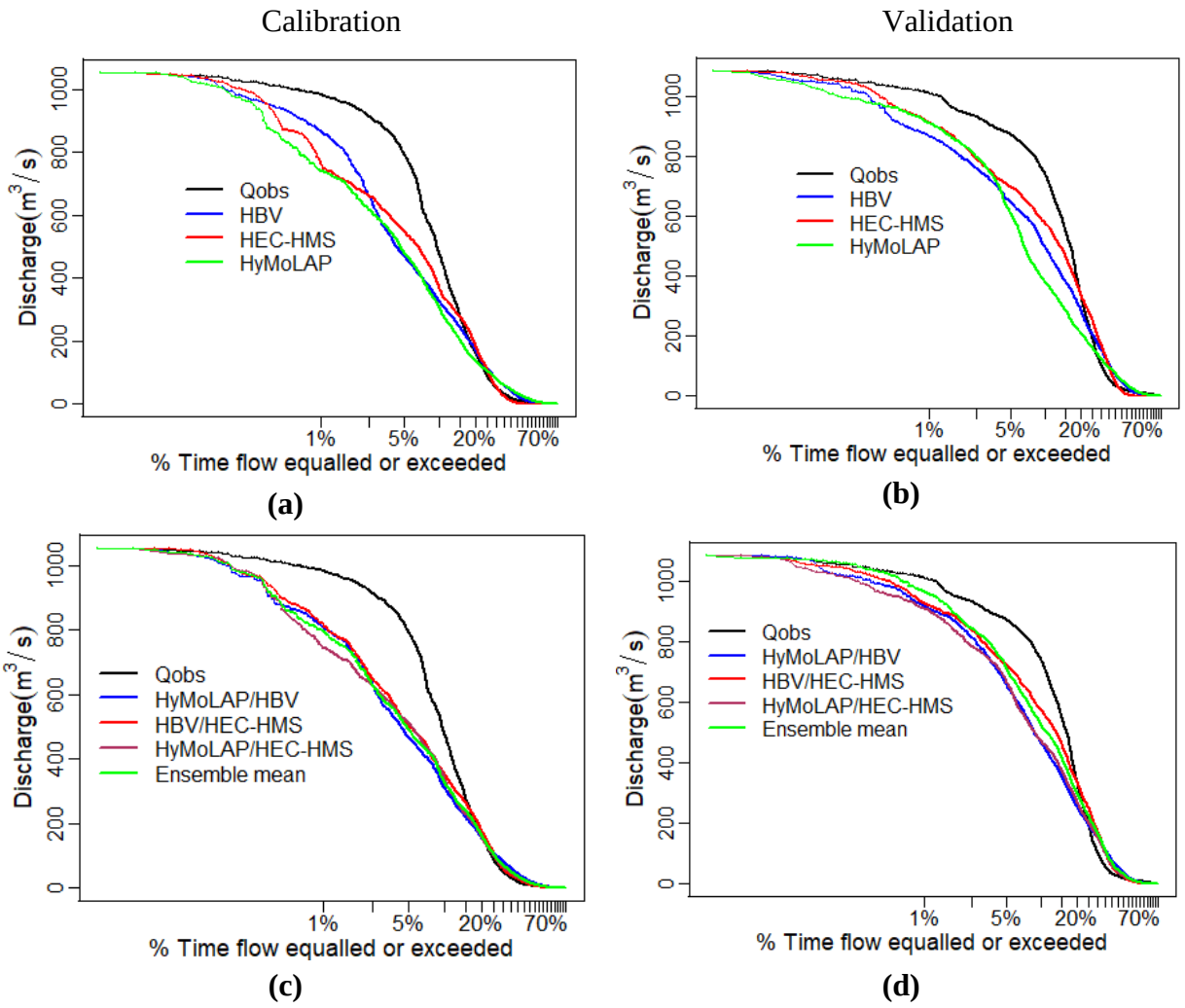

Figure 41. one by one model calibration (a) and validation (b) as well as ensemble model calibration (c) and validation (d)

6.5. Peak flow comparison

Observed and simulated discharge trends are shown on Table 33. Peak flows from HBV, HEC-HMS and HBV/HEC-HMS show increasing significant trend at 0.05 confidence level. Among these three models, HEC-HMS got the least significant Sen's slope.

Table 33. Peak flow trend statistics.

	Z-Value	Tau	Sen's Slope	P-value
Observation	1.164	0.135	5.677	0.244
HBV	**2.053**	**0.237**	**11.929**	**0.04**
HEC-HMS	**1.975**	**0.228**	**9.387**	**0.048**
HyMoLAP	1.452	0.168	7.775	0.147
HyMoLAP/HBV	1.896	0.219	10.169	0.058
HBV/HEC-HMS	**2.001**	**0.231**	**10.042**	**0.045**
HyMoLAP/HEC-HMS	1.792	0.207	9.457	0.073
Ensemble mean	1.87	0.216	9.501	0.061

In order to distinguish the best models among the three models HBV, HEC-HMS, and HBV/HEC-HMS to simulate peak flow in Ouémé catchment, performance criteria are computed as summarized in Table 34. It is noticed that HBV shows least percentage of peak bias of 5 % with higher MAE than that of HEC-HMS and HBV/HEC-HMS. In fact, the latter two models PBias are respectively of 8.5 and 5.6 underestimation of observation. They also hold similar MAE of respectively 130.19 and 135.4 m^3/s for HEC-HMS and HBV/HEC-HMS. However, KGE of HEC-HMS is the highest over peak flow 0.85 whereas that of HBV/HEC-HMS is 0.82.

Table 34. Model performance over peak flow.

	HBV	HEC-HMS	HyMoLAP	HyMoLAP/ HBV	HBV / HEC-HMS	HyMoLAP / HEC-HMS	Ensemble mean
MAE	158.18	130.19	238.86	194.97	135.4	182.11	171.15
PBias	-5	-8.5	-19.5	-16	-8.6	-15.8	-14.3
KGE	0.72	0.85	0.54	0.67	0.82	0.72	0.75

6.6. Discussion

HBV and HEC-HMS taken separately, showed good performance in simulating flow in Ouémé catchment. HEC-HMS was the best among all. HBV and HEC-HMS performance

look alike with a KGE of 0.90 and 0.94 respectively in calibration and 0.90 and 0.92 respectively in validation. The SMA loss used hereby performed slightly better in validation than the curve number loss method previously run [5]. In addition, KGE of HyMoLAP is 0.88 in calibration and 0.78 in validation. HyMoLAP highly underestimates flow peak by about 19.5 %. Considering daily flow, HBV overestimates more observation than HEC-HMS and HBV/HEC-HMS, whereas HyMoLAP underestimates most observed flow [143]. However, HEC-HMS underestimates peak flow by 8.5 % whereas HBV underestimates by 5 %. Flow overestimation by HBV is also noticed by Linde *et al.* (2008) during simulation of discharge in the Rhine catchment. This difference in models performance may be due not only to unfair rainfall distribution over the catchment whereas incertitude may have been introduced because of the homogenized rainfall used [133]. However, ensemble mean of HBV and HEC-HMS modeled well the peak flow in this area with 0.82 of KGE. The peak flow PBias is – 8.6 %. Therefore, even if the ensemble HEC-HMS performed almost similarly as HBV/HEC-HMS, it reduces the PBias and MAE. The performance of the ensemble model HBV/HEC-HMS may be due to the fact that HBV and HEC-HMS are both semi-distributed models and are almost alike. Even though they have a lot of modeling parameters, they have the advantages of taking more hydrological processes into computation than the lumped one. However, taking into account the equi-finality aspect as developed by Beven [11], HyMoLAP may be the best as it only has two parameters. Moreover, the use of it distributed form instead of the lumped may give improvements. Moreover, the main process that both HEC-HMS and HBV models take into account in difference of HyMoLAP is the storage component. HEC-HMS has canopy storage and accounts for surface interception storage before surface runoff [122]. HBV has only one storage component taking both canopy and surface storage into account. In contrary, HyMoLAP has no surface storage [123]. Storage acts as progressive loss and additional runoff within the distributed models but this part of runoff is missing in HyMoLAP. Therefore, storage component should be included in HyMoLAP as it is in HEC-HMS and HBV are highly sensitive to it [5]. Results attest of the high performance of HEC-HMS and the couple HBV/HEC-HMS as simulation was done over 40 years period including the driest period of 70s and the recovering period of 90s till nowadays [74].

6.7. Partial conclusion

Ouémé river peak flow simulation is conducted in this work using three hydrological models namely: HEC-HMS, HBV and HyMoLAP. Inter-comparison of models is firstly done

to assess their inner performance. Results show best performance of HEC-HMS ahead HBV and HyMoLAP. However, HBV and HEC-HMS performance look alike with KGE of more than 0.9 in calibration and validation. They hold the least PBias and MAE as well. HyMoLAP was average in simulating overall flow but underestimates much peak flows. In fact, KGE of HyMoLAP is 0.86 in calibration and 0.78 in validation, whereas the peak flow PBias is of -19.5 %. Considering ensemble models run, HBV/HEC-HMS is the best with the least percentage of bias over peak flow. Therefore, out of the various ensembles assessed in this study, the couple HBV/HEC-HMS is the best in Ouémé catchment. In addition, considering these models one by one HEC-HMS remains the best due to the storage components that it accounts for. Integrating storage components to HyMoLAP may be a good perspective for its improvement over peak flows.

Chapter 7: Flood mapping in Ouémé Delta

Chapter 7 presents results of Ouémé Delta flood events mapping. Section 7.1 provides natural color composition of Sentinel1A results, whereas Section 7.2 presents classes differentiation. In addition, Section 7.3 detailed flood mapping results while Section 7.4 maps built up and acadja over Nokoué Lake and Porto-Novo lagoon. Moreover, 7.5 and 7.6 respectively focused on discussion and partial conclusion.

7.1. Natural color composition of Sentinel1A

The mapping process presented hereby is based on the three main land use classification using color composition. The main task was to find the color composite that distinguish best into water, vegetation and soil based on Sentinel1A data. At end, such color composition will be used to extract water extent for flood mapping based on simple comparison approach between the optical sentinel 2A and radar sentinel1A images. Results from the true color composition (VV, VH, NDI) of the Sentinel1A from December 07, 2018 and that of the optical image Sentinel2A (4,3,2) from December 10, 2010 are shown on Figure 42.a. and Figure 42.b.

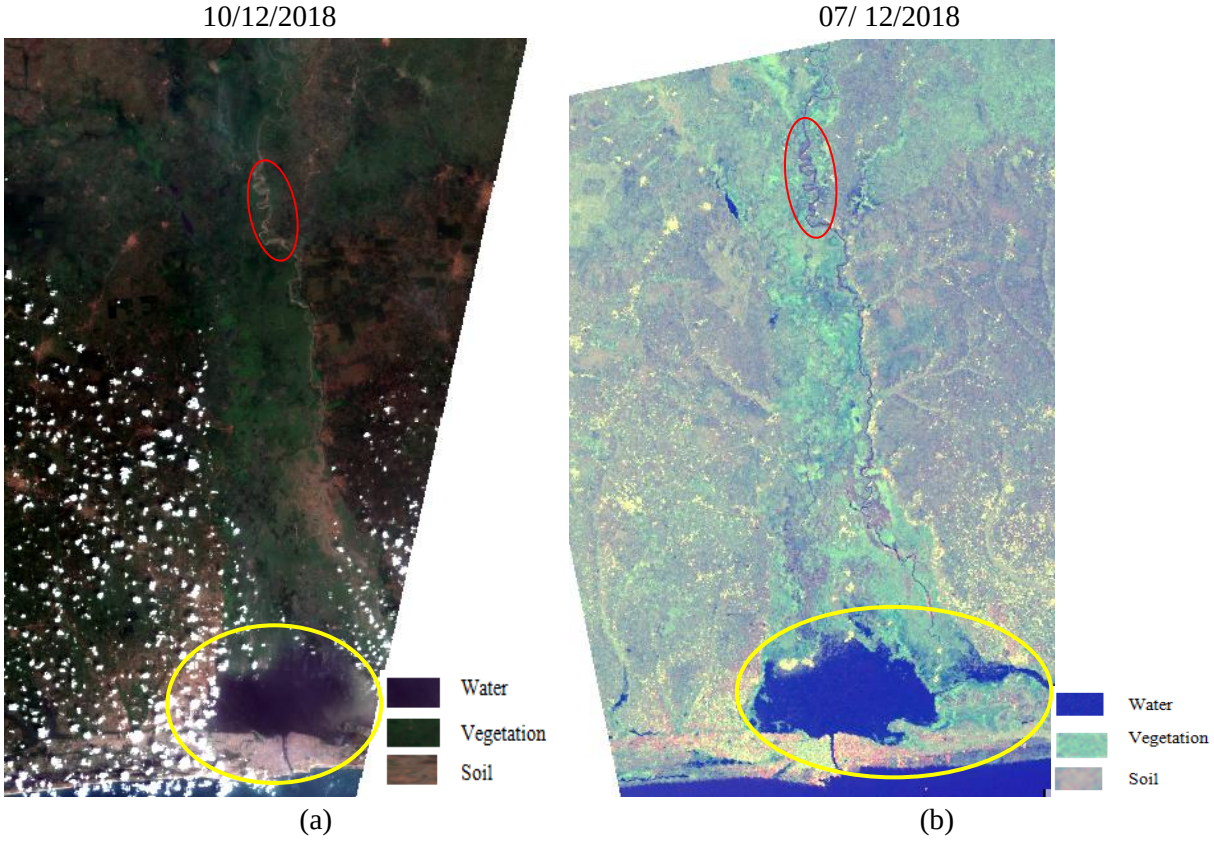

Figure 42. Visual comparison of Sentinel 2A (a) and Sentinel 1A (b) images.

Water extend is clearly the same and colored in blue (inside the yellow form). In addition, vegetation and soil or uncovered lands are also well visualized. On Figure 42.b yellowish areas are built up. Inside the red form, we noticed water extent on the Sentinel1A than on the Sentinel2A because of the images resolutions. In addition, the reddish areas are probably a mixture of water and other classes. Therefore, there is a need for more information for class differentiation.

7.2. Classes differentiation

Based on the reference land use and cover map, made by the European Space Agency (ESA) using Sentinel 2 data over Africa over the period of December 2015 till December 2016 [144], classes segmentation is provided. In fact, comparison is made between the natural color composition proposed in Figure 42.b and ESA map in 2016 as shown on Figure 43. We found that from both Figure 43.a and Figure 43.b built up are well distinguished as well as open water. However, from Figure 43.a there is no distinction between vegetation types as on Figure 43.b. In addition, there is confusion between flooded and non flooded vegetation.

Moreover, the class that was previously treated as soil as well as the reddish areas which were not well-known before are rather cropland as bare soils are rarely found in the Ouémé Delta based on Figure 43.b. Although, detailed class differentiation among vegetation cover types is limited using the proposed color composition, water level and built up classes is possible to be distinguished. Therefore, this color composition can be applied for quick views of water extend for flood mapping process, built up and vegetation.

SIA of 07/ 12/2016

ESA land use and cover map in 2016

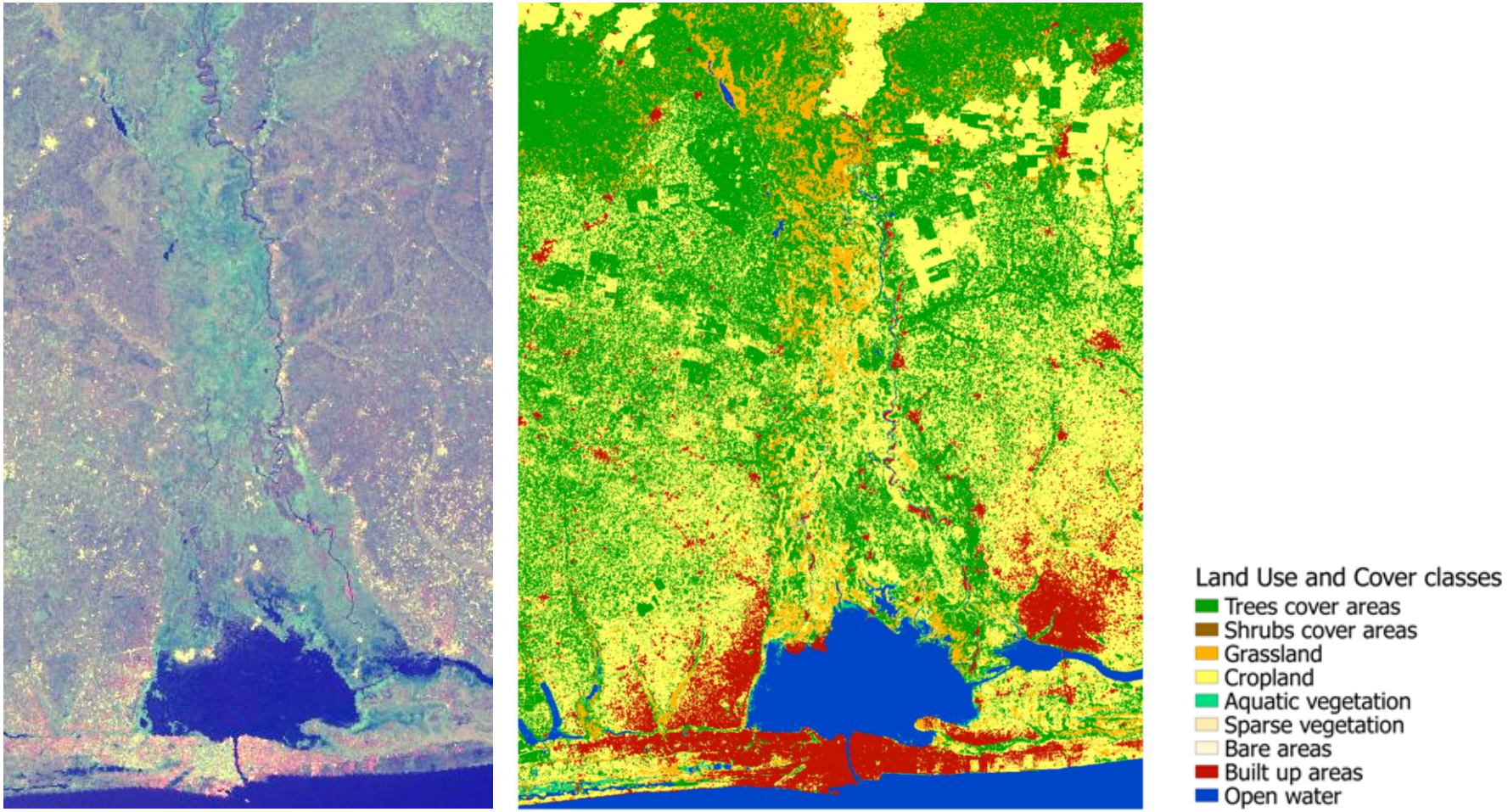

Figure 43. Comparison between natural color composition and ESA land use and cover map

7.3. Built up mapping on Nokoué Lake and Porto-Novo lagoon

By the means of the previous color composite Acadja and built up over Nokoué Lake and Porto-Novo lagoon is mapped. Acadja are fishing devices made of woods and branches for trapping fishes. Over the last decades, it has expended all over the Nokoué Lake and makes difficult fluvial circulation. Moreover, because of the branches degradation, the Lake is getting filled up with organic matters. Here is the map of Acadja over Nokoué Lake and Porto-Novo lagoon in December 2018 based on Sentinel1A data (Figure 44).

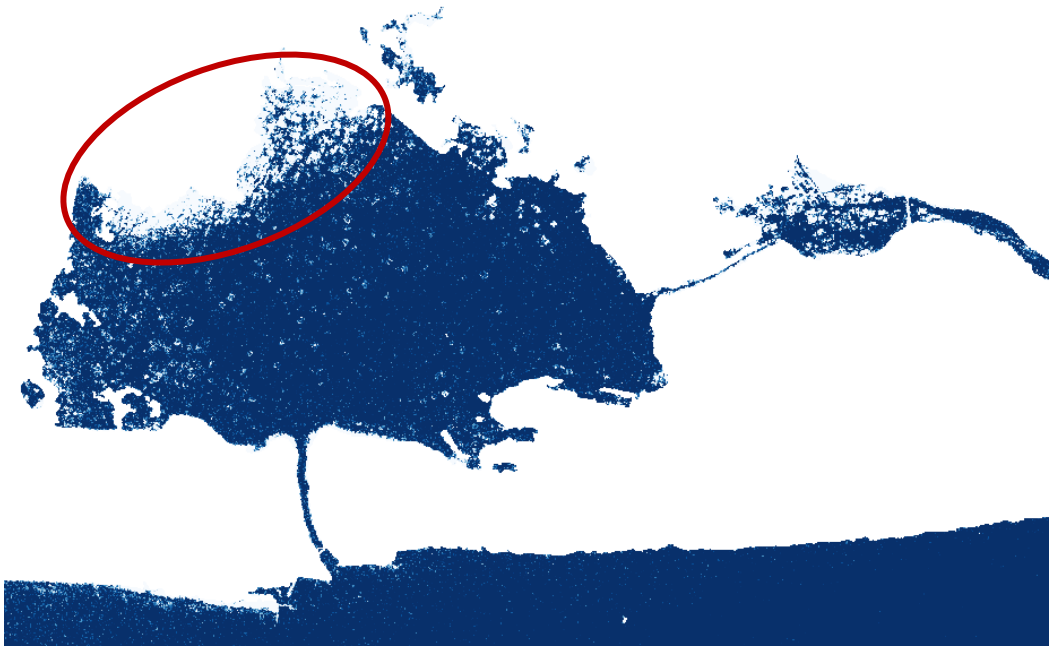

Figure 44. Acadja and built up map over Nokoué Lake and Porto-Novo lagoon on December 2018.

The white areas are acadja and built up. Although, what is viewed is a mixture of acadja and built up, there is more acadja than built up. In the Ganvié village that is built entirely on water here in the red form we noticed a large expansion of acadja and built up as well as on the Porto-Novo Lagoon.

7.4. Flood mapping in 2018

Based on this analogical method, the following color composition: VV polarization in the red, VH in green and NDI in blue is applied to sentinel 1A image from August 9th till November 13th, 2018 to visualized 2018 flood extend in Ouémé Delta. Results are illustrated on Figure 45. The reddish areas are flooded crop land. Water class differentiation is then processed through saturation to blue colored areas and water extents results are displayed as on Figure 46.

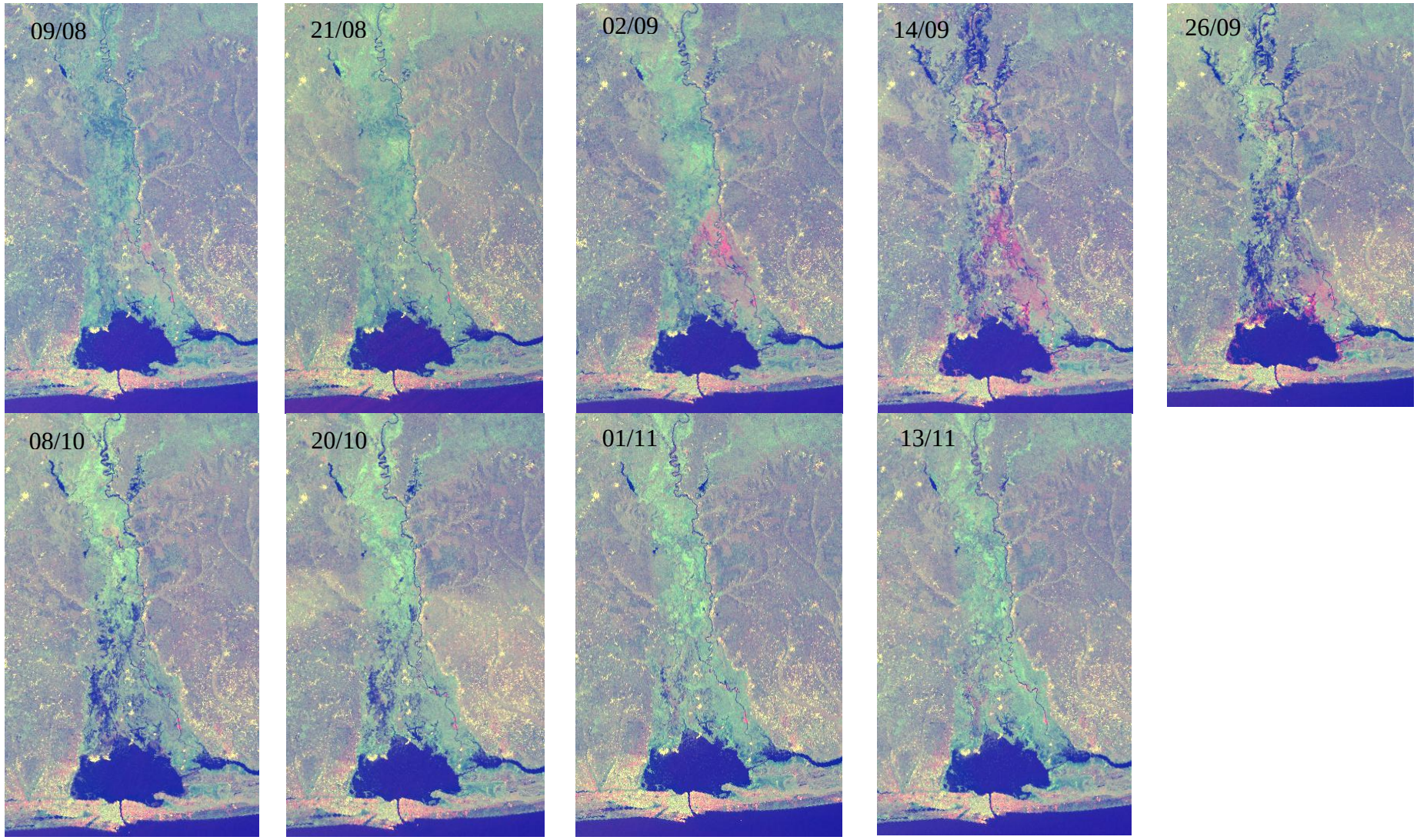

Figure 45. Ouémé Delta flood mapping results from September to November 2018.

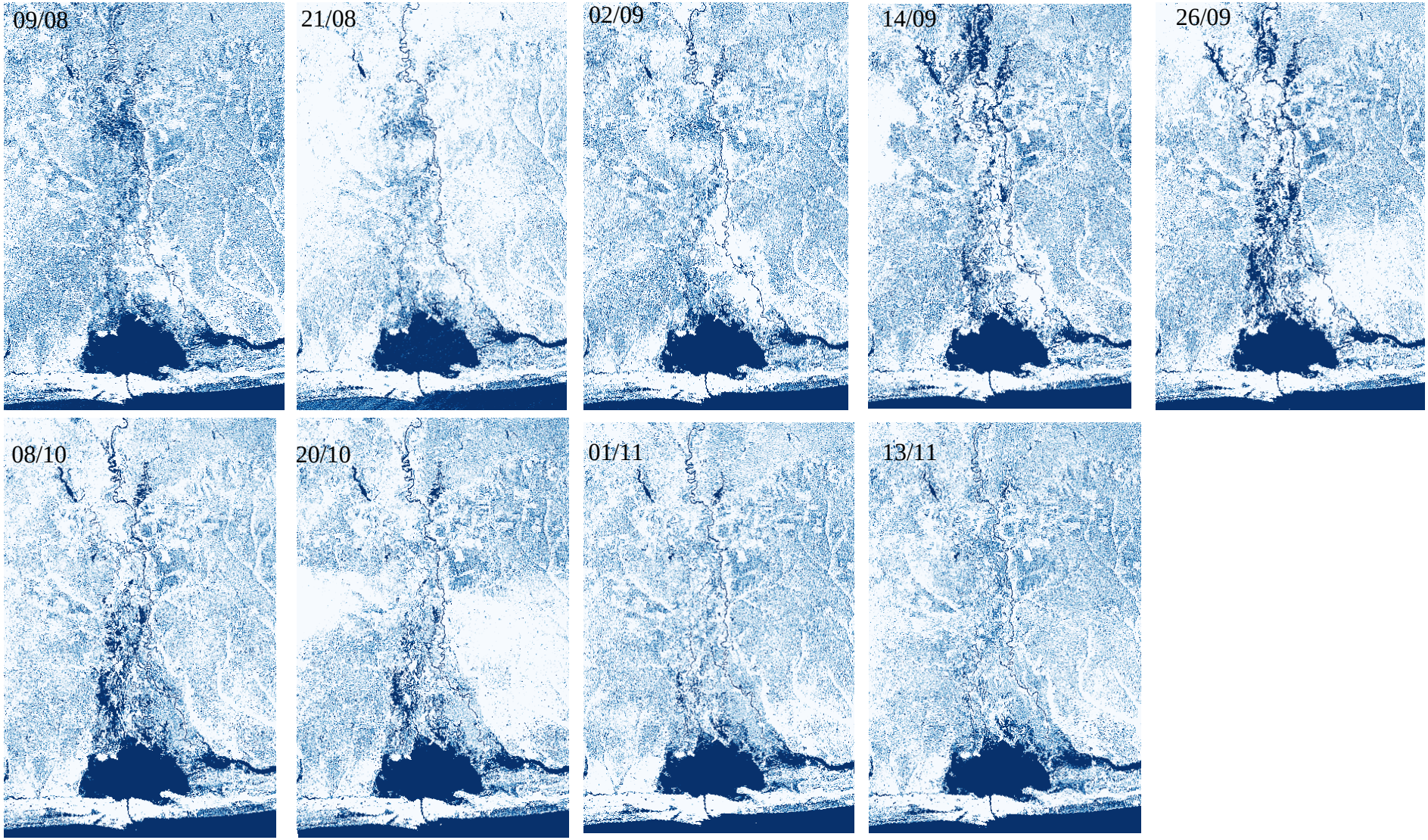

Figure 46. Water extent during 2018 Ouémé Delta flood event.

Based on Figure 46, it is observed either pluvial due to the local rainfall over Ouémé Delta or fluvial inundation due to rivers over flow. The high point of fluvial inundation on is more visible over September 14 and 26 maps where the confluence areas of Ouémé and Zou Rivers are well colored in blue. However, as the pluvial inundation depends on rainfall occurrence, comparison between satellite averaged rainfall records in 2018 from the NASA Global Precipitation Measurement (GPM) mission (Figure 47) and the images status is done.

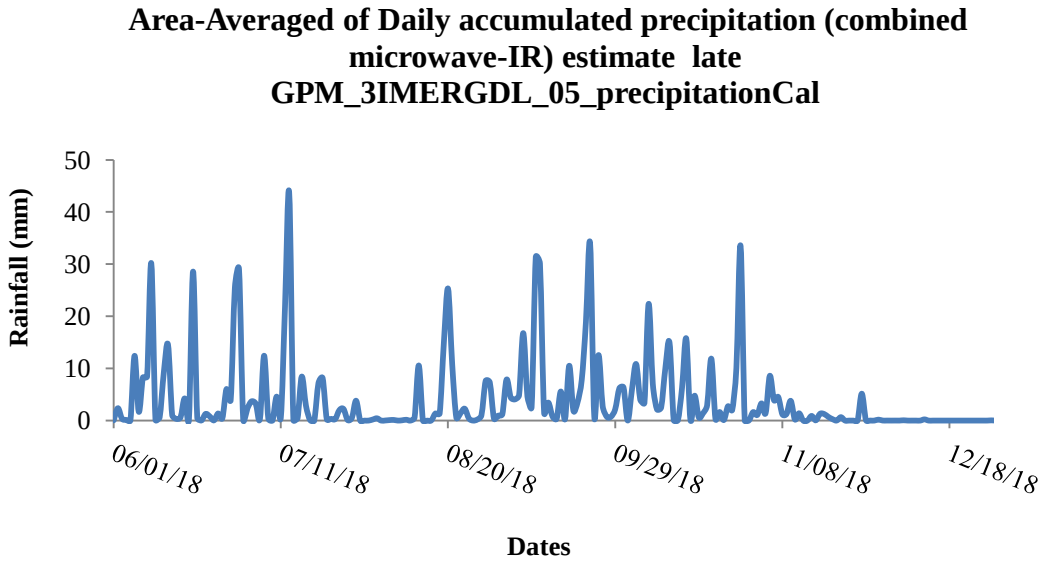

Figure 47. GPM rainfall over Ouémé Delta

From Figure 46, it is observed a dry condition (areas in the maps colored in white color) on October 20th is confirmed with the rainfall averaged record of 1.4 mm over Ouémé Delta displayed on Figure 47. In contrary, on August 21st there was a dry condition whereas the rainfall record is about 10.8 mm. Therefore, rainfall occurrence time and duration come to plays a key role. In fact, the Sentinel1A images used are taken around 6 PM. For instance, the 10.8 mm rainfall event happened between 1 and 4 AM, it has enough time to run into the Delta's rivers and floodplains before 6 PM. Thus, even though, we noticed considerable rainfall amount that day, it may not showed up on the satellite image.

7.5. Discussions

It is showed hereby, simple process for flood mapping based on a color composition on a free platform. It was done to show that at any point of the globe, such color composite is possible to roughly assess flooded areas. No flooded area quantification is conducted. In fact, the process was done only for visual effects. Quantification may not be precise at this stage unless using image classification which was not the aim. However, with the proposed color

composite hereby presented, built up and water extents are well distinguished. Moreover, vegetation cover is globally viewed but detailed about their types are not well perceived. As the Delta is a humid area, it is not easy to differentiate between flooded and non flooded vegetation as a lot of aquatic vegetation are spread around [145]. Therefore, detailed differentiation may need ground truth for validation. For water extent viewing, this color composite was already used over Chad Lake for monitoring water extent [146]

7.6. Partial conclusion

This chapter aims at mapping flooded areas in Ouémé Delta. Based on the color composite method proposed hereby not only land cover classes were visualized but also water extent in the Ouémé Delta. As the outputs are for visual aspect no area quantification is done. In addition, built up extent is well distinguished. Consequently, acadja and built up over Nokoué Lake was mapped in December 2018. However, it is noticed a confusion between pluvial and fluvial flood extent during high water period due to limited small scale time data. In fact, hourly scaled rainfall may be an input in correlating flood map and local rainfall influence in Ouémé Delta. In addition, distinction between flooded and non flooded vegetation is not easy as Ouémé Delta is a humid area. Moreover, an input may be determining water surface elevation based on such images in order to predict water level for early warning improvement.

Chapter 8: Hydrodynamic functioning of Ouémé Delta under climate change and dam construction scenario impacts

Chapter 8 provides results about hydrodynamic functioning of Ouémé Delta based on climate change and dam construction scenario. Section 8.1 exposed extreme events characteristics and Section 8.2 detailed the hydrodynamic model calibration and validation. In addition, Section 8.3 and 8.4 summarized respectively Ouémé River discharge data reconstruction in 2016 as well as the assessment of the hydrodynamic and hydrological models robustness in 2016 and 2018. Furthermore, Ouémé Delta hydrodynamic functioning is presented in Section 8.5, results of the combined impacts of climate change and dam construction scenario in Section 8.6 whereas a proposition of improvement of the existing early warning system is described in Section 8.7. This chapter ends up with the discussions in Section 8.8 as well as partial conclusion in Section 8.9.

8.1. Extreme events characterization

Based on Gumbel distribution, extreme event of 5, 20, 50 and 100 years return periods are detected as shown in Table 35. Gumbel method is used here since it is the simplest one for extremes estimation.

Table 35 . Extreme event corresponding to the return period 5, 20, 50 and 100.

Return period (year)	100	50	20	5
Discharge (m^3/s)	1554.0	1416.6	1233.2	943.9

It is observed that peak discharge with a return period of 5, 20, 50 and 100 years at Bonou station are respectively 943.9 m^3/s, 1233.2 m^3/s, 1416.6 m^3/s and 1554 m^3/s. Flow duration curve over the period 1971 – 2010 is shown on Figure 48.

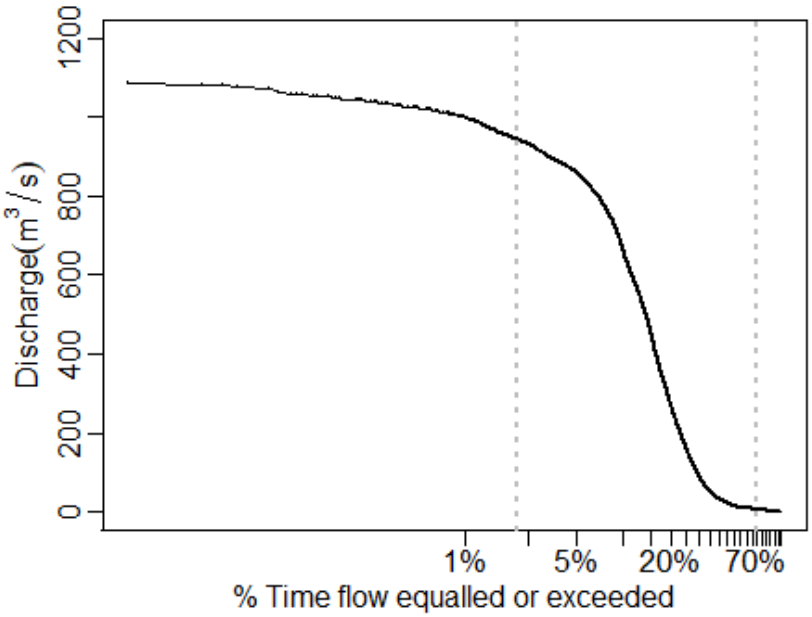

Figure 48. Flow duration curve over the period 1971 – 2010.

It is noticed that apart from the 5 years return period peak discharge (Q5) which is exceeded only 2.14 % of the time that is about 309 days over the period considered, none of the remaining is yet reached.

It is known that Ouémé Delta is flooded when Ouémé River water level reaches 8 meters (H8) at Bonou station [6]. Water level duration curve over the period 1971 – 2010 is plotted on Figure 49.

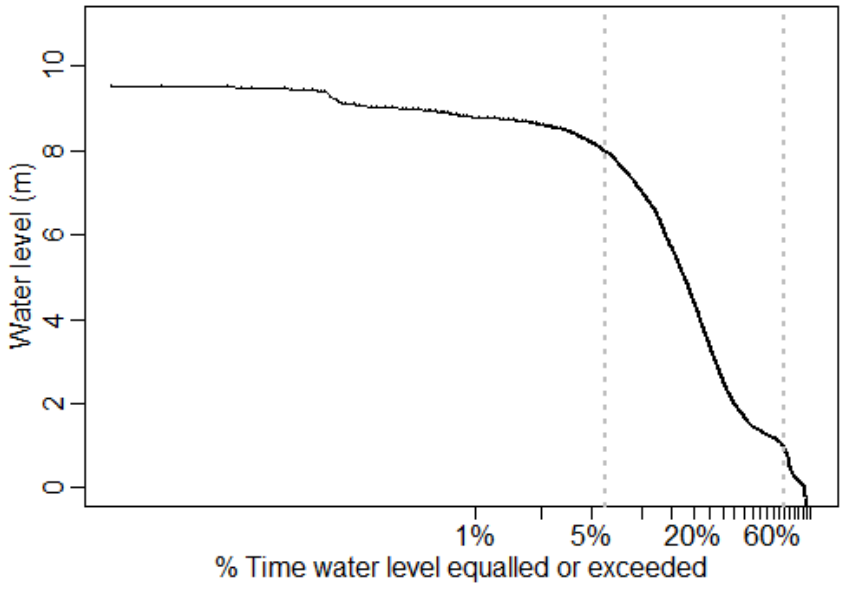

Figure 49. Water level duration curve over the period 1971 – 2010.

It is observed that H8 was exceeded about 5.95 % of the time that corresponds to 859 days over the forty years considered. Therefore, Ouémé Delta was flooded 2.35 years over the forty considered from 1971 to 2010. Daily water level plot in relationship with daily discharge is exhibited on Figure 50.

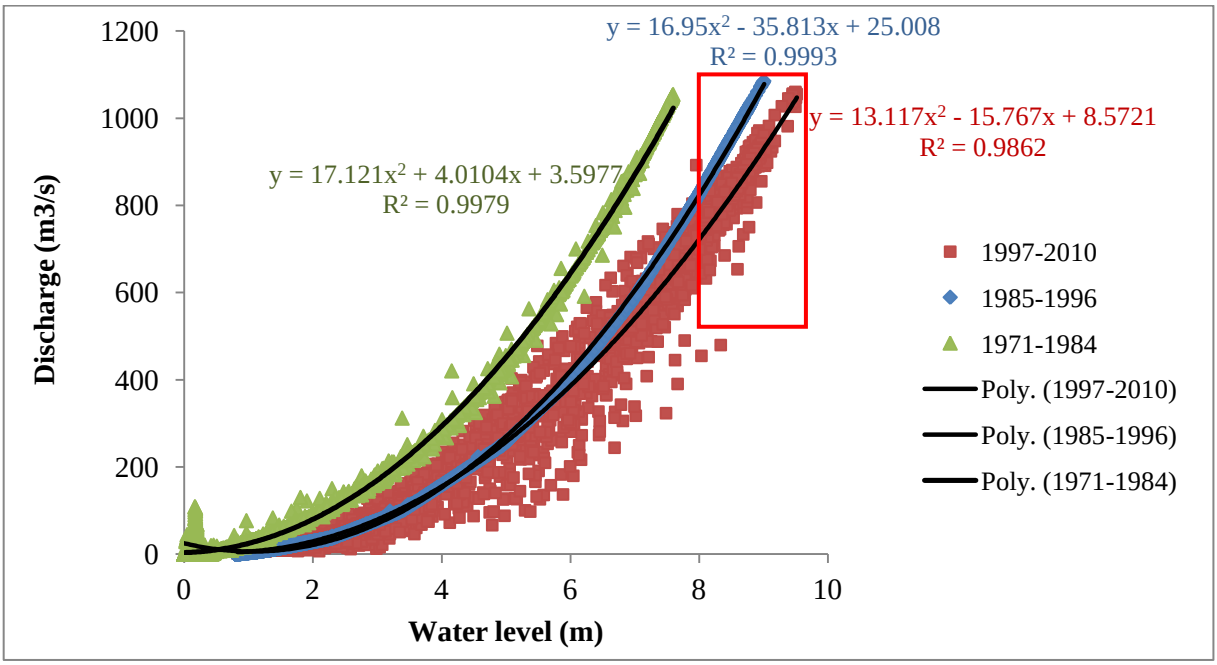

Figure 50. Plot of discharge in relation with water level from 1971 – 2010.

Daily discharges corresponding to water level exceeding H8 are inside the red box. It is observed that there is H8 of 8.04 m corresponding to 479.40 m^3/s. It was reached on July 26, 1999. That year H8 was exceeded 98 days. The maximum discharge over the period is 1085 m3/s and was obtained on August 30, 1991.

In addition, we noticed the use of three different rating curves at Bonou relatively to the periods 1971-1984, 1985-1996 and 1997-2010. Two degree polynomial regression equation over each period of time is as shown on Figure 48 respectively in green, blue and red colors. Comparing, these three rating curves, it is noticed that, from 1997-2010 the rating curve was not calibrated as data points are more dispersed compared to the others two.

8.2. Hydrodynamic model calibration and validation

The hydrodynamic model is calibrated and validated at the stations of Bonou and So-Ava only due to data availability. Actually, these are the stations were data are simultaneously available at least for one year. In fact, Bonou station represents the upstream forcing of the hydrodynamic model. As observed water level and discharge are available at Bonou, water

level data were used as upstream forcing to calibrate and validate discharge and vice-versa. In addition, So-Ava station is on So River and is influenced by tidal. Therefore calibration So-Ava increases the accuracy of the model.

Ouémé River discharge at Bonou station and water level at So-Ava station are calibrated and validated with efficiency coefficients summarized in Table 36.

Table 36. Efficiency coefficient of model calibration and validation results.

	Q_Bonou		H_So-Ava	
	Calibration	Validation	Calibration	Validation
MAE	16.23	17.66	0.11	0.10
PBias	-4.40	-4.80	2.70	-4.80
KGE	0.96	0.95	0.92	0.94

KGE between observed and simulated discharge at Bonou station is 0.95 with MAE of 17 m^3/s in average and about 4.6 % of underestimation either in calibration and validation. At So-Ava station, KGE is 0.92 in calibration and 0.94 in validation. MAE is respectively 0.11 m and 0.10 m in calibration and validation. There was an overestimation of 2.7 % and an underestimation of 4.8 % respectively in calibration and validation. Figure 51 showed calibrated and validated plots. It is observed a good agreement between observation and simulation.

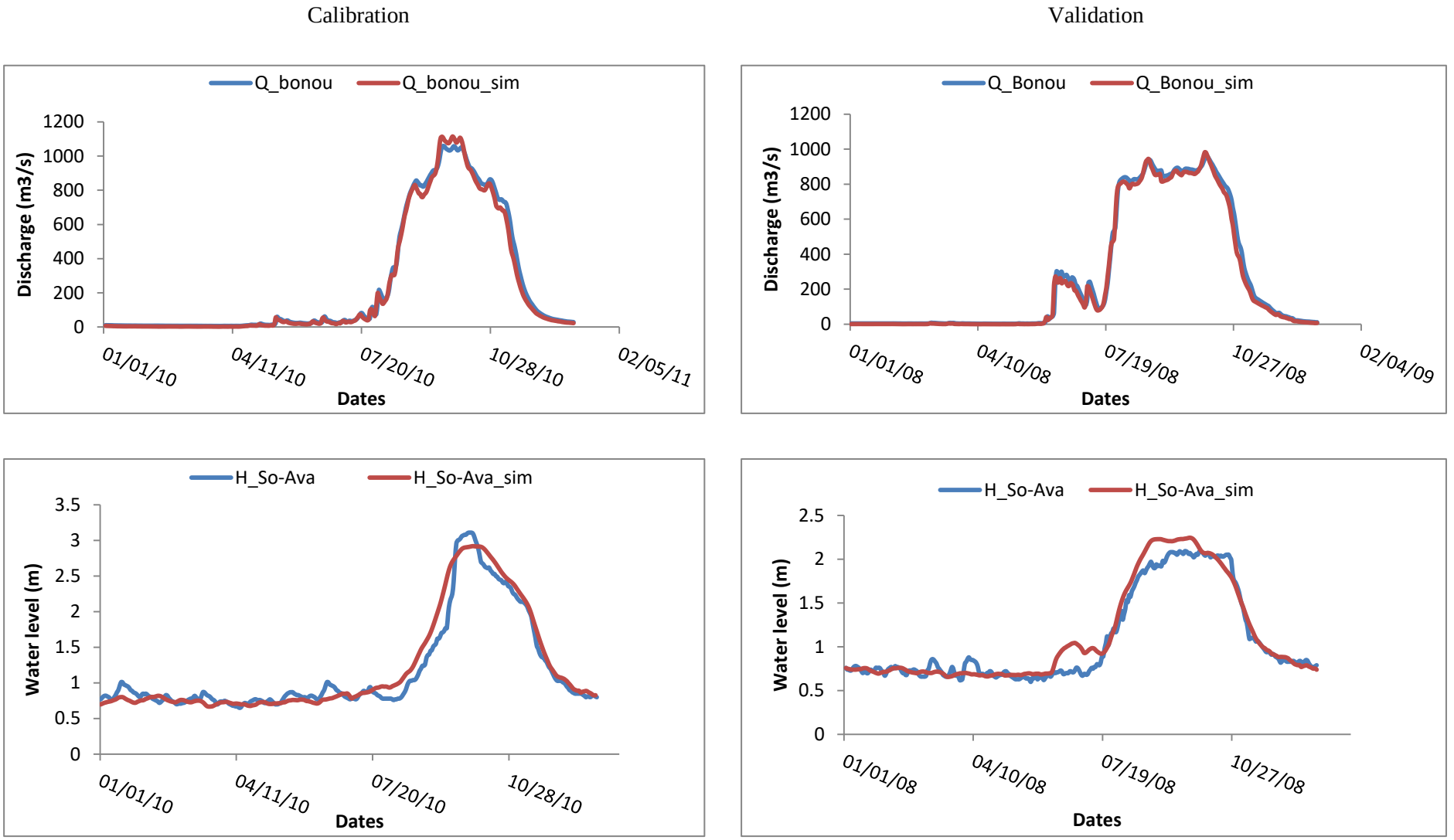

Figure 51. Calibration and validation of Ouémé River discharge at Bonou station and water level at So-Ava station.

In addition, flood map was extracted from the calibrated model and compared with existing satellite image. Figure 52 shows comparison between October 18, 2010 satellite image and simulated flood map of that same day.

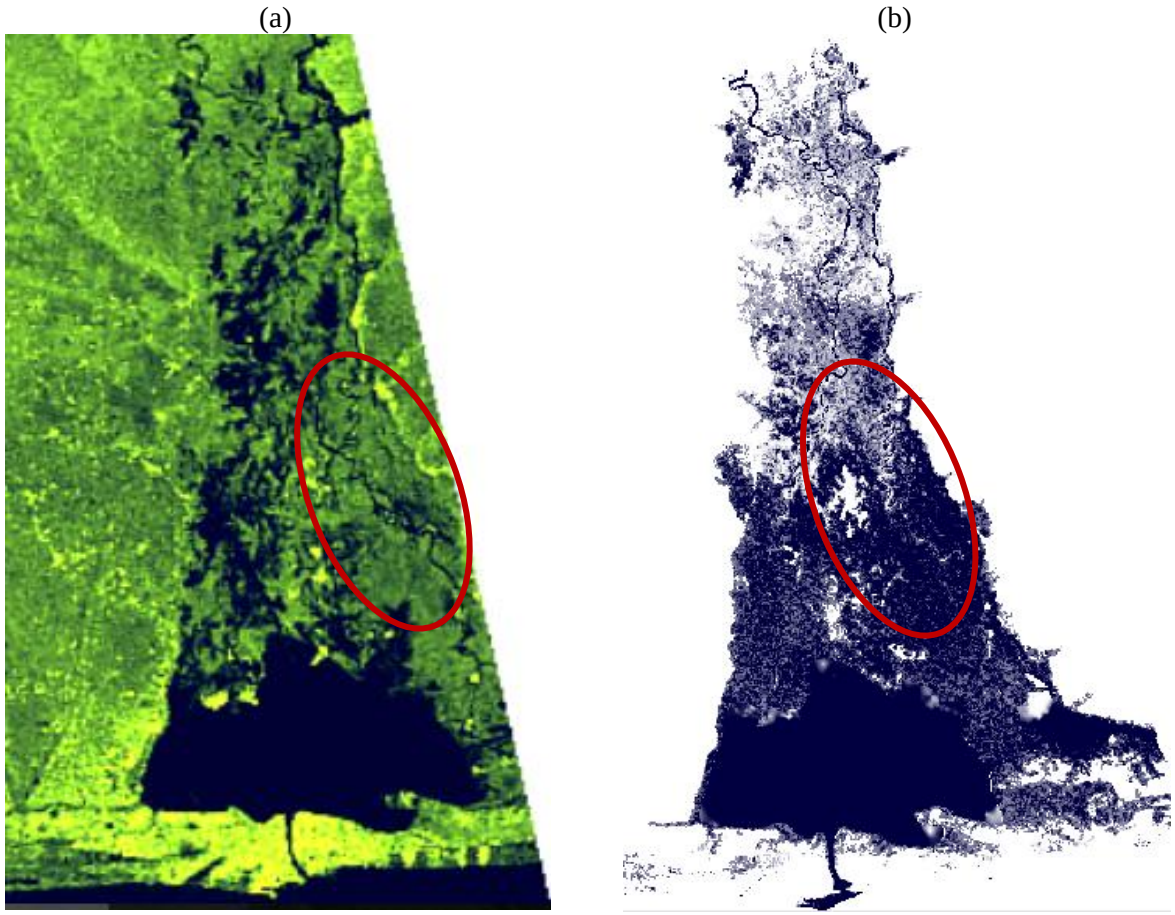

Figure 52. Comparison between October 18, 2010 satellite image (a) and simulated flood map (b).

It is noticed a matching between the satellite image and the simulated flood map everywhere apart from the eastern area hereby inside the red form. This visual mismatching is due to the mixture of water and vegetation which is not well perceived in the satellite image.

In addition, assessment of the calibrated roughness used over the Ouémé Delta showed good results with comparison to Chow manning's number classification relatively to land cover types [147].

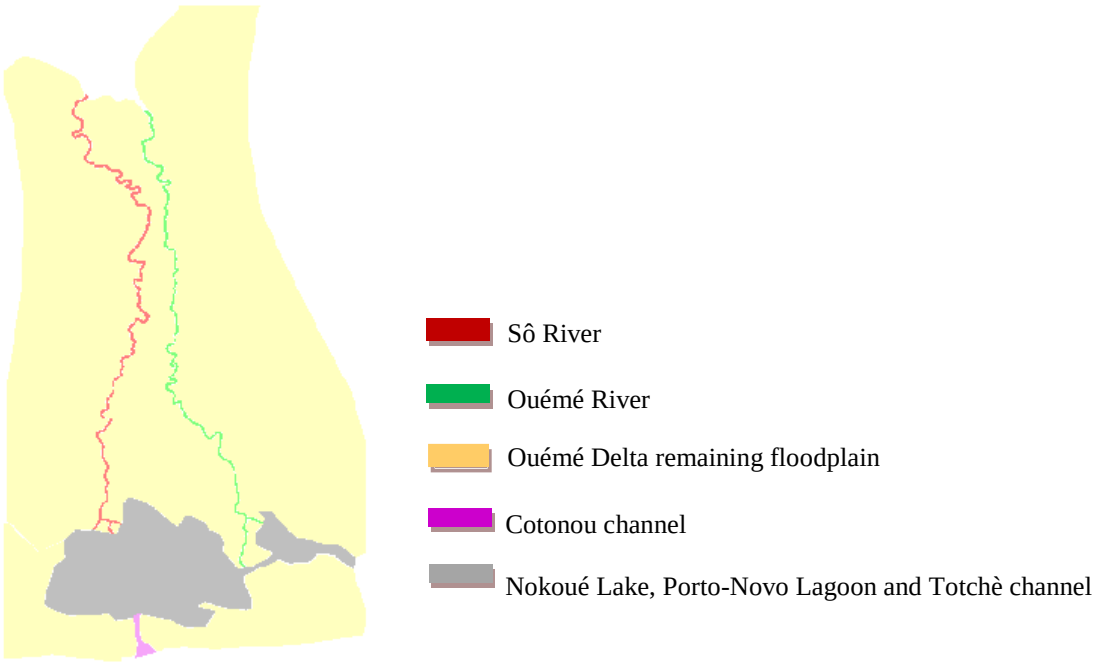

Figure 53. Calibrated Mannings number regions relatively to land cover types over Ouémé Delta

Figure 53 shows land cover regions distinction. In fact, various Rivers and channels as well as the floodplain were distinguished. The Manning's number used according to each region is as followed in Table 37.

Table 37. Calibrated Manning's numbers with actual region and chow description

Regions	Calibrated Mannings numbers	Corresponding Chow Manning's regions	Actual field description
Cotonou channel	0.05	Rivers	River with wastes
Sô River	0.06	Rivers	River with vegetaion
Ouémé Delta remaining floodplain	0.15	Farmland and residential areas	Farmland, grassland with scattered forests as well as build up
Nokoué Lake, Porto-Novo Lagoon and Totchè channel	0.045	Rivers	Rivers with acadja
Ouémé River	0.045	Rivers	Rivers with vegetation

Comparing Chow classification relatively to Manning's numbers and the actual field description, the roughness used are well calibrated.

8.3. Reconstruction of Ouémé River discharge at Bonou outlet in 2016 and Assessment of the hydrodynamic and hydrological models robustness in 2016 and 2018

8.3.1. Reconstruction of Ouémé River discharge at Bonou outlet in 2016

Adjohoun station is located on Ouémé River at 25 km downstream Bonou station [6]. There may be a relationship between these two stations' hydraulic characteristics. In order to assess that relationship, daily water level at Bonou from 1971 to 2010 was averaged and propagated. Water level data recorded at Adjohoun are then plotted against those of Bonou as shown on Figure 54.

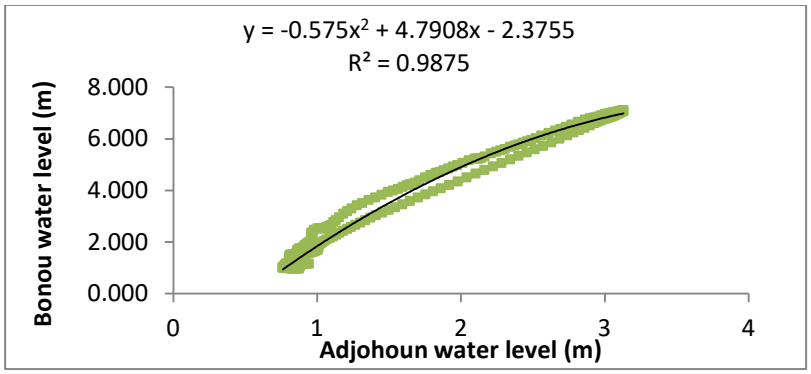

Figure 54. Relationship between Bonou and Adjohoun water level.

A linear relationship described by the following equation is found between the stations of Adjohoun and Bonou.

$$H_{Bonou} = -0.6 * H^{2}_{Adjohoun} + 4.8 * H_{Adjohoun} - 2.38 \quad (8)$$

8.3.2. Propagation results of the reconstructed discharge at Bonou in 2016

As water level data does not exist at Bonou in 2016 but is available at Adjohoun; Equation 8 is used to reconstruct missing data. In order to confirm the reconstruction, water level reconstructed at Bonou in 2016 was propagated. Water level recorded after the propagation is then compared with 2016 observation at Adjohoun. As water level data exist in 2016 at Hêtin-Sota and So-Ava, the same process is replicated for those stations. Efficiency between observation and water level recorded after propagation at each of the latter stations are summarized in Table 38. It is noticed a good representation of water level at Hêtin-Sota

and Adjohoun stations. Though, So-Ava station is still not well reproduced, the observed peak and the trend are well simulated.

Table 38. Data reconstruction efficiency in 2016.

	So-Ava	Hêtin-Sota	Adjohoun
MAE	0.12	0.16	0.09
PBias	1.10	-6.40	-1.80
KGE	0.65	0.94	0.96

Result plots are shown on Figure 55. As previously, described water level of 2016 is well validated.

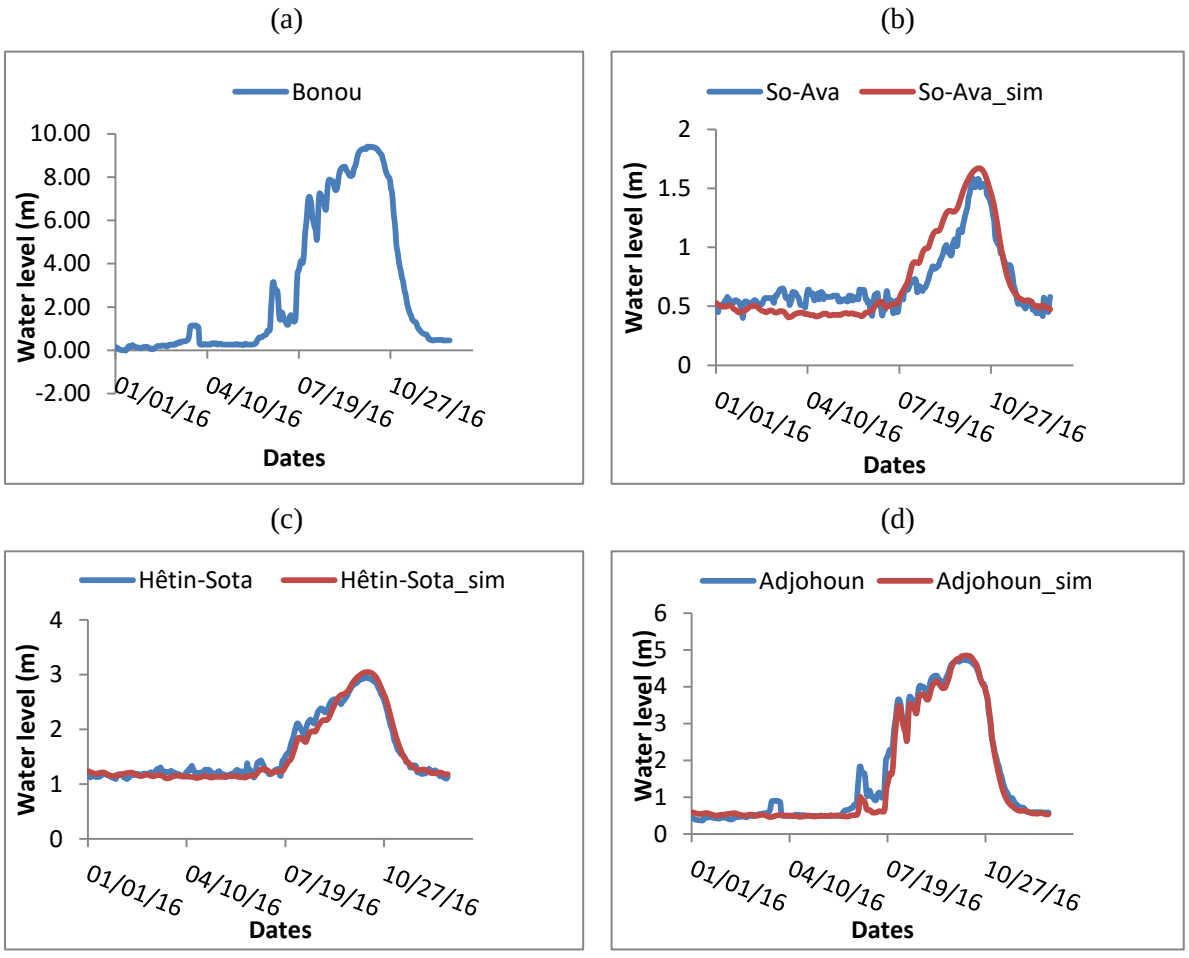

Figure 55. Bonou water level reconstructed (a), So-Ava validation (b), Hêtin-Sota validation (c) and Adjohoun validation (d) in the year 2016.

Therefore with one station data, the other ones are then predictable.

8.4. Assessment of the hydrodynamic and hydrological models robustness in 2016 and 2018

8.4.1. Assessment of the hydrodynamic and hydrological models robustness in 2016

In order, to assess the robustness of both hydrodynamic and hydrologic model outputs in the year 2016, comparison is made between discharge simulated at Bonou by the hydrodynamic model HEC-RAS and hydrologic model HEC-HMS. Result is shown on Figure 56. The trend is well represented although small scale rainfall distribution was not well represented by the regional climate model used.

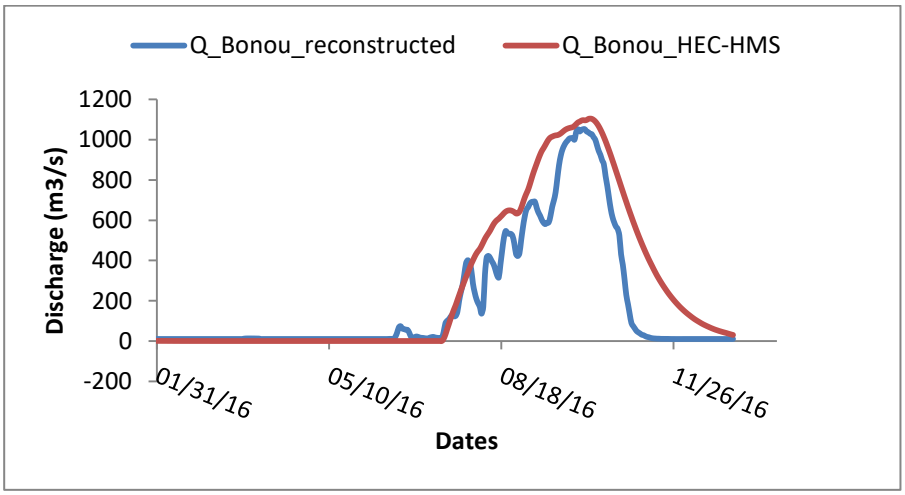

Figure 56. Comparison between simulated discharge from the hydrodynamic and hydrological model in 2016.

8.4.2. Assessment of the hydrodynamic and hydrological model combination robustness in 2018

As the Ouémé River discharge at Bonou outlet trends from the hydrological model and the reconstructed data from the hydrodynamic model matches (Figure 56), 2018 discharge at Bonou from the hydrological model is then propagated. As water level exists at Nokoué Lake station in 2018, comparison between water level recorded after propagation at Nokoué Lake station and observation is made. Efficiency coefficients of results are summarized in Table 39. Observations are underestimated at 1.1 %, with a mean absolute error of 0.03 m and a KGE of 0.96.

Table 39. Data reconstruction efficiency in 2018.

	Nokoué Lake
MAE	0.03
PBias	-1.1
KGE	0.96

Water level at the stations of Adjohoun Hêtin-Sota, So-Ava, Nokoué Lake and Bonou as well as discharge at Bonou are illustrated on Figure 57.

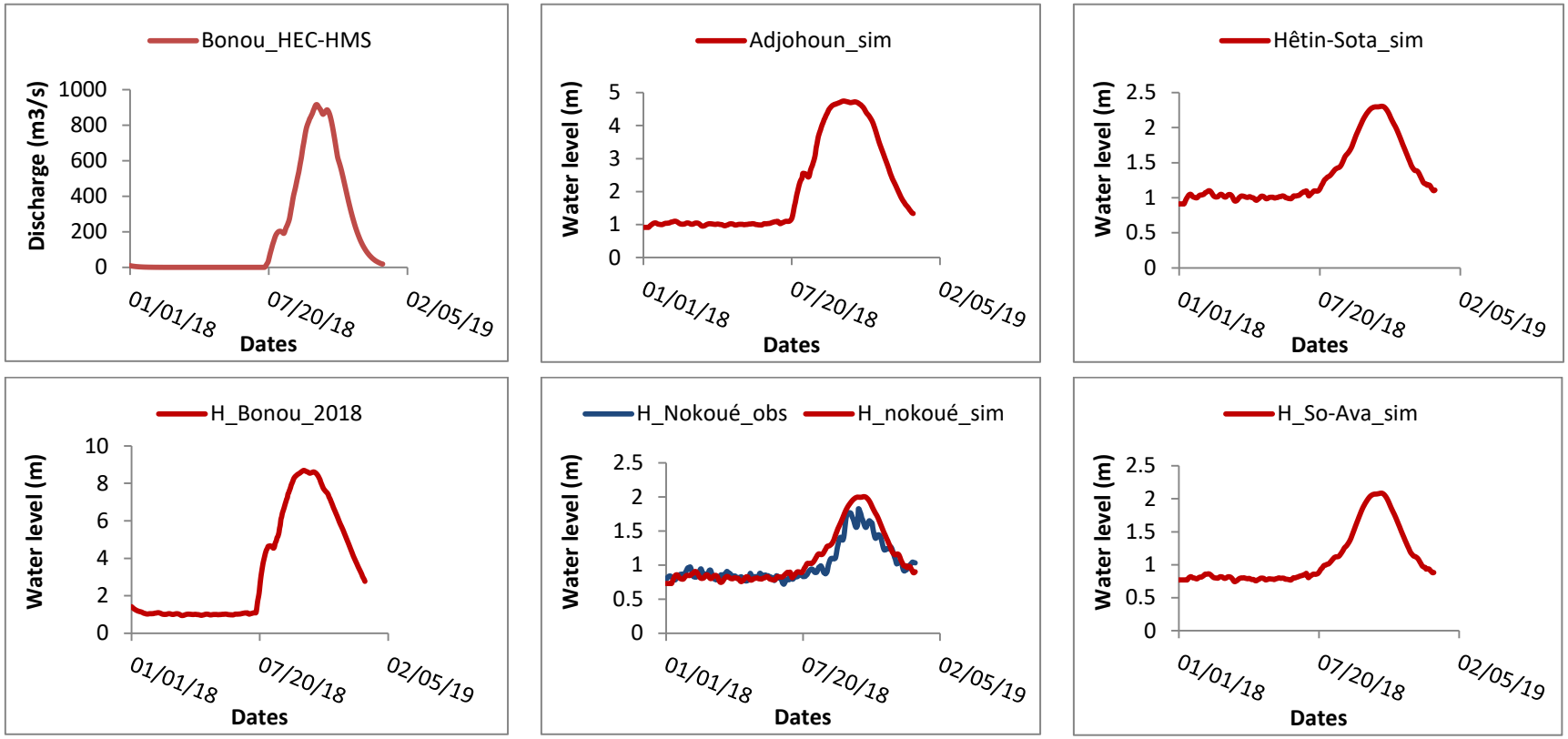

Figure 57. Water level reconstruction at Bonou, Adjohoun, Hêtin-Sota and Nokoué Lake station in 2018.

At the Nokoué lake station, a good matching between observed and propagated records is noticed.

8.5. Ouémé Delta hydrodynamic functionning

Ouémé delta hydrodynamic depends essentially on tidal, on Ouémé river inflow at Bonou and on inflow from So River in case where water level exceed 8 meters at Bonou station [6]. Local rainfall also plays a key role in the Ouémé Delta hydrodynamic.

Tidal effects extent is illustrated on Figure 58. It is noticed that tide is sensed from the coast till Hêtin-Sota latitude because of the flatness of these areas especially during the low flow and the first rainy season in Ouémé Delta from March to June. On Figure 59.a, a tidal impact is illustrated water level fluctuation in 2016 at Hêtin-Sota and So-Ava stations. Therefore, the water level variation observed during low water at Adjohoun and Bonou station is mainly due to the rainfall during the first rainy season in the Delta (Figure 59.b).

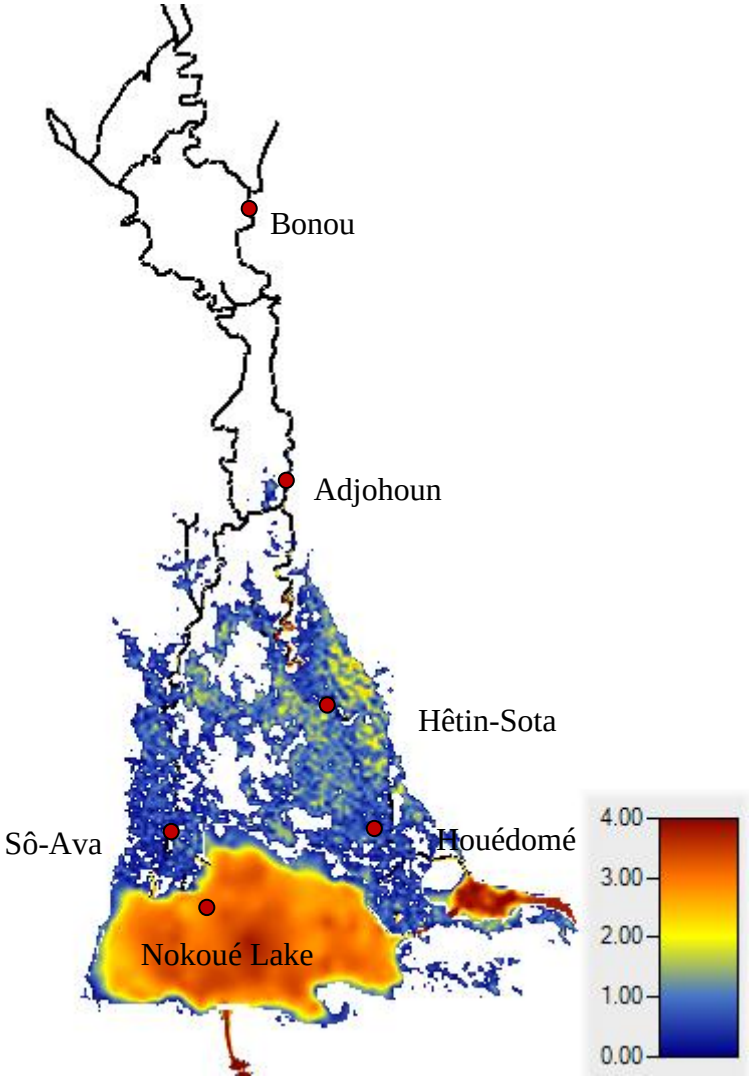

Figure 58. Tidal effect extent in Ouémé Delta.

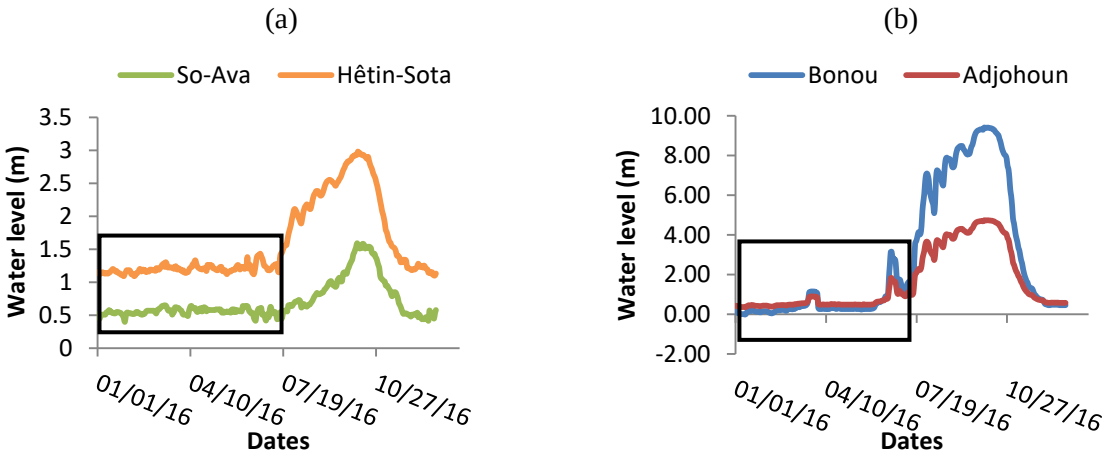

Figure 59. Tide influence on water level So and Hêtin (a) and Bonou and Adjohoun (b).

Because of Ouémé river slope from Bonou to Houédomé, it is noticed 50 % loss of water level almost each 25 km from July to November (Figure 60). As consequence, water level peak at Houédomé is half of Hêtin-Sota water level peak which is half of that of Adjohoun which in turn is half of water level peak at Bonou. It also noticed that water level at Houédomé is almost the same as that of So-Ava. The difference between both is due to the propagation time from Adjohoun to So-Ava which is higher than that Adjohoun to Houédomé. These relationships may be maintained only if So-Ava water level peak is less than 2 m. Out of this range, inflow from Ouémé River into So River in the upstream will be considerable and is not yet well known [6].

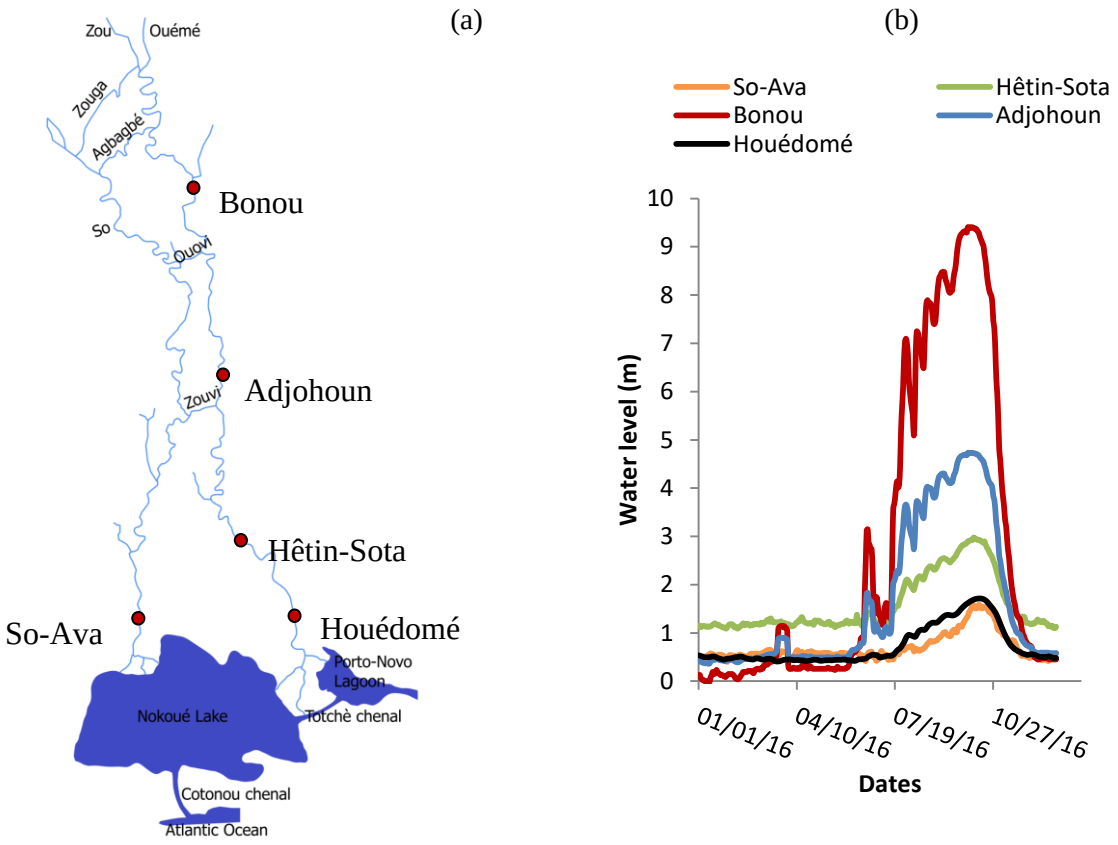

Figure 60. Water level station positions (a) and water level at each station (b).

Interrelationship between the stations of Bonou, Adjohoun, Hêtin-Sota, Houédomé and So-Ava is then deducted based on 2016 data recorded (Figure 60). We noticed that before the peak that stay from the end of September till the first week of October, water level relationship between the various stations followed more two degree polynomial shape (Figure 61). This

may be explained by the slow start from January till July, where it is noticed an abrupt rise in water level due to the rainy season start in the upstream over the Ouémé catchment. However, after that peak flow period, the relationship is linear (Figure 61).

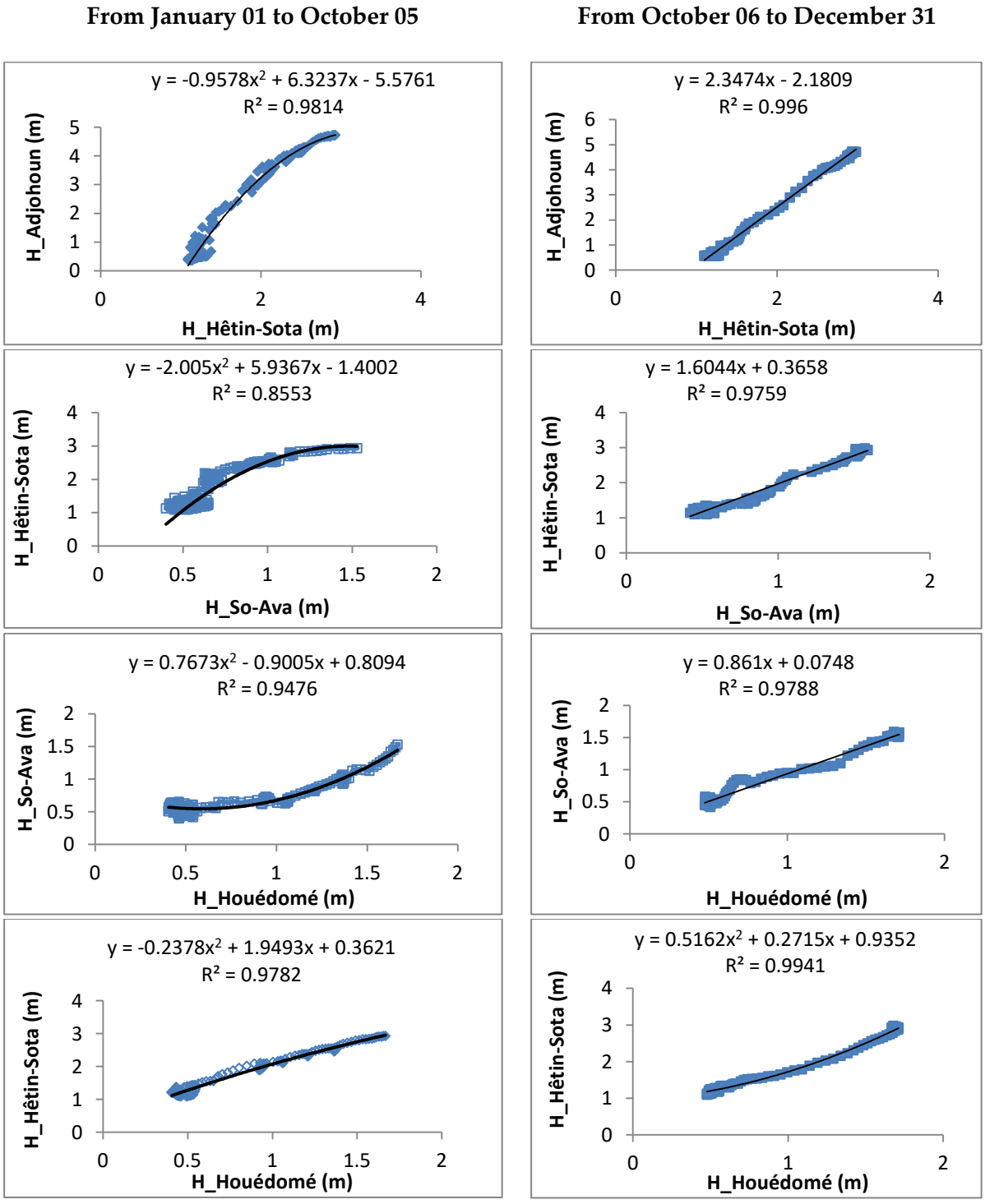

Figure 61. water level relationship between various stations

8.6. Dam construction scenario and climate change impacts on Ouémé Delta hydrodynamic

Considering the three main dams (Bétérou, Vossa and Dogo-Bis) projected on Ouémé catchment, 3.5 billion of annual water will be retained. In order, to assess its impact on Ouémé Delta, we considered the daily averaged discharge of Ouémé River at Bonou outlet over the period of 1971-2010. This period takes into account the dry period of 70s and the wet that started from the 90s. A potential retention based on the annual volume projected is deducted and plot on Figure 62 as dam retention.

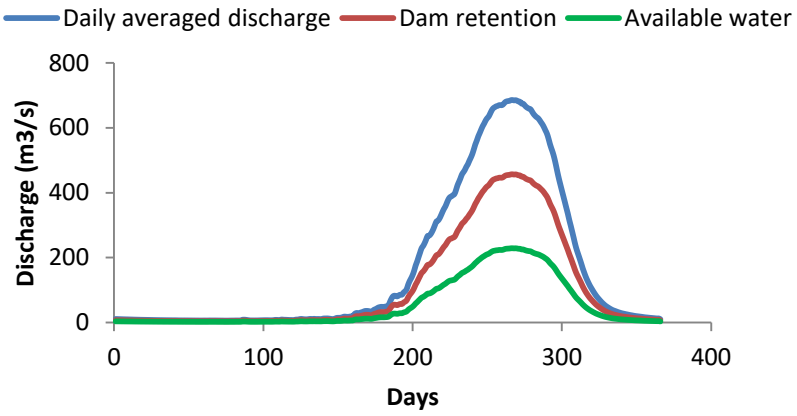

Figure 62. Daily discharge scenario in the case of dam construction.

Then the remaining volume of 1.8 billion of cubic meters (Table 40) is the available one plotted on the same graph.

Table 40. Annual volume of water corresponding to each discharge scenario

	Annual volume (Billion cubic meter)
Daily averaged discharge	5.3
Dam retention	3.5
Available water	1.8

The corresponding flood map to the scenario before and after dam construction is illustrated on Figure 63.

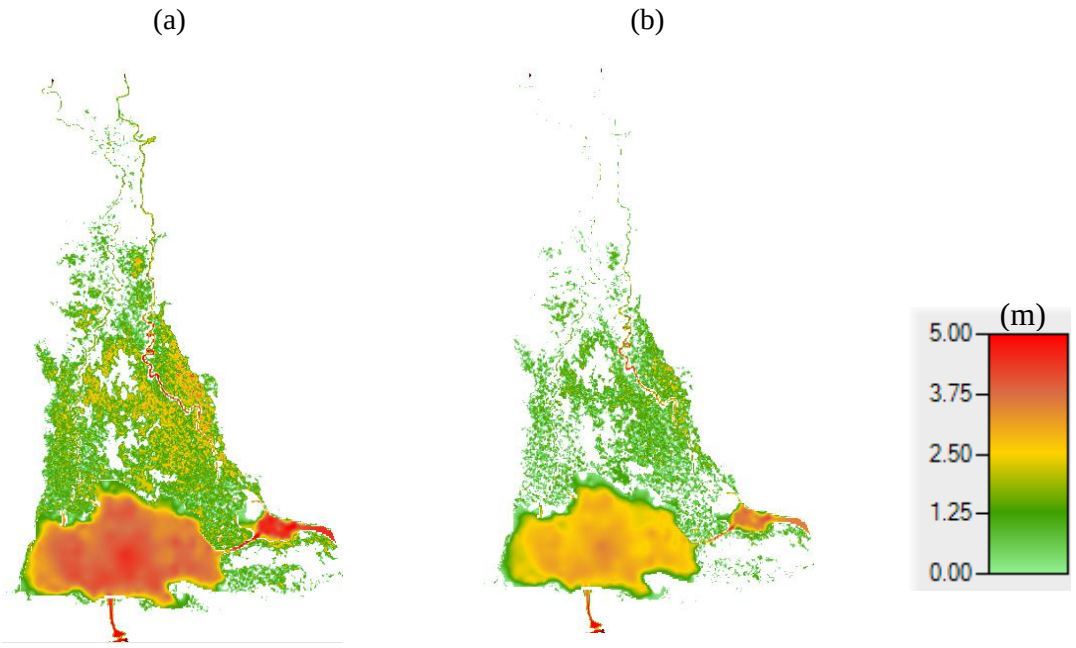

Figure 63. Ouémé Delta flood map before (a) and after (b) dam construction scenario with the scale in meters.

It is noticed that the southern part of the Delta is less flooded after dam construction scenario. In fact, in average the maximum water level is up to 5 m before dam scenario and decreases to almost 2.5 m after dam construction simulation. The drawback is that as the intensity of inundation is reduced less organic matters will be drained into the Delta for nourishing the soil. Another inconvenient is the reduction of water stagnation duration in the Ouémé Delta. In fact, most farmers in the Delta used to mow their land before flood events so that during flood they are rotted and fertilize the land for the following season. Moreover, this may cause difficulties to species that migrate through the floodplain up and down for hashing such as Heterotis or for other activities. Therefore, fishing activities will be impacted as well as agriculture. Considering salinity distribution, with the dam construction, dissolution effect will be reduced. Then, salinity along the rivers will be high and the species that are salinity sensitive will be quite influenced. An example is the Eucherichia crapisse (water jacinth) which does not resist to high salinity. This will also cause qualitative water issues for either consumption or

irrigation. A part from these overall impacts of dam construction, climate change impacts are not least.

In addition, as flow propagation is done by gravity, surface elevation plays a key role in the hydrodynamic functioning. Therefore, land use and cover degradation highly impact on flow propagation time. As land use and cover degradation is going to impact climate change effects on water resource by the means of discharge reduction based on the representative concentration pathway RCP4.5, the impacts of dam scenario will be enhanced. Therefore, the combined effects may double difficulties in socioeconomic aspects.

8.7. Early warning system improvement in Ouémé Delta

The existing early warning system is based on a statistical relationship between the main stations in the Delta. The improvement brought in this work is the automatization and the knowledge availability not only at station point but also at grid point. Based on the overall results, with knowledge about rainfall amount and temperature data in Ouémé catchment, water level and discharge is acknowledgeable at any point in Ouémé Delta. In fact, with inputs of rainfall and temperature into the hydrological model discharge is predicted. In addition, results showed that predicted discharge from the hydrodynamic and the hydrological models is well calibrated. Therefore, discharge obtained from the hydrological model could be propagated inside the Ouémé Delta using the hydrodynamic model set up for water level and discharge generation at any point of the Delta as shown on Figure 64. Moreover, based on the stations data of Adjohoun and Hêtin-Sota, Bonou station’s data can be deducted.

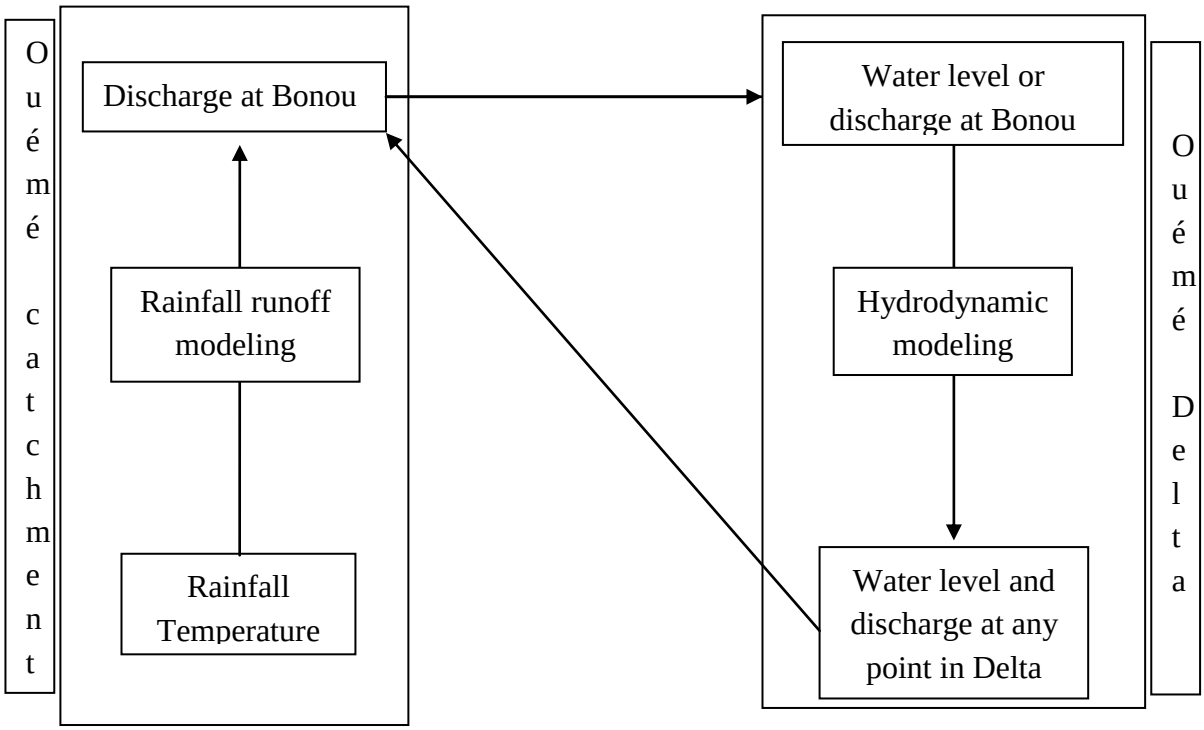

Figure 64. Early warning system improvement in Ouémé Delta.

This system could be improved using future updated data and further information.

8.8. Discussions

Results found showed good representation of observation using limited data. In fact, it is noticed that, the more the available data, the best the accuracy of results. Though, reconstruction of discharge based on the interrelationship between stations in 2016 was not quite good, it already gave the trend of the simulated discharge based on the hydrological model HEC-HMS. Therefore, in a case of limited data or for future projection, based on only precipitation scenarios over Ouémé catchment, water level can be simulated over Ouémé Delta. For instance in the year 2018, simulated discharge from the hydrological model HEC-HMS give good representation at Nokoué Lake station. However, more efforts should be made in data collection (water level, tide and satellite images) in order to reduce cumulative uncertainties from the modeling processes for better prevision and the early warning in Ouémé Delta.

8.9. Partial conclusion

In this chapter, the hydrodynamic model set up show ability of representing hydraulic characteristics (water level and discharge) over Ouémé Delta. Calibration and validation were conducted respectively over the year 2010 and 2008. Based on the sparse data available at the different stations over the Delta, 2016 and 2018 water level at those stations were reconstructed using a combination of the hydrological and the hydrodynamic models. Although, results are quite good, more data are needed for more accuracy. In fact, the difference between simulated discharge from HEC-HMS based on climate model data, and simulated discharge based on the internal relationships between stations in HEC-RAS may be reduced if uncertainties during the modeling processes are reduced. Moreover, the projected infrastructures should take into account the decreasing trend projected in discharge at 2050 horizon not only for sustainable investments but also the ecosystem services conservation through environmental protection over Ouémé catchment and Delta. Therefore, it is important to assess the environmental flow for Ouémé Delta before any hydraulic infrastructure construction for the Ouémé Delta sustainability.

Chapter 9: General conclusion and perspectives

Chapter 9 presents general conclusion in Section 9.1 and perspectives in Section 9.2.

9.1. Conclusion

This work focuses on analyzing climate change impacts on Ouémé Delta hydrodynamic and was structured on four parts. The first part focused on the current status of climatic extremes trends in Ouémé Delta. In order to reach this goal, prewhitened Mann–Kendal trend analysis in rainfall and temperature extremes, as well as pan evaporation influencing factors was conducted. Fifteen rainfall based climate indices; eight temperature based indices as well as minimal relative humidity, maximal relative humidity, sunshine duration, wind speed at 10 m altitude, and pan evaporation at annual scale were computed at eight gauging stations (including two synoptic stations) from 1960 to 2016. Results showed intensification in heavy rainfall frequency with increase in monthly maximum precipitation in the months of September, October, and November that represent the high water period in Ouémé Delta. In addition, the increase noted in extreme rainfall, especially heavy, very heavy rainfall, maximum consecutive 1, 2, 3, 5, and 10-day maximum will probably impact flood event in terms of damages and losses in Ouémé Delta. Moreover, most impacted areas are found to be the closest ones to Ouémé Delta. Therefore, extreme events tend to increase as stated in the hypothesis. Furthermore, the increase in temperature as a consequence of global warming and the decrease in relative humidity are going to put stress on plants in terms of water availability. The pan evaporation tends to significantly increase in Ouémé Delta. As a key measure of surface water loss, its climatic explanatory variables Ouémé Delta area are wind speed, mean temperature, and sunshine duration, with wind speed and sunshine explaining its variance at almost 50%. Consequently, water availability issue is probably going to be problematic with rise in conflicts between farmers and herders because of livestock migrations.

Therefore, the second part quantifies the impacts of climate change over Ouémé River discharge which catchment feed Ouémé Delta with water. Four regional climate models (RCM)

were used as well as land use and land cover change in Ouémé catchment. From 1971 to 2010, simulation of Ouémé River discharge showed 0.94 and 0.91 of Kling-Gupta efficiency respectively in calibration (1971-1990) and validation (1991-2010). In addition, underestimation of high flow is noted and should be taken into account in hydraulic scenario development. Moreover, in the next fifty years an increase in temperature is projected as proof of global warming. A significant decreasing trend is noticed in projected discharge based on the RCP 4.5 scenario as mentioned in the hypothesis. However, an insignificant increasing trend is projected in discharge based on the RCP 8.5 at mid-century term. Compared to previous works, HEC-HMS performed well and can be adopted in areas with limited soil data as in developing countries. However, future studies should explore the option of using soil moisture accounting (SMA) method for losses processing while using HEC-HMS over Ouémé catchment, in order to evaluate whether the model could better simulate high flow than it did under the curve number (CN) loss method.

The third part then explored ensemble model approach to simulate peak flow over Ouémé catchment. Two semi-distributed models based on the SMA (HEC-HMS, HBV) and one lumped model based on least action principle (HyMoLAP) were gathered through ensemble mean approach. Inter-comparison of models is firstly done to assess their inner performance. Results show best performance of HEC-HMS ahead HBV and HyMoLAP. However, HBV and HEC-HMS performance look alike with KGE of more than 0.9 in calibration and validation. They hold the least PBias and MAE as well. HyMoLAP was average in simulating overall flow but underestimates much peak flows. In fact, KGE of HyMoLAP is 0.86 in calibration and 0.78 in validation, whereas the peak flow PBias is of -19.5 %. Considering ensemble models run, HBV/HEC-HMS is the best with the least percentage of bias over peak flow. Therefore, out of the various ensembles assessed in this study, the couple HBV/HEC-HMS is the best in Ouémé catchment. In addition, considering these models one by one HEC-HMS remains the best due to the storage components that it accounts for. Integrating storage components to HyMoLAP may be a good perspective for its improvement over peak

flows. Moreover, the use of the distributed instead of the lumped as well as the stochastic version of HyMoLAP may be best since it initially takes into the stochastic aspect of natural phenomenon.

The next section was devoted to map flooded areas in Ouémé Delta for the hydrodynamic model results validation. Based on the color composite method proposed hereby not only land cover classes were visualized but also water extent in the Ouémé Delta. Acadja map is showed. In addition, correlation analysis between rainfall events and flood map is done for further flood map comprehension. As the outputs are for visual aspect no area quantification is done. Moreover, an input may be determining water surface elevation based on such images in order to predict water level for early warning improvement. The last part aimed at simulating hydrodynamic functioning of Ouémé Delta under climate change impacts and dam construction scenario. The hydrodynamic model set up, shows ability of representing hydraulic characteristics (water level and discharge) over Ouémé Delta. Calibration and validation were conducted respectively over the year 2010 and 2008. Based on the sparse data available at the different stations over the Delta, 2016 and 2018 water level at those stations were reconstructed using a combination of the hydrological and the hydrodynamic models. Therefore, Ouémé Delta early warning system could be improved using a combination of remote sensing, hydrologic and hydrodynamic tools as stated in the hypothesis. Although, results are quite good, more data are needed for more accuracy. In fact, the difference between simulated discharge from HEC-HMS based on climate model data, and simulated discharge based on the internal relationships between stations in HEC-RAS may be reduced if uncertainties during the modeling processes are reduced. Moreover, the projected infrastructures should take into account the decreasing trend projected in discharge at 2050 horizon for sustainable investments over Ouémé catchment. Therefore the environmental flow of Ouémé Delta should be assessed for it ecosystem services sustainability.

9.2. Perspectives

The objectives of this work were reached based on the scope designed at the beginning. As Ouémé Delta is a limited data area, more effort should be done on data collection with high resolution in space and time. In addition, future work should look at the use of Tropical Rainfall Measuring Mission (TRMM) data for averaged climatic data over the Ouémé catchment to fill missing. Ouémé Delta bathymetry data should be updated in order to integrate current change in the river bed to the hydrodynamic model. Moreover, fine resolute digital elevation model is needed for more accuracy. Stations data collection should be done for monitoring water level in order to produce daily discharge. Tele-transmitted stations should be prioritized to reduce disturbance and limit accessibility difficulties. This will easier short term early warning in Ouémé Delta. We have already start with one tele-transmitted stations acquired through IFS and two others through WASCAL founds. Only two are yet installed. One is located at Vêkky on the Nokoué Lake and the second at Yêgota not far from the confluence of Ouémé and Zou Rivers. The last one will be installed at Djigbé on So River next year. In addition, the use of remote sensing in water level prediction should be developed based on radar data for data reconstruction and inputs to the early warning system. The impact assessment should go beyond 2050 to far future (2100) for long term insight. Moreover, the use of the stochastic version of HyMoLAP may be a good option in modeling extreme flow. An appropriate radar mapping process should be developed using the semi automatic plugging for more accuracy. Moreover, the environmental flow assessment is important before any dam construction over Ouémé catchment for preserving Ouémé Delta ecosystem in this changing climate condition.

References

1. Marchand, M.; Bucx, T.; Makaske, B.; van de Guchte, C.; van Driel, W. Enabling Delta Life - What makes managing land and water in deltas different? Discussion paper. *Delta Alliance GWP* **2012**, 48.

2. World Bank Inondation au Bénin. Rapport d'Evaluration des Besoins Post Catastrophiques. **2011**.

3. Zannou, A. B.; Yabi, M.; Diallo, G.; Tokpon, M. S.; Agbakou, V.; Adimi, S.; Yamontche, S.; Kaka, D.; Kouazounde, J.; Medenon, A.; Koutchade, A. G.; Mama-sika, R.; Yergo, A.; Togbenou, M.; Badarou, R. M.; Dahome, E.; Mouzoun, P.; Agbegninou, R.; Fico, M. *Projet d ' aménagement des grands barrages hydroélectriques multifonctions sur le fleuve Ouémé au Bénin: Etude stratégique et technico-économique*; Cotonou, 2017;

4. Biao, E. I. Assessing the Impacts of Climate Change on River Discharge Dynamics in Oueme River Basin. *Hydrology* **2017**, *4*, 16, doi:10.3390/hydrology4040047.

5. Lawin, A. E.; Hounguè, R.; N 'Tcha M'Po, Y.; Hounguè, N. R.; Attogouinon, A.; Afouda, A. A. Mid-Century Climate Change Impacts on Ou é m é River Discharge at Bonou Outlet (Benin). *Hydrology* **2019**, *6*, 20, doi:10.3390/hyd6030072.

6. Le Barbe, L.; Ale, G.; Millet, B.; Texier, H.; Borel, Y.; Gualde, R. Les Ressources en Eaux Superficiels de la République du Bénin; ORSTOM.; Paris, 1993; ISBN 270990344X.

7. Mama, D. Méthodologie et résultats du diagnostic de l'eutrophisation du lac Nokoue (Bénin), Université de Limoges, 2010.

8. Hounguè, R.; Lawin, E.; Moumouni, S.; Afouda, A. A. Change in Climate Extremes and Pan Evaporation Influencing Factors over Ouémé Delta in Bénin. *Climate* **2019**, *7*, 22, doi:10.3390/cli7010002.

9. Alexander, L. Introduction to ClimPACT Background to ClimPACT • Written in R. **2013**.

10. Sylla, M. B.; Nikiema, P. M. Climate Change over West Africa : Recent Trends and Future Projections Chapter 3 Climate Change over West Africa : Recent Trends and Future Projections. **2016**, doi:10.1007/978-3-319-31499-0.

11. Beven, K. Modélisation Hydrologique Distribuée. **2002**, 3–7.

12. Riede, J. O.; Posada, R.; Fink, A. H.; Kaspar, F. What ' s on the 5th IPCC Report for West Africa ? **2016**, 7–24, doi:10.1007/978-3-319-31499-0.

13. Alterra, R. V. D. B.; Deltares, T. B.; Alterra, J. K.; Arcadis, P. W. Launching the Delta Alliance : Content report phase 3. **2014**.

14. Woodward, A.; Smith, K. R.; Campbell-Lendrum, D.; Chadee, D. D.; Honda, Y.; Liu, Q.; Olwoch, J.; Revich, B.; Sauerborn, R.; Chafe, Z.; Confalonieri, U.; Haines, A. Climate change and health: On the latest IPCC report. *Lancet* **2014**, *383*, 1185–1189, doi:10.1016/S0140-6736(14)60576-6.

15. Urama, K. C.; Ozor, N. Impacts of climate change on water resources in africa: the Role of Adaptation. *African Technol. Policy Stud. Netw.* **2010**, 1–29.

16. IEG World Bank Responding to Floods in West Africa: Lessons from Evaluation; Washington, DC, 2010;

17. Jha, A.; Lamond, J.; Bloch, R.; Bhattacharya, N.; Lopez, A.; Papchristodoulou, N.; Bird, A.; Poverbs, D.; Davies, J.; Barker, R. Five Feet High and Rising Cities and Flooding in the 21st Century. **2011**, 1–68, doi:10.1596/1813-9450-5648.

18. Mynett, A. E.; Vojinovic, Z. Hydroinformatics in multi-colours — part red: urban flood and disaster management. *J. Hydroinformatics* **2009**, *3–4*, 166–180, doi:10.2166/hydro.2009.027.

19. ECREEE GIS Hydropower Resource Mapping and Climate Change Scenarios for the ECOWAS Region, Country Report for Benin; ECOWAS Centre for Renewable Energy and Energy Efficiency (ECREEE): Praia, Cabo Verde, 2017;

20. Oguntunde, P. G.; Friesen, J.; Giesen, N. Van De; Savenije, H. H. G. Hydroclimatology of the Volta River Basin in West Africa: Trends and variability from 1901 to 2002. *Phys. Chem. Earth* **2006**, *31*, 1180–1188, doi:10.1016/j.pce.2006.02.062.

21. Panthou, G.; Lebel, T.; Vischel, T.; Quantin, G.; Sane, Y.; Ba, A.; Ndiaye, O.; Diongue-Niang, A.; Diopkane, M. Rainfall intensification in tropical semi-arid regions: the Sahelian case. *Environ. Res. Lett.* **2018**, *13*, 064013, doi:10.1088/1748-9326/aac334.

22. Nouaceur, Z.; Murărescu, O. Rainfall Variability and Trend Analysis of Annual Rainfall in North Africa. *Int. J. Atmos. Sci.* **2016**, *2016*, 1–12, doi:10.1155/2016/7230450.

23. Soro, G. E.; Noufé, D.; Albert, T.; Bi, G.; Shorohou, B. Trend Analysis for Extreme Rainfall at Sub-Daily and Daily Timescales in Côte d ' Ivoire. *Climate* **2016**, *4*, 1–15, doi:10.3390/cli4030037.

24. Oguntunde, P. G.; Abiodun, B. J.; Lischeid, G. Rainfall trends in Nigeria, 1901–2000. *J. Hydrol.* **2011**, *411*, 207–218, doi:10.1016/j.jhydrol.2011.09.037.

25. Kabo-bah, A. T.; Diji, C. J.; Nokoe, K.; Mulugetta, Y.; Obeng-ofori, D.; Akpoti, K. Multiyear Rainfall and Temperature Trends in the Volta River Basin and their Potential

Impact on Hydropower Generation in Ghana. *Climate* **2016**, *4*, 1–17, doi:10.3390/cli4040049.

26. Hountondji, Y.; Ozer, P. Submitted to the 1 st International Conference on Energy , Environment And Climate Changes Trends in extreme rainfall events in Benin (West Africa), 1960-2000. In *Proceedings of the 1st International Conference on Energy, Environment And Climate Changes*; Ho Chi Minh City, Vietnam; pp. 1–7.

27. Hounkpè, J.; Diekkrüger, B.; Badou, D.; Afouda, A. Change in Heavy Rainfall Characteristics over the Ouémé River Basin, Benin Republic, West Africa. *Climate* **2016**, *4*, 15, doi:10.3390/cli4010015.

28. Attogouinon, A.; Lawin, A. E.; M'Po, Y. N.; Houngue, R. Extreme Precipitation Indices Trend Assessment over the Upper Ouémé River Valley-(Bénin). *Hydrology* **2017**, *4*, 36, doi:10.3390/hydrology4030036.

29. N'Tcha M'Po, Y.; Lawin, E.; Yao, B.; Oyerinde, G.; Attogouinon, A.; Afouda, A. Decreasing Past and Mid-Century Rainfall Indices over the Ouémé River Basin, Benin (West Africa). *Climate* **2017**, *5*, 74, doi:10.3390/cli5030074.

30. Lawin, E. A.; Afouda, A.; Oguntunde, P. G.; Gosset, M.; Lebel, T. Rainfall variability at regional and local scales in the Ouémé upper valley in Benin. *Int. J. Sci. Adv. Technol.* **2012**, *2*, 46–55.

31. Bojang, F.; Ndeso-Atanga, A. Economic and social significance of forests for Africa's sustainable development. *Nat. Faune Enhancing Nat. Resour. Manag. food Secur. Africa* **2011**, *25*, 104.

32. IPCC Climate Change 2007: Synthesis Report. Contribution of Working Groups I, II and III to the Fourth Assessment Report of the Intergovernmental Panel on Climate Change *[Core Writing Team, Pachauri, R.K and Reisinger, A. (eds.)]*; ISBN 92-91.; IPCC: Geneva, Switzerland, 2007;

33. Diedhiou, A.; Bichet, A.; Wartenburger, R.; Seneviratne, S. I.; Rowell, D. P.; Mouhamadou, S. B.; Diallo, I.; Todzo, S.; Touré, N. E.; Camara, M.; Ngounou Ngatchah, B.; Kane, N. A.; Tall, L.; Affholder, F. Changes in climate extremes over West and Central Africa at 1 . 5 ◦ C and 2 ◦ C global warming. *Environ. Res. Lett.* **2018**, *13*, 1–11.

34. Cook, K. H.; Vizy, E. K. Impact of climate change on mid-twenty-first century growing seasons in Africa. *Clim. Dyn.* **2012**, *39*, 2937–2955, doi:10.1007/s00382-012-1324-1.

35. Touré, H. A.; Kalifa, T.; Kyei-Baffour, N. Assessment of changing trends of daily precipitation and temperature extremes in Bamako and Ségou in Mali from 1961- 2014. *Weather Clim. Extrem.* **2017**, *18*, 8–16, doi:10.1016/j.wace.2017.09.002.

36. Niang, I.; Ruppel; O.C. Abdrabo, M. A.; Essel, A.; Lennard, C.; Padgham, J.; Urquhart, P. Africa, Climate Change 2014: Impacts, Adaptation, and Vulnerability. Part B: Regional Aspects. Contribution of Working Group II to the Fifth Assessment Report of the Intergovernmental Panel on Climate Change [Barros, V.R., C.B. Field, D.J. Dokken, M.D. *Cambridge Univ. Press. United Kingdom New York, NY, USA*, **2014**, 1199–1265.

37. Nicholson, S. E.; Dezfuli, A. K. The Relationship of Rainfall Variability in Western Equatorial Africa to the Tropical Oceans and Atmospheric Circulation. Part I: The Boreal Spring. *J. Clim.* **2013**, *26*, 45–65.

38. New, M.; Hewitson, B.; Stephenson, D. B.; Tsiga, A.; Kruger, A.; Manhique, A.; Gomez, B.; Coelho, C. A. S.; Masisi, D. N.; Kululanga, E.; Mbambalala, E.; Adesina, F.; Saleh, H.; Kanyanga, J.; Adosi, J.; Bulane, L.; Fortunata, L.; Mdoka, M. L.; Lajoie, R. Evidence of trends in daily climate extremes over southern and west Africa. *J. Geophys. Res. Atmos.* **2006**, *111*, 1–11, doi:10.1029/2005JD006289.

39. Xing-Jie, J.; Ji-Jun, W.; Wan-Long, G.; Ye-Yu, Z.; Feng-Xiu, L. Trends in Annual and Seasonal Pan Evaporation in the Lower Yellow River Basin from 1961 to 2010. *Adv. Clim. Chang. Res.* **2012**, *3*, 195–204, doi:10.3724/SP.J.1248.2012.00195.

40. Oguntunde, P. G.; Abiodun, B. J.; Olukunle, O. J.; Olufayo, A. A. Trends and variability in pan evaporation and other climatic variables at Ibadan, Nigeria, 1973-2008. *Meteorol. Appl.* **2012**, *19*, 464–472, doi:10.1002/met.281.

41. Djaman, K.; Koudahe, K.; Ganyo, K. K. Trend Analysis in Annual and Monthly Pan Evaporation and Pan Coefficient in the Context of Climate Change in Togo. *J. Geosci. Environ. Prot.* **2017**, *5*, 41–56, doi:10.4236/gep.2017.512003.

42. Zhang, Q.; Wang, W.; Wang, S.; Zhang, L. Increasing trend of pan evaporation over the semiarid loess plateau under a warming climate. *J. Appl. Meteorol. Climatol.* **2016**, *55*, 2007–2020, doi:10.1175/JAMC-D-16-0041.1.

43. Helfer, F.; Lemckert, C.; Zhang, H. Impacts of climate change on temperature and evaporation from a large reservoir in Australia. *J. Hydrol.* **2012**, *475*, 365–378, doi:10.1016/j.jhydrol.2012.10.008.

44. Roudier, P.; Ducharne, A.; Feyen, L. Climate change impacts on runoff in West Africa: A review. *Hydrol. Earth Syst. Sci.* **2014**, *18*, 2789–2801, doi:10.5194/hess-18-2789-2014.

45. Mbaye, M. L.; Hagemann, S.; Haensler, A.; Stacke, T.; Gaye, A. T.; Afouda, A. Assessment of Climate Change Impact on Water Resources in the Upper Senegal Basin (West Africa). *Am. J. Clim. Chang.* **2015**, *04*, 77–93, doi:10.4236/ajcc.2015.41008.

46. Vinet, L.; Zhedanov, A. A "missing" family of classical orthogonal polynomials. *Clim. Chang. 2014 Synth. Report. Contrib. Work. Groups I, II III to Fifth Assess. Rep.*

Intergov. Panel Clim. Chang. **2010**, 2–26, doi:10.1088/1751-8113/44/8/085201.

47. Seneviratne, S. I.; Nicholls, I.; Easterling, D.; Goodess, C. M.; Kanae, S.; Kossin, J.; Luo, Y.; Marengo, J.; McInnes, K.; Rahimi, M.; Reichstein, M.; Sorteberg, A.; Vera, C.; Zhang, X. Changes in climate extremes and their impacts on the natural physical environment. *Manag. Risks Extrem. Events Disasters to Adv. Clim. Chang. Adapt. A Spec. Rep. Work. Groups I II Intergov. Panel Clim. Chang. (IPCC).* **2012**, 109–230.

48. Parry, M.; Canziani, O.; Palutikof, J.; Linden, P. van der; Hanson, C. *Climate Change 2007: Impacts, Adaptation and Vulnerability*; M.L. Parry, O.F. Canziani, J.P. Palutikof, P. J. van der L. and C. E. H., Ed.; Cambridge University Press, 2007; ISBN 9780521880107.

49. Giertz, S.; Diekkrüger, B.; Jaeger, a.; Schopp, M. An interdisciplinary scenario analysis to assess the water availability and water consumption in the Upper Ouémé catchment in Benin. *Adv. Geosci.* **2006**, *9*, 3–13, doi:10.5194/adgeo-9-3-2006.

50. Michael Case *Climate Change Impacts on East Africa: A Review of the Scientific Literature*; text 2006 WWF, Ed.; World Wide Fund for Nature: Gland, Switzerland, 2006;

51. Hawkins, E.; Osborne, T. M.; Kit Ho, C.; Challinor, A. J. Calibration and bias correction of climate projections for crop modelling : an idealised case study over Europe. *Agric. For. Meteorol.* **2013**, *Preprint*, 19–31.

52. Dosio, A. Projections of climate change indices of temperature high-resolution EURO-CORDEX regional climate models. **2016**, doi:10.1002/2015JD024411.

53. Serinaldi, F.; Kilsby, C. G. The importance of prewhitening in change point analysis under persistence. *Stoch. Environ. Res. Risk Assess.* **2016**, *30*, 763–777, doi:10.1007/s00477-015-1041-5.

54. Babur, M.; Babel, M. S.; Shrestha, S.; Kawasaki, A.; Tripathi, N. K. Assessment of Climate Change Impact on Reservoir Inflows Using Multi Climate-Models under RCP's—the case of Mangla Dam in Paskitan. *Water* **2016**, *8*, doi:10.3390/w8090389.

55. Yira, Y.; Diekkrüger, B.; Steup, G.; Bossa, A. Y. Impact of climate change on water resources in a tropical West African catchment using an ensemble of climate simulations. *Hydrol. Earth Syst. Sci. Discuss.* **2016**, 1–37, doi:10.5194/hess-2016-387.

56. Ali, S.; Li, D.; Congbin, F.; Khan, F. Twenty first century climatic and hydrological changes over Upper Indus Basin of Himalayan region of Pakistan. *Environ. Res. Lett.* **2015**, *10*, doi:10.1088/1748-9326/10/1/014007.

57. Koutroulis, A. G.; Tsanis, I. K.; Daliakopoulos, I. N.; Jacob, D. Impact of climate change on water resources status: A case study for Crete Island, Greece. *J. Hydrol.* **2013**,

doi:10.1016/j.jhydrol.2012.11.055.

58. Grillakis, M. G.; Koutroulis, A. G.; Daliakopoulos, I. N.; Tsanis, I. K. A method to preserve trends in quantile mapping bias correction of climate modeled temperature. **2017**, 889–900.

59. Oyerinde, G. T.; Hountondji, F. C. C.; Lawin, A. E.; Odofin, A. J.; Afouda, A.; Diekkrüger, B. Improving Hydro-Climatic Projections with Bias-Correction in Sahelian Niger Basin, West Africa. *Climate* **2017**, *5*, doi:10.3390/cli5010008.

60. Biao, I. E.; Alamou, A. E.; Afouda, A. Improving rainfall–runoff modelling through the control of uncertainties under increasing climate variability in the Ouémé River basin (Benin, West Africa). *Hydrol. Sci. J.* **2016**, *6667*, 02626667.2016.1164315, doi:10.1080/02626667.2016.1164315.

61. Obada, E.; Alamou Adéchina, E.; Zandagba, E. J.; Biao, I. E.; Chabi, A. Comparative study of seven bias correction methods applied to three Regional Climate Models in Mekrou catchment (Benin , West Africa). *Int. J. Curr. Eng. Technol.* **2016**, *6*, 1831–1840.

62. M'Po, Y. N. T. M.; Lawin, A. E.; Oyerinde, G. T. Comparison of Daily Precipitation Bias Correction Methods Based on Four Regional Climate Model Outputs in Ouémé Basin , Benin. **2017**, doi:10.11648/j.hyd.20160406.11.

63. Geleta, C. D.; Gobosho, L. Climate Change Induced Temperature Prediction and Bias Correction in Finchaa Watershed. **2018**, *18*, 324–337, doi:10.5829/idosi.aejaes.2018.324.337.

64. Foughali, A.; Tramblay, Y.; Bargaoui, Z.; Carreau, J.; Ruelland, D. Hydrological Modeling in Northern Tunisia with Regional Climate Model Outputs: Performance Evaluation and Bias-Correction in Present Climate Conditions. **2015**, 459–473, doi:10.3390/cli3030459.

65. Sorteberg, A. Challenges in bias correction of climate projections What are the challenges ? Examples from Norway.

66. Fung, F. UKCP18 Guidance : Bias correction; 2018;

67. Nicholson, S. E.; Funk, C.; Fink, A. H. Rainfall over the African continent from the 19th through the 21st century. *Glob. Planet. Change* **2018**, *165*, 114–127, doi:10.1016/j.gloplacha.2017.12.014.

68. Bouchardeau, A.; Bauduin, D. Monographie du delta de l'Ouémé; ORSTOM.; Paris, 1964;

69. Hounkpè, J.; Diekkrüger, B.; Afouda, A. A.; Sintondji, L. O. Land use change increases

flood hazard : a multi - modelling approach to assess change in flood characteristics driven by socio - economic land use change scenarios. *Nat. Hazards* **2019**, doi:10.1007/s11069-018-3557-8.

70. Lawin, E. A.; N Tcha M'Po, Y.; Biaou, C. A.; Komi, K.; Hounguè, R.; Yao, B. K.; Afouda, A. A. Mid-Century Daily Discharge Scenarios Based on Climate and Land Use Change in Ouémé River Basin at Bétérou Outlet. *Hydrology* **2019**, 1–14, doi:10.3390/hydrology5040069.

71. Barthel, R.; Sonneveld, B. G. J. S.; Götzinger, J.; Keyzer, M. A.; Pande, S.; Printz, A.; Gaiser, T. Integrated assessment of groundwater resources in the Ouémé basin , Benin , West Africa. *Phys. Chem. Earth* **2009**, *34*, 236–250, doi:10.1016/j.pce.2008.04.001.

72. Badou, D. F.; Kapangaziwiri, E.; Diekkrüger, B.; Hounkpè, J.; Afouda, A. Evaluation of recent hydro-climatic changes in four tributaries of the Niger River Basin (West Africa). *Hydrol. Sci. J.* **2016**, *0*, 1–14, doi:10.1080/02626667.2016.1250898.

73. Hounkpè, J.; Diekkrüger, B. Challenges in calibrating hydrological models to simultaneously evaluate water resources and flood hazard : a case study of Zou basin , Benin. *Episodes* **2018**, *41*, 105–114.

74. Gaba, O. U. C.; Biao, I. E.; Alamou, A. E.; Afouda, A. An Ensemble Approach Modelling to Assess Water Resources in the Mékrou Basin , Benin. **2015**, *3*, 22–32, doi:10.11648/j.hyd.20150302.11.

75. Linde, A. H.; Aerts, J. C. J. H.; Hurkmans, R. T. W. L.; Eberle, M. Comparing model performance of two rainfall-runoff models in the Rhine basin using different atmospheric forcing data sets. *Hydrol. Earth Syst. Sci.* **2008**, 943–957.

76. Dhami, B. S.; Pandey, A. Comparative review of recently developed hydrologic models. **2013**, 34–42.

77. Otieno, H.; Han, D. Comparative Study On Water Resources Assessment Between Kenya And England. In *International Conference on Hydroinformatics. HIC 2014*; New York City, USA, 2014.

78. PNUD Conception de modèles simplifies de prévision et la détermination des seuils et niveaux d 'alerte relatifs aux inondations; Rapport d'étude; Cotonou, 2014;

79. Iosub, M.; Minea, I.; Oana, H.; Romanescu, G. H. The use of HEC-RAS modelling in flood risk analysis. **2015**, doi:10.17378/AWC2015.

80. Patel, P. L. HEC-RAS based hydrodynamic model in prediction of stages of lower Tapi River. *ISH J. Hydraul. Eng.* **2012**, *17*, 10, doi:10.1080/09715010.2011.10515050.

81. Thakur, P. K.; Sumangala, A. Flood inundation mapping and 1-d hydrodynamic

modeling using remote sensing and gis technique. **2000**.

82. Tong, R.; Komma, J. Calibration of HEC-Ras hydrodynamic model using gauged discharge data and flood inundation maps. **2017**, *19*, 15805.

83. Marcinkowski, T.; Olszewski, T. Numerical modelling assumptions for deposition and spread of dumped material. *Bull. Marit. Inst.* **2015**, *2*, 1–9, doi:10.5604/12307424.1158129.

84. DHI Mike 21 flow model - Hints and recommendations in applications with significant flooding and drying. *Environment* **2003**, 1–8.

85. Kulkarni, R. R. Numerical Modelling of Coastal Erosion using MIKE21. **2013**.

86. Shahzad, M.; Faizan, K.; Tariq, A.; Saeed, U.; Sharif, M.; Sheraz, K.; Ahmed, A. Floodplain Mapping Using HEC-RAS *and* ArcGIS : A Case Study of Kabul River. **2015**, doi:10.1007/s13369-015-1915-3.

87. Patel, D. P.; Pandya, U. 1D HEC-RAS Hydrodynamic Modeling of River Flow Simulation Using DEM Extracted River Cross-Sections - A Case of Sabarmati River , Gujarat , India 1D HEC-RAS Hydrodynamic Modeling of River Flow Simulation Using DEM Extracted River Cross-Sections - A Case of. **2018**, 0–1.

88. Alaghmand, S.; Bin, A. R.; Abustan, I. Comparison between capabilities of HEC-RAS and MIKE11 hydraulic models in river flood risk modelling (a case study of Sungai Kayu Ara River basin , Malaysia). **2012**, *2*, 270–291.

89. Giustarini, L.; Chini, M.; Hostache, R.; Pappenberger, F.; Matgen, P. Flood hazard mapping combining hydrodynamic modeling and multi annual remote sensing data. *Remote Sens.* **2015**, *7*, 14200–14226, doi:10.3390/rs71014200.

90. Zhang, P.; Lu, J.; Feng, L.; Chen, X.; Zhang, L.; Xiao, X.; Liu, H. Hydrodynamic and inundation modeling of China's largest freshwater lake aided by remote sensing data. *Remote Sens.* **2015**, *7*, 4858–4879, doi:10.3390/rs70404858.

91. Forkuor, G. Agricultural Land Use Mapping in West Africa Using Multi-sensor Satellite Imagery. **2014**, 191.

92. Manavalan, R.; Rao, Y. S.; Mohan, B. K. Comparative flood area analysis of C-band VH , VV , and L-band HH polarizations SAR data. *Int. J. Remote Sens.* **2017**, *38*, 4645–4654, doi:10.1080/01431161.2017.1325534.

93. Riazanoff, S.; Xavier, J. A Statistical Approach to Preprocess and Enhance C-Band SAR Images in Order to Detect A Statistical Approach to Preprocess and Enhance C-Band SAR Images in Order to Detect Automatically Marine Oil Slicks. **2018**, doi:10.1109/TGRS.2017.2760516.

94. Zannou, A. B. Y. Analyse et modélisation du cycle hydrologique continenetal pour la Gestion Intégrée des Ressources en Eau au Bénin. Cas du bassin de l'Ouémé à Bétérou, 2011.

95. Tappan, G. G., Cushing, W.M., Cotillon, S.E., Mathis, M.L., Hutchinson, J.A., and Dalsted, K. J. *West Africa Land Use Land Cover Time Series: U.S. Geological Survey data release*; 2017;

96. SEARCY, J. K.; HARDISON, C. H. Double-Mass Curves. *UNITED STATES Gov. Print. Off. Washingt.* **1960**.

97. Herold, N.; Alexander, L. V ClimPACT: Software for quantifying climate extremes for sector applications; poster; 2016;

98. Tank, A. M. G. K.; Zwiers, F. W. Guidelines on Analysis of extremes in a changing climate in support of informed decisions for adaptation; WMO.; Geneva, Switzerland, 2009;

99. Wang, L.; Liu, H. An efficient method for identifying and filling surface depressions in digital elevation models for hydrologic analysis and modelling. *Int. J. Geogr. Inf. Sci.* **2006**, *Vol. 20*, 193–213.

100. Alexander, L. V Global observed long-term changes in temperature and precipitation extremes : A review of progress and limitations in IPCC assessments and beyond. *Weather Clim. Extrem.* **2016**, *11*, 4–16, doi:10.1016/j.wace.2015.10.007.

101. Teutschbein, C.; Seibert, J. Is bias correction of regional climate model (RCM) simulations possible for non-stationary conditions ? **2013**, 5061–5077, doi:10.5194/hess-17-5061-2013.

102. Gericke, A.; Kiesel, J.; Deumlich, D.; Venohr, M. Recent and Future Changes in Rainfall Erosivity and Implications for the Soil Erosion Risk in Brandenburg, NE Germany. *Water (Switzerland)* **2019**.

103. Afouda, A.; Lawin, Agnidé Emmanuel Lebel, T. A stochastic streamflow model based on a minimum energy expenditure concept. In *Contempory problems in mathematical physics: Proceeding 3rd Intern Workshop.*; Word scientific publishing Co. Ltd., 2004; p. pp 153-169.

104. Alamou, A. E. Application du principe de moindre action a la modélisation pluie – débit., Université d' Abomey Calavi., 2011.

105. Mann, H. B. Nonparametric tests against trend. *J. Econom. Soc.* **1945**, *Vol. 13*, 245–259.

106. Kendall, M. G. Ranks and Measures. *Biometrika* **1962**, *49*, 133–137, doi:10.2307/2333473.

107. Patakamuri, S. K.; Brien, N. O. Modified Mann Kendall Trend Tests; 2018;

108. Tabari, H.; Somee, B. S.; Zadeh, M. R. Testing for long-term trends in climatic variables in Iran. *Atmos. Res.* **2011**, *100*, 132–140, doi:10.1016/j.atmosres.2011.01.005.

109. Salmi, T.; Maatta, A.; Anttila, P.; Airola, T. R.; Amnell, T. Detecting Trends of Annual Values of Atmospheric Pollutants by the Mann-Kendall Test and Sen's Slope Estimates: The Excel Template Application Makesens; Helsinki, 2002;

110. Yue, S.; Pilon, P.; Phinney, B.; Cavadias, G. The influence of autocorrelation on the ability to detect trend in hydrological series. *Hydrol. Process.* **2002**, *16*, 1807–1829, doi:10.1002/hyp.1095.

111. Blain, G. C. The Mann-Kendall test: the need to consider the interaction between serial correlation and trend. *Acta Sci.* **2013**, *35*, 393–402, doi:10.4025/actasciagron.v35i4.16006.

112. Bayazit, M.; Önöz, B. To prewhiten or not to prewhiten in trend analysis? *Hydrol. Sci. J.* **2007**, *52*, 611–624, doi:10.1623/hysj.52.4.611.

113. Yue, S.; Wang, C. Y. Applicability of Prewhitening to Eliminate the Influence of Serial Correlation on the Mann- Kendall Test. *Water Resour. Res.* **2002**, *38*, doi:10.1029/2001WR000861.

114. Liu, C.; Zhang, J.; Wang, G.; He, R. Changes of pan evaporation and its influencing factors in different climate zones of China. In *Proceedings of symposium J-H02 held during IUGG2011*; Melbourne, Australia, 2011; pp. 93–98.

115. Lawin, A. E.; Hounguè, N. R.; Biaou, C. A.; Badou, D. F. Statistical Analysis of Recent and Future Rainfall and Temperature Variability in the Mono River Watershed. **2019**, doi:10.3390/cli7010008.

116. Zambrano-Bigiarini, M. Package ' hydroGOF ': Goodness-Of-Fit Functions for Comparison of Simulated and Observed Hydrological Time Series 2017, 76.

117. Nash, J. E.; Sutchliffe, J. V. River flow forecasting through conceptual models. Part 1-A discussion of principles. *J. Hydrol* **1970**, *10*, 282–290.

118. Asuero, A. G.; Sayago, A.; Gonz, A. G. The Correlation Coefficient : An Overview. *Crit. Rev. Anal. Chem.* **2006**, *36*, 41–59, doi:10.1080/10408340500526766.

119. Sorooshian, S.; Duan, Q.; Gupta, V. K. Calibration of rainfall-runoff models: Application of global optimization to the Sacramento Soil Moisture. *Water Resour. Res.* **1993**, *29*, 1185–1194, doi:10.1029/92WR02617.

120. Gupta, H. V; Kling, H.; Yilmaz, K. K.; Martinez, G. F. Decomposition of the mean squared error and NSE performance criteria : Implications for improving hydrological

modelling. *J. Hydrol.* **2009**, *377*, 80–91, doi:10.1016/j.jhydrol.2009.08.003.

121. Oudin, L.; Hervieu, F.; Michel, C.; Perrin, C.; Andréassian, V.; Anctil, F.; Loumagne, C. Which potential evapotranspiration input for a lumped rainfall – runoff model ? Part 2 — Towards a simple and efficient potential evapotranspiration model for rainfall – runoff modelling. **2005**, *303*, 290–306, doi:10.1016/j.jhydrol.2004.08.026.

122. USACE HEC-HMS Hydrologic Modeling System; Washington, DC, 2000;

123. Bergström, S. Experience from applications of the HBV hydrological model from the perspective of prediction in ungauged basins. *IAHS Publ* **2006**, 97–107.

124. Center for Ecology and Hydrology A review of applied methods in Europe for flood-frequency analysis in a changing environment; Wallingford, UK, 2013;

125. Halwatura, D.; Najim, M. M. M. Application of the HEC-HMS model for runoff simulation in a tropical catchment. **2013**, doi:10.1016/j.envsoft.2013.03.006.

126. Koneti, S.; Sunkara, S. L.; Roy, P. S. Hydrological Modeling with Respect to Impact of Land-Use and Land-Cover Change on the Runoff Dynamics in Godavari River Basin Using the HEC-HMS Model. **2018**, doi:10.3390/ijgi7060206.

127. Sampath, D. S.; Weerakoon, S. B.; Herath, S. HEC-HMS Model for Runoff Simulation in a Tropical Catchment with Intra- HEC-HMS Model for Runoff Simulation in a Tropical Catchment with Intra-Basin Diversions Case Study of the Deduru Oya River Basin , Sri Lanka. *Eng. - J. Inst. Eng.* **2015**, *XLVIII*, 1–9, doi:10.4038/engineer.v48i1.6843.

128. Pascual-ferrer, J.; Candela, L.; Pérez-foguet, A. Ethiopian Central Rift Valley basin hydrologic modelling using HEC-HMS and ArcSWAT. **2013**, *15*, 10563.

129. Zhang, H. L.; Wang, Y. J.; Wang, Y. Q.; Li, D. X.; Wang, X. K. The effect of watershed scale on HEC-HMS calibrated parameters : a case study in the Clear Creek watershed in Iowa , US Solid Earth. *hess* **2013**, *17*, 2735–2745, doi:10.5194/hess-17-2735-2013.

130. Roy, D.; Begam, S.; Ghosh, S.; Jana, S. Calibration and validation of HEC-HMS model for a river basin in eastern India. **2013**.

131. Awa, W.; Ou, A.; Raude, J. M. Continuous Modeling of the Mkurumudzi River Catchment in Kenya Using the HEC-HMS Conceptual Model : Calibration , Validation , Model Performance Evaluation and Sensitivity Analysis. **2018**, doi:10.3390/hydrology5030044.

132. Biao, E. I.; Gaba, C.; Alamou, A. E.; Afouda, A. Influence of the uncertainties related to the Random Component of Rainfall Inflow in the Ouémé River Basin (Benin , West Africa). *Int. J. Curr. Eng. Technol.* **2015**, *5*, 1618–1629.

133. Tegegne, G.; Park, D. K.; Kim, Y. Comparison of hydrological models for the assessment of water resources in a data-scarce region , the Upper Blue Nile River Basin. *J. Hydrol. Reg. Stud.* **2017**, *14*, 49–66, doi:10.1016/j.ejrh.2017.10.002.

134. European Space Agency Sentinel-1 processing in snap 2017, 4.

135. Nka, B. N.; Oudin, L.; Karambiri, H.; Paturel, J. E.; Ribstein, P. Trends in floods in West Africa : analysis based on 11 catchments. *Hydrol. Earth Syst. Sci.* **2015**, *19*, 4707–4719, doi:10.5194/hess-19-4707-2015.

136. Guhathakurta, P.; Sreejith, O. P.; Menon, P. A. Impact of climate change on extreme rainfall events and flood risk in India. *J. Earth Syst. Sci.* **2011**, *120*, 359–373.

137. Bodegom, A. J. Van; Satijn, B. *Climate Change Profile Benin*; 2015;

138. Zhao, N.; Gou, S.; Zhang, B.; Yu, Y.; Han, S. Changes in Pan Evaporation and Their Attribution to Climate Factors in the Zoige Alpine Wetland, the Eastern Edge of the Tibetan Plateau (1969–2014). *Water* **2017**, *9*, 971, doi:10.3390/w9120971.

139. Hoffman, M. T.; Cramer, M. D.; Gillson, L.; Wallace, M. Pan evaporation and wind run decline in the Cape Floristic Region of South Africa (1974-2005): Implications for vegetation responses to climate change. *Clim. Change* **2011**, *109*, 437–452, doi:10.1007/s10584-011-0030-z.

140. Ganfon, H.; Diallo, T.; Nanga, C.; Coulibaly, N.; Benao, V.; Ekanmian, G.; Sandouidi, A. Private pharmacy staff in five main towns in Benin , Burkina Faso and Mali: knowledge and practices concerning malaria care in 2014. *Med. Sante Trop.* **2017**, *27*, 164–169.

141. Essou, G. R. C.; Brissette, F. Climate Change Impacts on the Ouémé River , Benin , West Africa. *Earth Sci. Clim. Chang.* **2017**, doi:10.4172/2157-7617.1000161.

142. Stanzel, P.; Kling, H.; Bauer, H. Climate change impact on West African rivers under an ensemble of CORDEX climate projections. *Clim. Serv.* **2018**, *11*, 36–48, doi:10.1016/j.cliser.2018.05.003.

143. GABA, O. U. C. Improvement and comparative assessment of a new hydrological modelling approach to catchments in Africa and the USA Towards an application to ungauged catchments, University of Abomey Calavi (Benin), 2016.

144. ESA-CCI Internal Release of Global Land Cover Map with Improved Accuracy over the Existing State of the Art (75.6%) Available online: http://2016africalandcover20m.esrin.esa.int/download.php (accessed on Jun 5, 2019).

145. Cazals, C.; Rapinel, S.; Frison, P.-L.; Bonis, A.; Mercier, G.; Mallet, C.; Corgne, S.; Rudant, J.-P. Mapping and Characterization of Hydrological Dynamics in a Coastal

Marsh Using High Temporal Resolution Sentinel-1A Images. *Remote Sens.* **2016**, *8*, 570, doi:10.3390/rs8070570.

146. Sentinel Vision team VisioTerra Lac Tchad vu des satellites; Paris, 2018;

147. Chow, V. Te *Open-Channel Hydraulics*; McGraw-Hill, New York, 1959; ISBN ISBN 0-07-010810- 2.

Annexes

List of published papers

Hounguè, R.; Lawin, E.; Moumouni, S.; Afouda, A. A. Change in Climate Extremes and Pan Evaporation Influencing Factors over Ouémé Delta in Bénin. *Climate* **2019**, *7*, 22, doi:10.3390/cli7010002.

List of co-authors published papers

Attogouinon, A.; Lawin, A. E.; M'Po, Y. N.; Hounguè, R. Extreme Precipitation Indices Trend Assessment over the Upper Ouémé River Valley-(Bénin). *Hydrology* **2017**, *4*, 36, doi:10.3390/hydrology4030036.

Lawin, E. A.; N Tcha M'Po, Y.; Biaou, C. A.; Komi, K.; Hounguè, R.; Yao, B. K.; Afouda, A. A. Mid-Century Daily Discharge Scenarios Based on Climate and Land Use Change in Ouémé River Basin at Bétérou Outlet. *Hydrology* **2019**, 1–14, doi:10.3390/hydrology5040069.

Lawin, A. E.; Hounguè, R.; N 'Tcha M'Po, Y.; Hounguè, N. R.; Attogouinon, A.; Afouda, A. A. Mid-Century Climate Change Impacts on Ou é m é River Discharge at Bonou Outlet (Benin). *Hydrology* **2019**, *6*, 20. doi:10.3390/hyd6030072

Akokponhoué, N. , Yalo, N. , Akokponhoué, B. , Hounguè, R. and Agbahoungba, G. (2019) Contribution of Electrical Resistivity Tomography and Boring Technique in the Realization of Ten (10) Large Boreholes in a Crystalline Basement Rocks in the Centre-West of Benin. *Journal of Geoscience and Environment Protection*, **7**, 114-130. doi: 10.4236/gep.2019.79009.

Rita HOUNGUE is born on April 27, 1989 at Adjaha in the southern Benin. She spent 14 years in Comé where she did her primary and secondary school before getting her baccalaureat in 2006. She then started a bachelor in physics before steping into hydrological science in 2008. She holds a bachelor in physics and a bachelor and master in quantitative hydrology. She is now completing a PhD in climate change and water resources. She is sympathic, moderate and altruistic. Her perspectives lie in improving people wellbeing through everyday actions.

Abstract:

Ouémé Delta is known as the food basket that feeds southern Benin with protein and agricultural products. These resources have to be well managed and preserved for sustainability. In fact, under effects of anthropogenic activities due to population growth as well as climate variability, there is a need of resource quantification and planning for better management. Moreover, Ouémé Delta is the buffer zone of Ouémé catchment drainage and used to be flooded seasonally during high water period. In addition, the existing early warning system does not account in detail for the Delta due to lack of data. In order, to contribute to flood event management in Ouémé Delta while taking into account anthropogenic activities and climate *variability, the present work focuses on climate change impacts on the hydrodynamic functioning of Ouémé Delta. The objective of this work is: 1) to assess current state of extreme event in Ouémé Delta using trend analysis of climate extreme indices; 2) to quantify impact of climate change over Ouémé River discharge at Bonou outlet from 1971 to 2050; 3) design simple flood mapping process for Ouémé Delta; 4) to model Ouémé Delta hydrodynamic under climate change effects. The data collected are mainly climatic and hydrometric. The climatic data are observations from 1971 to 2010 and climate projection from 2020 to 2050 based on the representative concentration pathways 4.5 and 8.5. The hydrometric data are water level and river discharge at station points. Trend analysis is conducted using the prewhitened Mann Kendall method. Rainfall runoff modeling is based on three hydrological models among which are two distributed ones (HBV, HEC-HMS) and one lumped and locally developed HyMoLAP for comparison over peak flows. In HEC-HMS two loss methods are applied: the curve number (CN) method which takes into account land use and cover change aspect in one hand and the soil moisture accounting method (SMA) in the other hand for peak flow simulation. SMA loss method is the one used under HBV model. Futhermore, hydrodynamic modeling is done using HEC-RAS. The efficiency coefficients retained are the Kling–Gupta Efficiency (KGE), the percentage of bias (PBias) and the Mean Absolute Error (MAE). Results showed that extreme events tend to increase with climate variability. Temperature is increasing as proof of the global warming. HEC-HMS showed ability to simulate runoff while taking into account land use and cover change. Comparing HEC-HMS, HBV and HyMoLAP, HEC-HMS is found to be the best followed by HBV. Moreover, the coupling process through mean ensemble approach exhibits the high performance of the couple HBV/HEC-HMS. The same performance is shown over Ouémé River peak flows at Bonou outlet. The low performance of HyMoLAP is probably due to the lack of storage components which HEC-HMS and HBV were found to be sensitive to. The hydrodynamic model also* showed ability in simulating flow propagation in Ouémé Delta. As input for the existing early warning system, the current hydrodynamic model informs on detailed hydraulic characteristics in Ouémé at grid points instead of station points only. Dam construction and climate change are projected to impact on water quality, quantity and fluvial transport in Ouémé Delta with issue on soci-economical activities.

Key words: *Trend analysis, hydrological modeling, land use and cover dynamic, hydrodynamic modeling, Ouémé Catchment, Ouémé Delta early warning system in Benin.*

PhD

Rita HOUNGUE

Climate change impacts on hydrodynamic functioning of Ouémé Delta (Benin)

GRP/CCWR/INE/WASCAL – UAC February, 2020